Femtosekundenpuls injizierte kleine Polaronen in Lithiumniobat:

Bildungs- und Transportdynamiken, Nachweis der Gitterverzerrung und nichtlinear optische Eigenschaften im mittleren infraroten Spektralbereich

Kumulative Dissertation

Felix Freytag
Fachbereich Physik

UNIVERSITÄT OSNABRÜCK

30. November 2018

Inhaltsverzeichnis

1 Einleitung **1**

2 Bildungs- und Transportdynamiken kleiner Polaronen **4**
2.1 Publikationen 5

3 Nachweis der Gitterverzerrung kleiner Polaronen **7**
3.1 Publikationen 8

4 Nichtlinear optische Eigenschaften im mittleren infraroten Spektralbereich **9**
4.1 Publikationen 10
4.2 Unveröffentlichte Daten: MIR-Holographie 12
4.2.1 Intensitäts-, Energiedichte- und Ladungsträgermodulation bei Überlagerung dreier Lichtpulse 13
4.2.2 Experimentelle Methoden und Beobachtungen 16
4.2.3 Experimentelle Daten 17
4.2.4 Auswertung - Diskussion 21

5 Zusammenfassung **26**

Literaturverzeichnis **28**

A Berechnung linearer und nichtlinearer Absorptionskoeffizienten **34**

B Publikationen **36**
B.1 Scanning nonlinear absorption in lithium niobate over the time regime of small polaron formation 36
B.2 The role of self-trapped excitons in polaronic recombination processes in lithium niobate 52
B.3 Atomic insight to lattice distortions caused by carrier self-trapping in oxide materials 75
B.4 Mid-Infrared photorefractivity with non-degenerate two-photon absorption 87
B.5 Dynamic grating mediated energy transfer between two sub-picosecond pulses in $LiNbO_3$ 91
B.6 Transient energy transfer on the femtosecond timescale in lithium niobate 95
B.7 Picosecond near-to-mid-infrared absorption of pulse-injected small polarons in lithium niobate 98

C Beiträge zu Konferenzen **108**

1 Einleitung

Schönheit liegt im Auge des Betrachters.
Auch wenn gewisse Charakteristiken des menschlichen Gesichtes wie die Symmetrie als allgemein attraktiv empfunden werden, gibt es individuelle Präferenzen der Schönheit, welche auf die Erfahrungen der jeweiligen Person zurückzuführen sind [1]. Beispielsweise kann im Auge eines liebenden Partners ein altes, faltiges, Gesicht eine ästhetische Harmonie besitzen. Schönheit ist nicht jedem Auge zugänglich. Das Auge der Physik sind Experimente, durch deren Weiterentwicklung und Kombination sich der Blick für Dinge öffnet, die anderen Betrachtern verborgen bleiben. Vornehmlich gilt dieses für optische Experimente, die die Limitationen des menschlichen Auges aufheben können und beispielsweise das „Sehen“ außerhalb des sichtbaren Spektralbereichs erlauben.

Den Grundstein für ein komplett neues Verständnis der Umwelt durch die Optik setzte Theodore Harold Maiman mit der Entdeckung des ersten Rubin Lasers im Jahr 1960 [2]. Durch die Wechselwirkung des Laserlichtes mit Materie und den damit verbundenen hohen elektrischen Feldstärken im Material wurden die am Atomkern gebundenen Elektronen so stark ausgelenkt, dass der Zusammenhang zwischen der elektrischen Polarisation und dem elektrischen Feld um zusätzliche nichtlineare Terme ergänzt werden musste [3]. Hieraus resultierten intensitätsabhängige nichtlinear optische Prozesse wie die Frequenzverdopplung [4], die Änderung des Brechungsindex' [5, 6] oder die gleichzeitige Absorption mehrerer Photonen [7].

Durch das semiklassische Modell zur nichtlinearen Optik von Nicolas Bloembergen [3] und die Entdeckung neuer Herstellungsverfahren für synthetische nichtlinear optische Kristalle wie KTP [8], BBO [9], LBO [10] oder $LiNbO_3$ [11] wurde in den folgenden Jahren der Weg für neue Technologien wie den Femtosekundenlaser [12–14] oder optisch parametrische Verstärker/Oszillatoren, welche lückenlos Licht vom Ultravioletten bis ins mittlere Infrarote (MIR) mit einer Konversionseffizienz von bis zu 40% erzeugen können [15], geebnet. Diese Technologien führten zu einer Revolution der Physik, Chemie und Biologie, da es nun erstmals möglich war, neben der statischen Betrachtung von Molekülstrukturen durch Röntgen/Elektronenbeugung, AFM, STM oder NMR auch den Prozess der Entstehung und des Zerfalls von (Molekül-)Bindungen mit einer Femtosekundenzeitauflösung in einem weiten Spektralbereich zu betrachten [16, 17].

Mit diesem neuen Blick auf Materialien gehen außerdem ultrakurze (sub-Pikosekunden) Laserpulse mit Spitzenintensitäten von mehreren Petawatt pro Quadratmeter einher, welche in nichtlinear optischen Materialien zu hohen Ladungsträgerdichten über Multi-Photonen-Absorption (MPA) führen können. Die durch Femtosekundenpuls *injizierten* Ladungsträger können in nichtlinear optischen Medien mit starker Elektronen/Loch-Phononen-Kopplung in kleine, stark-koppelnde, Polaronen zerfallen - Ladungsträger, welche sich durch Verzerrung des Gitters in der Nähe von intrinsischen oder extrinsischen Defekten selbst lokalisieren [18–20]. Kleine Polaronen beeinflussen maßgeblich die (nicht-linear) optischen und elektronischen Eigenschaften im Material wie die Leitfähigkeit

[21], die Absorption [22, 23], den Brechungsindex [24] oder den laserinduzierten Schaden [25]. Für das Verständnis dieser Prozesse ist hinsichtlich photonischer Anwendungen eine genaue Analyse der elektronischen Dynamik sowie der strukturellen Änderung während der Bildung und der Rekombination notwendig. Als Referenzmaterial zur Erforschung von kleinen Polaronen fungiert Lithiumniobat, $LiNbO_3$ (LN), welches sich durch eine gut bekannte Defektstruktur, seine starke Elektronen-Phononen Kopplung, seinen hohen nichtlinearen Koeffizienten, eine hohe Laserzerstörungsschwelle, ein weites Transmissionsfenster, sowie seinen ausgeprägten Photorefraktiven-Effekt auszeichnet [11, 22, 26, 27].

In dieser Arbeit wird eine Kombination von elektronischen, strukturellen und nichtlinear optischen Verfahren an Lithiumniobat verwendet, um ein erweitertes Bild von Femtosekundenpuls *injizierten* kleinen Polaronen zu erhalten (vgl. Fig. 4.10).

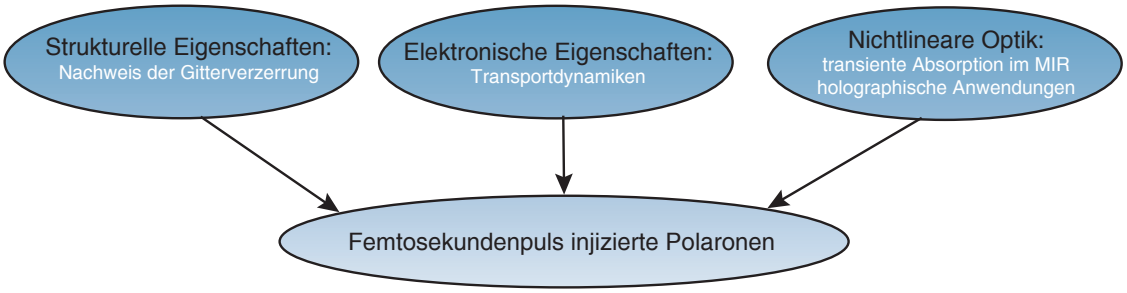

Abbildung 1.1: Schematischer Aufbau der Arbeit: Erst eine kombinierte Betrachtung der elektronischen (Kapitel 2), strukturellen (Kapitel 3) und nichtlinear optischen Eigenschaften (Kapitel 4) ermöglicht ein umfassendes Bild von Femtosekundenpuls *injizierten* Polaronen.

In Kapitel 2 werden die Bildungs- und Transportdynamiken von kleinen Polaronen analysiert. Polaronendynamiken sind elementar für das Verständnis der ultraschnellen Response von vielen oxidischen Materialien und müssen für photonische Anwendungen wie bei der Ultrakurzzeit-Holographie für bspw. die Realisierung von holographischen 3D-Displays [28], optischen Korrelatoren [29] oder THz-Schaltern [30] herangezogen werden. In dieser Arbeit wird zum Einen ein Schwerpunkt auf die ultrakurzen Dynamiken von Femtosekundenpuls *injizierten* Polaronen und die Beiträge zur Absorption im sichtbaren Spektralbereich gelegt. Zum Anderen wird ein aktualisiertes Polaronentransportmodell postuliert, das sowohl offene Fragestellungen der bisherigen Literatur beantworten kann als auch erstmals den Einfluss von Exzitonen auf den Transport berücksichtigt. Hierdurch können die Daten der transienten Absorption von Polaronen auch für tiefe Temperaturen ($T < 200\,°C$) beschrieben werden.

In Kapitel 3 wird erstmals eine Verzerrung der Gitterstruktur durch Femtosekundenpuls *injizierte* Polaronen nachgewiesen. Polaronische Eigenschaften wie Bindungsenergie, Absorptionsquerschnitte oder die Hopping-Rate basieren sowohl auf den Eigenschaften des Gitters (Steifigkeit, Phononenfrequenz, Temperatur,...) als auch auf der lokalen Verzerrung der Gitterstruktur [31]. Eine dynamische Analyse der Struktur hat einen großen Einfluss auf das generelle Verständnis der Polaroneneigenschaften und könnte Aufschluss über den Polaronenradius oder die Polaronenkopplungsstärke geben. Obwohl es eine

Vielzahl an Methoden gibt um statisch Gitterparameter zu bestimmen (vgl. [32]), so kann die Gitterstruktur bisher nicht während der Polaronenbildung und Rekombination beobachten werden. In dieser Arbeit wird eine Methode vorgestellt mit der es möglich ist polaronische Gitterverzerrungen bei Raumtemperatur im Nichtgleichgewichtszustand mit bis zu Femtosekundenzeitauflösung zu betrachten, um einen neuen Blickwinkel auf Polaroneneigenschaften zu gewinnen.

Im letzten Teil dieser Arbeit (Kapitel 4) werden nichtlinear optische Eigenschaften von LN mit Schwerpunkt auf den infraroten Spektralbereich bestimmt. Das Verständnis von Femtosekundenpuls *injizierten* Polaronen ist in diesem Spektralbereich von besonderer Bedeutung, da dieser auf der einen Seite für medizinische Anwendungen bspw. dem zielgenauen Abtragen von Gewebe große Relevanz hat [33], auf der anderen Seite kohärentes Licht in diesem Spektralbereich nur über optisch parametrische Prozesse erreicht werden kann [34]. Um Materialien für die Erzeugung von Femtosekunden im mittleren Infraroten zu optimieren, werden transiente Absorptionsmessungen im mittleren Infraroten durchgeführt. Über die Realisierung einer Methode zum Schreiben von (transienten) holographischen Gittern im mittleren Infraroten Spektralbereich, können außerdem neue Erkenntnisse zur Kontrolle und Charakterisierung von Infrarotpulsen gewonnen werden.

2 Bildungs- und Transportdynamiken kleiner Polaronen

Kleine Polaronen können ursächlich für ultraschnelle Wechselwirkungen von Licht mit Materie sein und spielen eine entscheidende Rolle, um grundlagenphysikalische Fragestellungen auf Gebieten der Defektphysik oder Ladungsträgerlokalisierung in Nichtgleichgewichtszuständen auf der ultraschnellen Zeitskala zu untersuchen [35]. Das Aufkommen des Feldes der nichtlinearen Photonik - der Übertrag von optischen Verfahren auf den Bereich der *Informations- und Kommunikationstechnologie* - bedingt einen steigenden Bedarf an nichtlinear optischen Materialien mit instantanen/ultraschnellen Kopplungen und führt zu einer Notwendigkeit der Beantwortung dieser Fragestellungen hinsichtlich dynamischer Prozesse im Material. Lithiumniobat, auch häufig als „Silizium der Photonik“ bezeichnet [36, 37], dient in dieser Studie auf Grund der Vielzahl an Defektzentren als oxidisches Referenzmaterial zur Analyse der Bildungs- und Transportdynamiken von durch Licht *injizierten* kleinen, stark koppelnden, Polaronen.

In der Veröffentlichung ([38], siehe B.1) werden die nichtlinearen (instantanen) und polaronischen (ultraschnellen) Beiträge zur transienten Absorption auf der Femtosekundenzeitskala untersucht und durch Simulation der Polaronendynamiken separiert. Mit Variation der Pulsdauer von $\tau = 70\,\mathrm{fs} - 1{,}000\,\mathrm{fs}$ können Aussagen zur Polaronenbildungszeit getroffen werden und ein Zeitraum von ca. 80 fs nach Anregung kann bestimmt werden, in dem nur instantane Prozesse zu einer Kopplung von Licht mit Materie führen. Diese Ergebnisse sind von großer Bedeutung beim Einsatz von Lithiumniobat als zukünftiges Material der nichtlinearen Photonik und für nichtlinear optische Anwendungen bspw. als Frequenzkonverter.

In der Studie ([39], siehe B.2) wird das bisherige mikroskopische Bild zur dynamischen Ladungsträgerlokalisierung und Rekombination in Lithiumniobat durch Kombination von transienten Absorptionsmessungen und Lumineszenzmessungen in einem weiten Temperaturbereich überarbeitet. Erstmals wird im Rahmen dieses Modells der Einfluss von selbstlokalisierenden Exzitonen untersucht, welchen eine Absorption im ultravioletten/blauen Spektralbereich zugeordnet werden kann. Diese Studie gibt einen neuen Blickwinkel auf die Rekombination und die Absorptionsquerschnitte kleiner Polaronen und ist ein erster Schritt für einen Exzitonenlaser im blauen Spektralbereich.

2.1 Publikationen

Der Autor hat zu den im Folgenden aufgeführten Artikeln im Bereich Bildungs- und Transportdynamiken kleiner Polaronen in Lithiumniobat beigetragen:

- H. Badorreck, S. Nolte, F. Freytag, P. Bäune, V. Dieckmann, M. Imlau. *Scanning nonlinear absorption in lithium niobate over the time regime of small polaron formation* Opt. Mater. Exp. 5, 2729-2741, (2015). doi: 10.1364/OME.5.002729.

  Abstract: Nonlinear absorption is studied in presence of small polaron formation in lithium niobate using the z-scan technique and ultrashort laser pulses with pulse durations of 70 - 1,000 fs. A model for the analysis of the transmission loss as a function of pulse duration is introduced that considers (i) the individual contributions of two-photon and small polaron absorption, (ii) the small polaron formation time and (iii) an offset time between the optical excitation of free carriers by two-photon absorption and the appearance of small polarons. It is shown that the model allows for the analysis of the experimentally determined z-scan data with high precision over the entire range of pulse durations using a two-photon absorption coefficient of $\beta = (5.6 \pm 0.8)\,\mathrm{mm/GW}$. A significant contribution by small polaron absorption to the nonlinear absorption is uncovered for pulse durations exceeding the characteristic small polaron formation time of $\approx 100\,\mathrm{fs}$. It can be concluded that the small polaron formation time is as short as (70 - 110) fs and the appearance of small polaron formation is delayed with respect to two-photon absorption by an offset of about 80 fs.

  © 2015 Optical Society of America. Users may use, reuse, and build upon the article, or use the article for text or data mining, so long as such uses are for non-commercial purposes and appropriate attribution is maintained. All other rights are reserved.

- S. Messerschmidt, A. Krampf, F. Freytag, M. Imlau, L. Vittadello, M. Bazzan, G. Corradi. *The role of self-trapped excitons in polaronic recombination processes in lithium niobate*, J. Phys. Cond. Mat., (2018). doi: 10.1088/1361-648X/aaf4df

  Abstract: Transient absorption and photoluminescence are experimentally investigated in the polaronic reference system lithium niobate, $LiNbO_3$ (LN), with the aim to refine the microscopic model of small polaron dynamics in materials with strong electron-phonon coupling. As a unique feature, our study is performed by using two different spectroscopic methods, in crystals with dopants enhancing photorefraction or damage resistance, and over a broad temperature range from $15 - 400\,\mathrm{K}$. Although being self-consistent for particular experimental conditions, the hitherto used microscopic polaronic models reveal inconsistencies when applied to this larger data set. We show that comprehensive modeling is unlocked by the inclusion of an additional type of polaronic state with the following characteristics: (i) strongly temperature- and dopant-dependent relaxation times, (ii) an absorption feature in the blue-green spectral range, and (iii) a Kohlrausch-Williams-Watts decay shape with a temperature-dependent stretching factor $\beta(T)$ showing a behavior contrary to that of small, strong-coupling polarons. The hypothesis of

self-trapped excitons (STEs, i.e., bound electron-hole pairs strongly coupled to Nb^{5+} and O^{2-} within a niobium-oxygen octahedron) and their pinning on defects as the microscopic origin of these characteristics is supported by a spectroscopic linkage of photoluminescence at low (15 K) and elevated (300 K) temperatures and explains the long-lifetime components in transient absorption as due to pinned STEs.

Die Zusammenfassung der ersten Arbeit wurde mit freundlicher Genehmigung der *The Optical Society (OSA)* und des *American Institute of Physics* angegeben. Die Zusammenfassung der zweiten Arbeit wurde mit freundlicher Genehmigung der *IOP Publishing Ltd.* angegeben. Die vollständigen Artikel finden sich im Anhang unter B.1,B.2.

3 Nachweis der Gitterverzerrung kleiner Polaronen

Spätestens seitdem es Eigler und Schweizer im Jahr 1990 gelang, einzelne Xe-Atome mit einem Rasterkraftmikroskop (AFM) zu positionieren, um den IBM Schriftzug zu schreiben [40], ist das Beobachten und die Kontrolle von Strukturen auf Atomebene nicht mehr wegzudenken. Neben der auf Oberflächenanalyse beschränkten Rasterkraftmikroskopie haben sich Messmethoden etabliert, um statische strukturelle Parameter von Gitterverbänden zu bestimmen. Hierbei handelt es sich bspw. um eine Kombination aus Röntgenbeugung und Elektronenspinresonanz (EPR), Elektronen-Kernspin-Doppelresonanz (ENDOR) oder die winkelaufgelöste Photoelektronenspektroskopie (APRES) [41–45].

Trotz dieser Vielzahl an Methoden ist es bis zum heutigen Tag nur schwer möglich, strukturelle Veränderungen/Dynamiken insbesondere auf der Femtosekundenzeitskala im Gitterverband zu beobachten. Bei der Bildung eines durch Femtosekundenpulse *injizierten* Polarons wird jedoch vermutet, dass es zu einem Selbsteinfang des Ladungsträgers durch Elektronen/Loch-Phononen-Kopplung kommt und eine Verzerrung der Gitterstruktur resultiert [31]. Bildungszeiten von einigen hundert Femtosekunden und Zerfallszeiten auf der Pikosekunden bis Sekunden Zeitskala (siehe [39] und [32]) führen zu der Notwendigkeit, eine neue Methodik zu entwickeln, um die polaronisch bedingte Gitterverzerrung nachzuweisen.

In der Veröffentlichung ([46], siehe B.3) kann eine Gitterverzerrung durch kleine Polaronen in Lithiumniobat nachgewiesen werden. Hierzu wird die Schwingungsbande eines zweiatomigen Moleküls als lokale Sonde verwendet, um die strukturellen Veränderungen der direkten Umgebung zu tasten. Dieses geschieht durch eine Kombination aus Anreg-Abtast Spektroskopie im mittleren infraroten Spektralbereich und einer Modellierung der Umgebung über Coulomb- und Morsepotential. Diese Methode ermöglicht einen neuen Einblick, um Veränderungen von oxidischen Materialien im Allgemeinen zu untersuchen und dynamische strukturelle Fragestellungen über die Formation, den Hopping-Transport oder das Rekombinationsverhalten von Polaronen auch auf der ultrakurzen Zeitskala zu beantworten.

3.1 Publikationen

Der Autor hat zu den im Folgenden aufgeführten Artikeln im Bereich des Nachweises der Gitterverzerrung kleiner Polaronen beigetragen:

- F. Freytag, G. Corradi, M. Imlau. *Atomic insight to lattice distortions caused by carrier self-trapping in oxide materials* Sci. Rep. 6, 36929, (2016). doi: 10.1038/srep36929.

  Abstract: We gain hitherto missing access to the spatio-temporal evolution of lattice distortions caused by carrier self-trapping in the class of oxide materials - and beyond. The joint experimental/theoretical tool introduced combines femtosecond mid-infrared probe spectroscopy with potential landscape modeling and is based on the original approach that the vibration mode of a biatomic molecule is capable to probe strongly localized, short-lived lattice distortions in its neighborhood. Optically generated, small, strong-coupling polarons in lithium niobate, mediated by OH^- ions present as ubiquitous impurities, serve as a prominent example. Polaron trapping is found to result in an experimentally determined redshift of the OH^- stretching mode amounting to $\Delta\nu_{\mathrm{vib}} = -3\,\mathrm{cm}^{-1}$, that is successfully modeled by a static Morse potential modified by Coulomb potential changes due to the displacements of the surrounding ions and the trapped charge carrier. The evolution of the trapping process can also be highlighted by monitoring the dynamics of the vibrational shift making the method an important tool for studying various systems and applications.

  This work is licensed under a Creative Commons Attribution 4.0 International License. The images or other third party material in this article are included in the article's Creative Commons license, unless indicated otherwise in the credit line; if the material is not included under the Creative Commons license, users will need to obtain permission from the license holder to reproduce the material. To view a copy of this license, visit http://creativecommons.org/licenses/by/4.0/

Die Zusammenfassung wird hier mit freundlicher Genehmigung der *Nature Publishing Group* angegeben, die vollständige Publikation findet sich im Anhang unter B.3.

4 Nichtlinear optische Eigenschaften im mittleren infraroten Spektralbereich

In diesem Kapitel werden die nichtlinear optischen Eigenschaften von LN mittels Holographie und transienter Absorptionsspektroskopie im mittleren Infraroten im Hinblick auf die Femtosekundenpuls *Injektion* kleiner Polaronen untersucht. Die Ergebnisse dieser Studie beeinflussen den Einsatz von LN als Frequenzkonverter, als Medium für holographische Anwendungen und für die Diagnostik und Kontrolle von MIR-Pulsen. Auf Grund der hohen Absorption von Wasser im mittleren infraroten Spektralbereich ist letztere besonders relevant für medizinische Anwendungen, in denen zielgenau Gewebe abgetragen oder geschnitten werden muss, ohne thermische Schädigungen der Umgebung hervorzurufen [33]. Hierzu sind ultrakurze Pulse in einem Wellenbereich $\lambda \approx$ 3-6 μm notwendig, welche über mehrstufige Prozesse in optisch parametrischen Verstärkern oder Oszillatoren in nichtlinearen Medien, häufig LN, erzeugt werden. Die *Injektion* von kleinen Polaronen durch Femtosekundenpulse beeinflusst die transiente Absorption und limitiert damit die Konversionseffizienz und die Zerstörschwelle des nichtlinear optischen Materials (siehe [32]). Für die Entwicklung neuer Lichtquellen ist daher die genaue Kenntnis der transienten (Absorptions-)Prozesse von entscheidender Bedeutung.

In der Arbeit ([32], siehe B.7), welche bei *Optics Letters* eingereicht ist, kann gezeigt werden, dass durch Femtosekundenpulsbeleuchtung mit sichtbaren Pulsen ($\lambda = 488\,\mathrm{nm}$) kleine freie Polaronen *injiziert* werden, welche die transienten Absorptionseigenschaften bis in den mittleren infraroten Spektralbereich beeinflussen. Kleine Polaronen werden in der Veröffentlichung ([47], siehe B.5 und [48], siehe B.6) als mögliche Ursache für einen retadierten transienten Energietransfer bei der Selbstbeugung betrachtet. In der Veröffentlichung ([49], siehe B.4) wird das Aufzeichnen eines PR-Gitters im mittleren infraroten Spektralbereich mit ultrakurzen Pulsen ($\geq 1600\,\mathrm{nm}$) mittels nicht degenerierter Zwei-Photonen-Absorption (NDTPA) in LN gezeigt. Der Anregungsmechanismus wird in unveröffentlichten Daten bei simultaner Überlagerung zweier infraroter Pulse mit einem sichtbaren Lichtpuls als Entstehungsursache des PR-Gitters und eines transienten Gitters betrachtet. Die Entstehung des transienten Gitters wird zum Einen über den Kerr-Effekt und die MPA diskutiert, zum Anderen wird die Möglichkeit eines retadierten Mehr-Stufen-Prozesses über Femtosekundenpuls *injizierte* kleine Polaronen in Betracht gezogen.

4.1 Publikationen

Der Autor hat zu den im Folgenden aufgeführten Artikeln im Bereich nichtlinear optischer Eigenschaften im mittleren infraroten Spektralbereich beigetragen:

- B. Bourdon, F. Freytag, M. Imlau, A. Shumelyuk, S. Odoulov.
  Mid-Infrared photorefractivity with non-degenerate two-photon absorption
  IOP Conf. Series: Journal of Physics: Conf. Series 867 (2017) 012006. doi: 10.1088/1742-6596/867/1/012006

  Abstract: Photorefractive grating recording with mid-infrared sub-picosecond light pulses (1.6 μm and longer wavelengths) might be possible in $LiNbO_3$ crystals if the interaction area is illuminated additionally with pulses of visible light. Two processes can enable the experimentally observed MIR recording: One is related to the direct photoexcitation of a free electron via nonlinear absorption of two photons with different frequencies, one in the MIR and one in the visible range. The alternative possibility consists in an enhancement, caused by the diffraction of a visible pulse, of a very weak space-charge grating seeded solely by MIR radiation.

  Content from this work may be used under the terms of the Creative Commons Attribution 3.0 licence. Any further distribution of this work must maintain attribution to the author(s) and the title of the work, journal citation and DOI.

- S. Nolte, B. Bourdon, F. Freytag, M. Imlau, A. Shumelyuk, S. Odoulov.
  Dynamic grating mediated energy transfer between two subpicosecond pulses in $LiNbO_3$
  IOP Conf. Series: Journal of Physics: Conf. Series 867 (2017) 012003. doi: 10.1088/1742-6596/867/1/012003

  Abstract: Two ultrashort pulses that interact in a nonlinear medium can excite a grating of the nonlinear absorption and refraction and their characteristics can be modified as a result of selfdiffraction from this grating. In this work, we adress an energy transfer between pulses of different energies and/or different frequencies within the visible spectral range in congruent, nominally undoped LiNbO 3 aiming to reveal new features that distinguish this process from the known transient and steady-state coupling of cw laser beams.

  Content from this work may be used under the terms of the Creative Commons Attribution 3.0 licence. Any further distribution of this work must maintain attribution to the author(s) and the title of the work, journal citation and DOI.

- S. Nolte, B. Bourdon, F. Freytag, M. Imlau, A. Shumelyuk, S. Odoulov.
  Transient energy transfer on the femtosecond timescale in lithium niobate
  CLEO/Europe-EQEC pp. 1-1 (2017). doi: 10.1109/CLEOE-EQEC.2017.8087516

  In reference to IEEE copyrighted material which is used with permission in this thesis, the IEEE does not endorse any of University Osnabrück's products or services. Internal or personal use of this material is permitted. If interested in

reprinting/republishing IEEE copyrighted material for advertising or promotional purposes or for creating new collective works for resale or redistribution, please go to http://www.ieee.org/publications_standards/publications/rights/rights_link.html to learn how to obtain a License from RightsLink.

- F. Freytag, S. Messerschmidt, A. Krampf, G. Corradi, M. Imlau.
  Picosecond near-to-mid-infrared absorption of pulse-injected small polarons in lithium niobate, Opt. Mat. Exp. **8**, 6, 1505-1514 (2018) . doi: 10.1364/OME.8.001505

  Abstract: Fs-pulse-induced (E_{pump}=2.5 eV) picosecond mid-infrared (MIR) absorption is studied in the spectral region between 0.30 eV and 1.05 eV in $LiNbO_3$. We find a non-instantaneous MIR absorption peak in the time domain up to 1 ps and a broad-band, long-lived absorption (maximum at 0.85 eV, width $\approx$ 0.5 eV), for $t > 1$ ps. Modelling suceeds by considering small Nb_{Nb}^{4+} electron polaron formation along the sequence: (i) two-photon injection of hot electron-hole pairs at Nb-O-octahedra, (ii) electron cooling by electron-phonon-scattering, and (iii) electron self-localization by strong electron-phonon-coupling.

  © 2018 Optical Society of America. Users may use, reuse, and build upon the article, or use the article for text or data mining, so long as such uses are for non-commercial purposes and appropriate attribution is maintained. All other rights are reserved.

Die Zusammenfassungen der ersten beiden Publikationen werden hier mit freundlicher Genehmigung von *IOP Publishing Ltd.* angegeben die dritte Publikation mit Genehmigung von *IEEE Xplore*, die vierte Publikationmit Genehmigung von der *Optical Society of America (OSA)* eingereicht worden. Die vollständigen Artikel finden sich im Anhang unter B.4,B.5,B.6,B.7.

4.2 Unveröffentlichte Daten: MIR-Holographie

Die Holographie (*griech. holos - ganz, graphein - aufzeichnen, schreiben*) beschreibt ein von Dennis Gabór in 1947 entwickeltes bildgebendes Verfahren [50], welches im Gegensatz zur klassischen Fotografie zusätzlich zur Intensität auch die Tiefeninformationen über die Phase der Lichtwelle aufnimmt. Die Konservierung der Phase erfolgt durch die Überlagerung einer vom Objekt ausgehenden Lichtwelle mit einer Referenzwelle in einem photosensitiven Medium durch eine Modulation des Brechungsindex' bzw. der Phase oder der Absorption bzw. der Amplitude. Das im Medium entstandene Hologramm kann unter Verwendung der Referenz- bzw. der Signalwelle ausgelesen werden und ermöglicht so eine Rekonstruktion des Objektes. Die Holographie findet nicht nur Einsatz in der Industrie wie in der Archivierung von 3D-Bildern oder der zerstörungsfreien Werkstoffprüfung [51], sondern auch bei der Entwicklung neuer Technologien - dynamischen Displays oder der holographischen CD, welche Daten von über 10 TB speichern könnte [52–54]. Da das Anwendungsgebiet der Holographie stark von der Lebensdauer τ des Hologramms abhängt, wird im Folgenden zwischen ultrakurzen ($\tau \ll 1\,\mathrm{ns}$) und statischen Hologrammen ($\tau \gg 1\,\mathrm{s}$) unterschieden.

Statische Hologramme finden ihren Einsatz in der persistenten Datenspeicherung, wobei hierzu häufig photorefraktive Kristalle wie Bariumnitrat ($BaTiO_3$), Gallium-Arsenid (GaAs) oder Lithiumniobat verwendet werden [55]. Bei dem Photorefraktiven Effekt (PR-Effekt) führt inhomogene Lichteinstrahlung zu einer Anhebung von Elektronen aus Defektzentren ins Leitungsband. Es folgt eine Umverteilung der Ladungsträger über Diffusion und den Volumen Photovoltaischen Effekt in nicht beleuchtete Bereiche, sodass positiv geladene Defektzentren zurück gelassen werden [56, 57]. Die Ladungsträger können in den nicht beleuchteten Bereichen an Defektzentren als Polaronen gefangen werden, welche auf Grund der Abwesenheit von Licht stabil sind, bis eine Rekombination mit Löchern erfolgt. Die räumliche Trennung der Ladungsträger führt durch die Poissongleichung [56] zur Ausprägung eines elektrischen Raumladungsfeldes, wodurch über den linearen elektrooptischen Effekt der Brechungsindex moduliert wird [58].

Ultrakurze Hologramme sind für Anwendungen wie die transiente Datenspeicherung oder den transienten Energietransfer (vgl. Publikation [47] und [48]) relevant und häufig in Kombination mit sub-Pikosekunden Lichtpulsen zu finden. Sehr hohe Lichtintensitäten können zu einer intensitätsabhängigen Änderung der Absorption und/oder des Brechungsindex' über MPA bzw. den quadratisch elektrooptischen Effekt (Kerr-Effekt) führen [59, 60]. Da durch die Interferenz zweier Pulse die Intensität räumlich variiert, wird nur in Bereichen konstruktiver Interferenz die Absorption bzw. der Brechungsindex zusätzlich zum linearen Effekt moduliert. Hierdurch prägt sich ein intensitätsabhängiges Gitter aus, welches nur bei zeitlicher Überlagerung zweier Pulse auftritt. Im Gegensatz zum photorefraktiven Gitter muss beim ultrakurzen Gitter die Anregung der Ladungsträger nicht aus einem photorefraktiven Zentrum erfolgen [61]. Eine Modulation der Amplitude bzw. des Brechungsindex' kann jedoch nicht nur durch instantane Prozesse, sondern auch durch retardierte Prozesse auftreten. Reckenthaeler et al. [62] berichten über die Separation des instantanen Gitters durch MPA und der verzögerten Reaktion des Materials über ein freies Ladungsträgergitter. In Lithiumniobat lokalisieren sich nach einigen hundert Femtosekunden [38, 63, 64] die freien Ladungsträger als kleine

Polaronen, welche wiederum die Absorptionseigenschaften des Materials beeinflussen [35]. Die Lebensdauer des so entstandenen Absorptionsgitters hängt von der Zerfallszeit des Polarons ab. Auf Grund der starken Absorption von freien Polaronen im mittleren Infraroten ist es daher zu erwarten, dass sich auch im MIR ein retadiertes Absorptionsgitter ausprägt. Vorherige Studien beschreiben das Aufzeichnen von photorefraktiven Gittern mit IR-Strahlung in LN für degenerierte Drei-Photonen-Absorption bis maximal $1.55\,\mu$m [65–67].

Im Folgenden wird eine Methode vorgestellt, um sowohl photorefraktive Gitter als auch ultrakurze Gitter für Wellenlängen bis in den mittleren infraroten Spektralbereich zu schreiben. Grundlegend werden hierzu zwei infrarote Pulse zusätzlich mit einem sichtbaren Lichtpuls überlagert, sodass ein freies Elektron nicht nur durch lineare Absorption und degenerierte Zwei-Photonen-Absorption zweier Photonen im Sichtbaren (Pump-Photonen), sondern auch durch nicht degenerierte Zwei-Photonen-Absorption eines sichtbaren und eines infraroten Photons erzeugt werden kann.

4.2.1 Intensitäts-, Energiedichte- und Ladungsträgermodulation bei Überlagerung dreier Lichtpulse

Im Folgenden wird die Intensitäts-, Energiedichte- und Ladungsträgermodulation für die Überlagerung von drei Lichtpulsen theoretisch untersucht. Es wird verifiziert, dass auch bei Anregung durch nicht degenerierte Zwei-Photonen-Absorption eine Modulation der Intensität, Energiedichte und Ladungsträgerdichte mit dem Gitterabstand $\Gamma_{\mathrm{IR}} = 2\pi/\left|\mathbf{k}_{\mathrm{R}} - \mathbf{k}_{\mathrm{S}}\right|$ ($\mathbf{k}_{\mathrm{R,S}}$: Wellenvektoren) der beiden Schreibstrahlen, Referenz- (R) und Signalstrahl (S), entsteht, deren Periodizität nicht vom Pumpstrahl (P) abhängt.

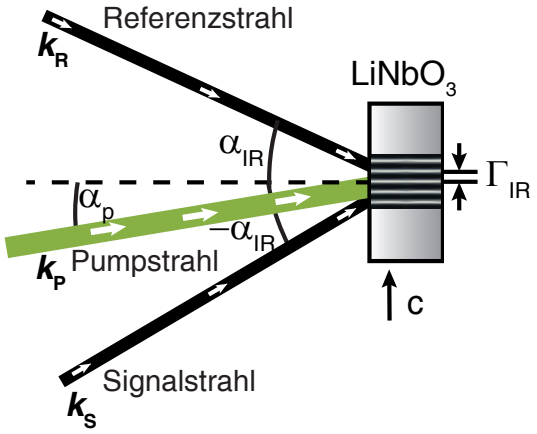

Abbildung 4.1: Nicht degeneriertes Anregungsschema: Zwei infrarote Pulse erzeugen mit einem sichtbaren Puls überlagert eine Intensitätsmodulation im LN-Kristall, die zu einem Gitter mit einer Periode $\Gamma_{\mathrm{IR}} = 2\pi/\left|\mathbf{k}_{\mathrm{R}} - \mathbf{k}_{\mathrm{S}}\right|$ führt.

Diese Betrachtung ist eine Erweiterung der Studie von Odoulov et al. [68], in der erstmals die Interferenz zweier Femtosekundenpulse verschiedener Frequenzen postuliert und beobachtet werden konnte. Abbildung 4.1 zeigt den auf der nicht degenerierten

Zwei-Photonen-Absorption basierenden schematischen Aufbau. Die infraroten Strahlen, treffen unter einem Winkel von α_{IR} bzw. $-\alpha_{\mathrm{IR}}$ auf die Probe. Zusätzlich wird ein Pumpstrahl , welcher in Bezug auf die infraroten Strahlen mit Δt verzögert werden kann, unter dem Braggwinkel α_{P} zum Gittervektor des IR-Gitters räumlich mit den infraroten Strahlen überlagert. Das elektrische Feld der zueinander kohärenten, ebenen Wellen R, S und P, ist gegeben durch:

$$\mathbf{E}_{\mathrm{R,S}}(\mathbf{r},t) = a_{\mathrm{R,S}}\mathbf{e}_{R,S} \cdot \mathrm{f_{R,S}(t)} \exp(-\mathrm{i}\omega_{\mathrm{R,S}}\mathrm{t}) \exp(-\mathrm{i}\mathbf{k}_{\mathrm{R,S}}\mathbf{r}) \tag{4.1}$$

$$\mathbf{E}_{\mathrm{P}}(\mathbf{r},t,\Delta t) = a_{\mathrm{P}}\mathbf{e}_{\mathrm{P}} \cdot \mathrm{f_P(t,\Delta t)} \exp(-\mathrm{i}\omega_{\mathrm{P}}(\mathrm{t}-\Delta\mathrm{t})) \exp(-\mathrm{i}\mathbf{k}_{\mathrm{P}}\mathbf{r}), \tag{4.2}$$

wobei $a_{\mathrm{R,S,P}}$ die Amplitude, $\mathbf{e}_{\mathrm{R,S,P}}$ die Polarisation und f den zeitlichen Verlauf der Einhüllenden angeben. Die Intensitätsmodulation der drei Wellen ist über $I(\mathbf{r},t) = |\mathbf{E}_{\mathrm{R}} + \mathbf{E}_{\mathrm{S}} + \mathbf{E}_{\mathrm{P}}|^2$ mit dem Frequenzunterschied $\Omega_{\mathrm{ij}} = \omega_{\mathrm{i}} - \omega_{\mathrm{j}}$ und dem Gittervektor $\mathbf{K}_{\mathrm{ij}} = \mathbf{k}_{\mathrm{i}} - \mathbf{k}_{\mathrm{j}}$ bestimmt:

$$\begin{aligned} I(\mathbf{r},t,\Delta t) &= a_{\mathrm{S}}^2\mathrm{f_S(t)}^2 + \mathrm{a_R^2 f_R(t)}^2 + \mathrm{a_P^2 f_P(t,\tau)}^2 \\ &+ 2a_{\mathrm{S}}a_{\mathrm{R}}\mathbf{e}_{\mathrm{S}}\mathbf{e}_{\mathrm{R}}\mathrm{f_{RS}(t)}^2 \cos(\Omega_{\mathrm{RS}}\mathrm{t} + \mathbf{K}_{\mathrm{RS}}\mathbf{r}) \\ &+ 2a_{\mathrm{S}}a_{\mathrm{P}}\mathbf{e}_{\mathrm{S}}\mathbf{e}_{\mathrm{P}}\mathrm{f_{RS}(t)f_P(t,\Delta t)} \cos(\Omega_{\mathrm{SP}}\mathrm{t} + \mathbf{K}_{\mathrm{SP}}\mathbf{r} - \omega_{\mathrm{P}}\Delta\mathrm{t}) \\ &+ 2a_{\mathrm{R}}a_{\mathrm{P}}\mathbf{e}_{\mathrm{R}}\mathbf{e}_{\mathrm{P}}\mathrm{f_{RS}(t)f_P(t,\Delta t)} \cos(\Omega_{\mathrm{RP}}\mathrm{t} + \mathbf{K}_{\mathrm{RP}}\mathbf{r} - \omega_{\mathrm{P}}\Delta\mathrm{t}). \end{aligned} \tag{4.3}$$

Die Intensität in Gl. (4.3) wird über die ersten drei konstanten Terme und die letzten drei Terme, welche eine Modulation hervorrufen, beschrieben. Die Modulation der beiden infraroten Strahlen tritt nur für parallele Polarisation von R und S auf und führt mit $\lambda_{\mathrm{R}} = \lambda_{\mathrm{S}}$ zu einem von der Zeit unabhängigen stationärem Gitter mit dem Gittervektor $\mathbf{K}_{\mathrm{RS}}$. Die Überlagerung eines Pumpstrahls mit einem infraroten Strahl ergibt ein dynamisches Gitter mit der Geschwindigkeit $v_{\mathrm{SP,RP}} = \Omega_{\mathrm{SP,RP}}/\left|\mathbf{K}_{\mathrm{SP,RP}}\right|$. Der große Frequenzunterschied bedingt, dass sich das Gitter mit nahezu Lichtgeschwindigkeit ($v_{\mathrm{SP,RP}} > 0{,}995c_{\mathrm{n}}$) durch den Kristall bewegt. Der innerhalb einer Pulsdauer zurückgelegte Weg ist wesentlich größer als die Periodenlänge des Gitters, welches zum Verschwimmen des Gitters führt [68]. Quantitativ kann der Kontrast des Gitters über die Integration der Intensität über die Zeit für eine bestimmte Pulsform ermittelt werden [68]. Die Energiedichteverteilung für einen Gaußpuls ist für die Verzögerungszeit $\Delta t = 0\,\mathrm{fs}$ gegeben durch:

$$\begin{aligned} \mathcal{E}(\mathbf{r},0\,\mathrm{fs}) &= \frac{1}{2}\tau\sqrt{\frac{\pi}{\log(2)}}(a_{\mathrm{S}}^2 + a_{\mathrm{R}}^2 + a_{\mathrm{P}}^2 \\ &+ 2a_{\mathrm{R}}a_{\mathrm{S}}\mathbf{e}_{\mathrm{R}}\mathbf{e}_{\mathrm{S}} \exp(-\frac{\tau^2\Omega_{\mathrm{RS}}^2}{16\log 2}) \cos(\mathbf{K}_{\mathrm{RS}}\mathbf{r}) \\ &+ 2a_{\mathrm{R}}a_{\mathrm{P}}\mathbf{e}_{\mathrm{R}}\mathbf{e}_{\mathrm{P}} \exp(-\frac{\tau^2\Omega_{\mathrm{RP}}^2}{16\log 2}) \cos(\mathbf{K}_{\mathrm{RP}}\mathbf{r}) \\ &+ 2a_{\mathrm{S}}a_{\mathrm{P}}\mathbf{e}_{\mathrm{S}}\mathbf{e}_{\mathrm{P}} \exp(-\frac{\tau^2\Omega_{\mathrm{SP}}^2}{16\log 2}) \cos(\mathbf{K}_{\mathrm{SP}}\mathbf{r})). \end{aligned} \tag{4.4}$$

Die mittlere Modulationstiefe der Energiedichteverteilung ist für die Wechselwirkung eines infraroten Pulses mit einem sichtbaren Puls auf Grund des sehr großen Frequenzunterschiedes $\Omega_{\mathrm{RP,RP}}$ bei einer Pulslänge $\tau = 100\,\mathrm{fs}$ vernachlässigbar klein. Die Modulation des infraroten Gitters hingegen kann über das Verhältnis der Amplituden zu $\overline{m}_{\mathrm{RS}} = 2\mathrm{a_R a_S}\mathbf{e}_{\mathrm{R}}\mathbf{e}_{\mathrm{S}}/(\mathrm{a_R^2} + \mathrm{a_S^2})$ beschrieben werden und wird maximal, wenn die Wellen sowohl die gleiche Amplitude als auch parallele Polarisation aufweisen. Für die Überlagerung von drei Pulsen prägt sich daher unter der gegebenen Anordnung nur eine Modulation der Energiedichte mit der Gitterperiode des IR-Gitters aus. Da für die Betrachtung der Beugungseffizienz beim instantanen und PR-Gitter die Zahl der Ladungsträger von entscheidender Bedeutung ist, erfolgt im Folgenden eine Berechnung der Ladungsträgerdichte N. Nach Badorreck et al. [38] ist diese über die Ratengleichung:

$$\frac{\partial N(\mathbf{r},t,\Delta t)}{\partial t} = \frac{\alpha I_{\mathrm{P}}}{h\omega_{\mathrm{P}}} + \frac{\beta I_{\mathrm{P}}^2}{2h\omega_{\mathrm{P}}} + \frac{\beta_{\mathrm{ND}} I_{\mathrm{P}} I_{\mathrm{R,S}}}{h(\omega_{\mathrm{P}} + \omega_{\mathrm{R,S}})} + \frac{\gamma I_{\mathrm{R,S}}^3}{3h\omega_{\mathrm{R,S}}} \tag{4.5}$$

definiert, wobei im Gegensatz zu Badorreck die nicht degenerierte Zwei-Photonen-Absorption und die Absorption von drei IR-Photonen mit berücksichtigt werden. Die Parameter α, β_{ND}, γ beschreiben die Koeffizienten der Ein- (ein Pump-Photon), Zwei- (ein Pump-Photon, ein IR-Photon) und Drei-Photonen-Absorption (drei IR-Photonen) aus dem photorefraktiven Zentrum und β den Zwei-Photonen-Absorptionskoeffizienten bei Anregung aus dem Valenzband (zwei Pump-Photonen), wobei die Intensität und die Kreisfrequenz des Pumpstrahls bzw. der infraroten Strahlen über $I_{\mathrm{P;R,S}}$ und $\omega_{\mathrm{P;R,S}}$ definiert sind. Die Ladungsträgermodulation ist über die Differenz der Ladungsträgerdichte beim Interferenzmaximum- bzw. Minimum ($r_{\max} = 0$, $r_{\min} = \Gamma_{\mathrm{IR}}/2$) gegeben. Abbildung 4.2 stellt die theoretische Ladungsträgermodulation bei Variation der (a) IR-Intensität (b) Pump-Intensität für $\lambda_{\mathrm{P}} = 510\,\mathrm{nm}$ und $\lambda_{\mathrm{S,R}} = 1600\,\mathrm{nm}$ dar. Die Parameter: $\alpha = 472\,\mathrm{m}^{-1}$, $\beta = 1{,}05 \cdot 10^{-11}\,\mathrm{m/W}$, $\gamma = 2{,}25 \cdot 10^{-28}\,\mathrm{m/W}$, $\tau = 100\,\mathrm{fs}$ wurden für die in dieser Studie verwendete Probe gemessen (siehe Anhang A); für den nicht degenerativen Zwei-Photonen-Absorptions-Koeffizienten wurde $\beta_{\mathrm{ND}} = \beta$ angenommen[1].

Die Variation der gesamten IR-Intensität (Abb. 4.2(a)) bei fester Pump-Intensität $I_{\mathrm{P}} = 10^{14}\,\mathrm{Wm}^{-2}$ führt bei niedrigen Intensitäten zu einem linearen- und bei hohen Intensitäten zu einem kubischen Zusammenhang. Es gilt festzuhalten, dass für ein verschwindendes γ, wie es bei $\lambda_{\mathrm{S,R}} = 2400\,\mathrm{nm}$ der Fall ist ($\gamma_{2400} = (0{,}30 \pm 0{,}30) \cdot 10^{-28}\,\mathrm{m/W}$ (siehe Anhang A)), auch bei hohen Intensitäten nur ein linearer Zusammenhang zu erkennen ist (nicht abgebildet). Eine Variation der Pump-Intensität (Abb. 4.2(b)) führt bei fester IR-Intensität $I_{\mathrm{IR}} = 10^{15}\,\mathrm{W/m^2}$ bei niedrigen Intensitäten zu keiner Änderung der Differenz der Ladungsträger, bei hohen Intensitäten zu einem linearen Zusammenhang. Die Ergebnisse aus Abb. 4.2 werden in Kapitel 4.2.4 verwendet, um näheren Aufschluss über die Anregungsmechanismen bei photorefraktiven und ultrakurzen Gittern zu erhalten.

[1] Beyer et al. zeigten für $\lambda_{\mathrm{Pump}} = 388\,\mathrm{nm}$ und $\lambda_{\mathrm{R,S}} = 776\,\mathrm{nm}$, dass sich β_{ND} in der gleichen Größenordnung wie β befindet [69].

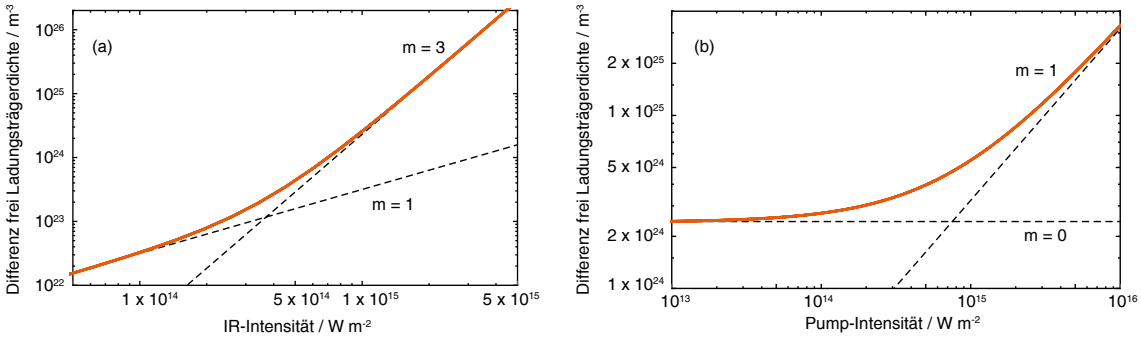

Abbildung 4.2: Doppelt-logarithmische Darstellung der Differenz der angeregten Ladungsträger zwischen Maximum und Minimum für Variation der (a) IR-Intensität (b) Pump-Intensität mit: $\alpha = 472\,\mathrm{m}^{-1}$, $\beta = 1{,}05 \cdot 10^{-11}\,\mathrm{m/W}$, $\beta_{\mathrm{ND}} = 1{,}05 \cdot 10^{-11}\,\mathrm{m/W}$, $\gamma = 2{,}25 \cdot 10^{-28}\,\mathrm{m/W}$, $\tau = 100\,\mathrm{fs}$.

4.2.2 Experimentelle Methoden und Beobachtungen

Für die Messungen wird ein eisendotierter Lithiumniobat Kristall, $LiNbO_3$:Fe (0,1 % wt.), mit einer Dicke $d = 1\,\mathrm{mm}$ verwendet. Zwei IR-Strahlen mit $\lambda_{\mathrm{R,S}} = \lambda_{\mathrm{IR}} = 1600\,\mathrm{nm}$ bzw. $\lambda_{\mathrm{IR}} = 2400\,\mathrm{nm}$ werden in einem Intensitätsverhältnis von 1:1,5 unter einem äußeren Winkel $2\alpha_{\mathrm{IR}} \approx 19°$ überlagert (vgl. Abb. 4.1). Diese Strahlen werden von einem der zwei optisch parametrischen Verstärkern (Coherent Inc., OPerA solo) mit einer Reptitionsrate $f = 1\,\mathrm{kHz}$ und einer Pulslänge $\tau \approx 100\,\mathrm{fs}$ mit einer Polarisation senkrecht zur optischen Achse des Kristalls erzeugt. Zusätzlich können beide IR-Strahlen mit einem sichtbaren Puls ($\lambda_{\mathrm{P}} = 470\,\mathrm{nm}$ - $750\,\mathrm{nm}$) unter dem Braggwinkel zum IR-Gitter $\alpha_{\mathrm{P}} \approx 2.1°$ überlagert werden, welcher vom zweiten OPA generiert wird, dessen Querschnittsflächen im Überlagerungsbereich im Verhältnis 1:1,5-2 (IR zu Pump) stehen. Die Weg- bzw. Zeitdifferenz Δt des sichtbaren Strahls und der infraroten Strahlen kann über eine motorisierte Verzögerungstrecke (MFA-CC, Newport Corporation) auf $\Delta t = (-1{,}5 - 1{,}5)\,\mathrm{ps}$ mit einer Genauigkeit von 10 fs eingestellt werden. Die Intensität der Strahlen wird über ein Filterrad variiert, ohne den zeitlichen Versatz zu verändern. Zum Auslesen des photorefraktiven Gitters wird ein HeNe-Laser ($\lambda_{\mathrm{HeNe}} = 632{,}8\,\mathrm{nm}$) verwendet, welcher unter dem Braggwinkel $\alpha_{\mathrm{HeNe}} \approx 2{,}5°$ zum IR-Gitter auf den Kristall trifft und mittels optischen Siliziumsensors (Coherent Inc., LM2-VIS oder Thorlabs Inc., DET10A/M) detektiert wird. Sowohl der HeNe-Strahl als auch der sichtbare Puls sind, falls nicht anders beschrieben senkrecht zur optischen Achse des Kristalls polarisiert. Dadurch wird die r_{13}-Komponente des elektrooptischen Tensors angesprochen, womit Verzerrungen in der Wellenfront wegen des optischen Schadens im Vergleich zur r_{33}-Komponente reduziert werden [56].

In Abb. 4.3 ist ein typisches Beugungsmuster nach 5 minütiger Beleuchtung mit dem sichtbaren Puls ($\lambda_{\mathrm{P}} = 510\,\mathrm{nm}$), den infraroten Pulsen ($\lambda_{\mathrm{P}} = 2400\,\mathrm{nm}$) und dem HeNe-Laser für $\Delta t = 0$ dargestellt.
Aus der Entstehung und dem Zerfall des Beugungsmusters lassen sich folgende allgemeine experimentelle Beobachtungen festhalten:

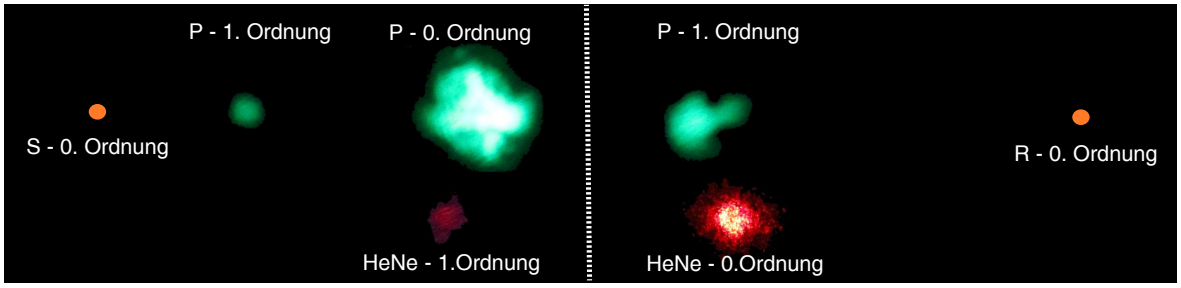

Abbildung 4.3: Beugungsmuster nach einer Bestrahlungsdauer von 5 Minuten bei Überlagerung zweier IR-Strahlen ($\lambda_{\mathrm{IR}} = 2400\,\mathrm{nm}$) mit einem Pumpstrahl ($\lambda_{\mathrm{P}} = 510\,\mathrm{nm}$). Eine Beugung am Gitter mit dem Gittervektor $\mathbf{K}_{\mathrm{RS}}$ tritt sowohl für den Pumpstrahl als auch für den HeNe-Strahl auf. Zur Übersichtlichkeit wurden beide IR-Strahlen in orange mit eingezeichnet und zur besseren Ansicht ein Höhenversatz zwischen Pump- und HeNe-Strahl hinzugefügt. Die gestrichelte weiße Linie entspricht der Flächennormalen des Kristalls.

- Bei der gleichzeitigen Beleuchtung mit allen Strahlen tritt (i) nahezu instantan eine Beugung des Pump-Pulses und (ii) ein langsamer Anstieg der Beugungsintensität des HeNe-Strahls auf.
- Nach Beleuchtung bleibt die Beugungintensität des HeNe-Strahls auch bei Abwesenheit aller anderen Strahlen nahezu konstant. Das geschriebene Gitter lässt sich durch Bestrahlung mit diffusem Weißlicht über ca. eine Stunde oder homogener Beleuchtung mit dem Pump-Puls löschen.
- Unter den Winkeln $\alpha_{\mathrm{P,Beugung}} = 4{,}1° \pm 0{,}2°$ und $\alpha_{\mathrm{HeNe,Beugung}} = 4{,}9° \pm 0{,}2°$ tritt Beugung auf, welche im Rahmen des Fehlers mit den über die Bragg-Bedingung berechneten Werten $\alpha_{\mathrm{P,Bragg}} = 4{,}14°$ und $\alpha_{\mathrm{HeNe,Bragg}} = 5{,}03°$ bei einer Beugung an einem IR-Gitter mit dem Gitterabstand Γ_{IR} übereinstimmen.
- Es bildet sich keine Beugung bei Abwesenheit von mindestens einem IR-Strahl aus.

4.2.3 Experimentelle Daten

Im Folgenden werden die aus dem Beugungsmuster resultierenden Beobachtungen für Dauerstrichbeleuchtung und gepulste Beleuchtung verifiziert und die für die Beugung ursächlichen Prozesse experimentell untersucht. In der Publikation [49] konnte der langsame Anstieg bei $\lambda_{\mathrm{IR}} = 1600\,\mathrm{nm}$ unter Auslesen mit Dauerstrichbeleuchtung dem PR-Effekt zugeordnet werden. Hierbei fehlte jedoch eine systematische Betrachtung des Aufbaus und des Zerfalls des photorefraktiven Gitters, eine Abhängigkeit der Beugungsintensität von der IR-Intensität und ein Durchstimmen der Pumpwellenlänge, um ein genaueres Bild der zu Grunde liegenden Anregungseffekte zu bekommen. Die ultrakurze Beugung (vgl. ultrakurze Hologramme 4.2) wurde nicht untersucht, ist jedoch für diese Arbeit von besonderer Relevanz, da diese entweder auf instantanen Nichtlinearitäten wie dem Kerr-Effekt oder der Zwei-Photonen-Absorption [38] beruht,

oder durch verzögerte Nichtlinearitäten wie durch die periodische *Injektion* kleiner Polaron durch Femtosekundenpulse gegeben ist.

Beugung Dauerstrich-Laser:
Abbildung 4.4(a) beschreibt den zeitlichen Anstieg der auf das Maximum normierten Intensität der ersten Beugungsordnung des HeNe-Strahls ($I_P = 0{,}26\,PW/m^2$, $I_{IR} = 1{,}73\,PW/m^2$) bei gleichzeitiger Beleuchtung aller Strahlen bei $t = 0\,s$.

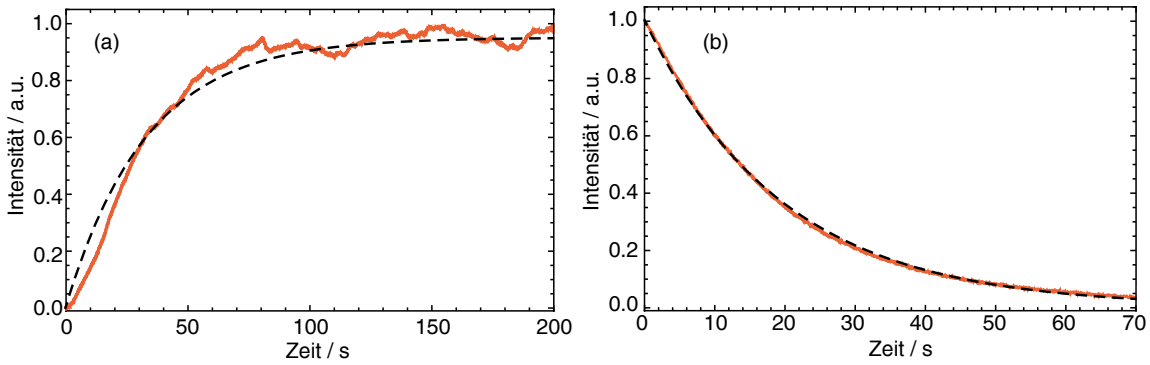

Abbildung 4.4: Beugungsintensität der ersten Beugungsordnung des HeNe-Strahls ($I_P = 0{,}26\,PW/m^2$, $I_{IR} = 1{,}73\,PW/m^2$) (a) Aufbau (b) Zerfall nach einer Beleuchtungszeit von 300 s. Die Anpassung der Graphen (schwarze gestrichelte Linie) erfolgt über Gl. (4.6) bzw. Gl. (4.7). Vielen Dank an Dr. Alexandr Shumelyuk für die Erstellung dieser Messung.

Die Beugungsintensität steigt mit zunehmender Zeit an und geht in Sättigung. Nach Ausschalten der Pump- und IR-Strahlen ist das Hologramm über mehrere Stunden stabil, kann jedoch durch homogene Beleuchtung mit dem Pump-Puls innerhalb einiger zehn Sekunden ausgelöscht werden (Abb. 4.4(b)). Die Gleichungen:

$$I_{\text{Aufbau}}(t) = I_0(1 - \exp(\frac{-t}{\tau_{\text{Aufbau}}})) \tag{4.6}$$

$$I_{\text{Zerfall}}(t) = I_0 \exp(\frac{-t}{\tau_{\text{Zerfall}}}) \tag{4.7}$$

mit der normierten Maximalintensität I_0, der Aufbaukonstante τ_{Aufbau} und der Zerfallskonstante τ_{Zerfall} beschreiben die Abhängigkeit der Beugungsintensität von der Zeit (vgl. [70]). Die Daten in Abb. 4.4 lassen sich durch $\tau_{\text{Aufbau}} = (33 \pm 7)\,s$, $\tau_{\text{Zerfall}} = (20 \pm 1)\,s$ und $I_0 = 1$ anpassen.

In Abb. 4.5 ist die Beugungseffizienz als Funktion der IR-Intensität bei $\lambda_{IR} = 1600\,nm$ für vier verschiedene Beleuchtungszeiten ohne Beleuchtung mit dem Pumpstrahl dargestellt. Die Beugungseffizienz wurde über den Zusammenhang $\eta = I_{1.\text{Ordnung}} / (I_{0.\text{Ordnung}} + I_{1.\text{Ordnung}})$ bestimmt, um Extinktionseffekte durch Multi-Photonen-Absorption herauszurechnen [70]. Bei Intensitäten $I_{IR} > 0{,}5\,PW/m^2$ kann sich alleine durch die IR-Strahlen ein Gitter ausbilden, dessen Ausprägung mit wachsender Beleuchtungszeit zunimmt.

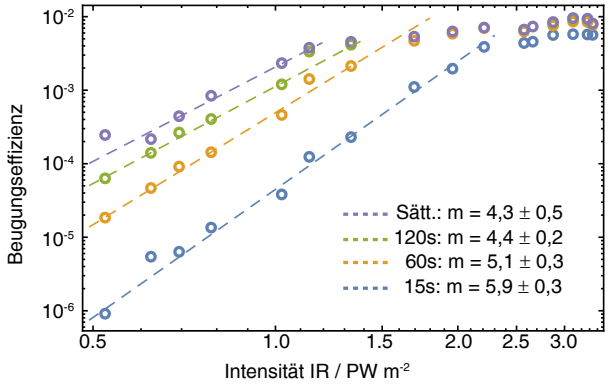

Abbildung 4.5: Beugungseffizienz als Funktion der IR-Intensität bei $\lambda_{IR} = 1600\,nm$ für vier verschiedene Beleuchtungszeiten. Die Achsen sind doppelt-logarithmisch skaliert. Vielen Dank an Björn Bourdon für die Erstellung dieser Messung.

Bei sehr hohen IR-Intensitäten (nach 15 s: $I > 2\,PW/m^2$, nach 120 s: $I > 1\,PW/m^2$) kommt es auch bei Erhöhung der IR-Intensität zu keinem weiteren Anstieg der Beugungseffizienz, welche einen konstanten Wert $\eta = 0{,}5\,\% - 1{,}0\,\%$ annimmt. Für kurze Beleuchtungszeiten ist die Beugungseffizienz proportional zu I_{IR}^6 und nähert sich gegen Sättigungsbeleuchtung dem Zusammenhang $\propto I_{IR}^4$ an. Bei $\lambda_{IR} = 2400\,nm$ konnte in diesem Intensitätsfenster keine Beugung alleine durch IR-Beleuchtung festgestellt werden.

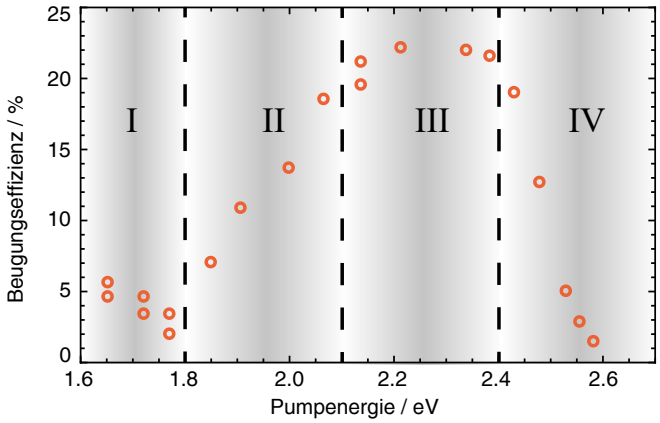

Abbildung 4.6: Beugungseffizienz als Funktion der spektralen Pumpenergie für $\lambda_{IR} = 1600\,nm$, $I_P = 0{,}14\,PW/m^2$ und $I_{IR} = 1{,}73\,PW/m^2$. Vielen Dank an Dr. Alexandr Shumelyuk für die Erstellung dieser Messung.

Die Beugungseffizienz in Abhängigkeit der spektralen Pumpenergie für $\lambda_{IR} = 1600\,nm$ (E_{IR}=0,77 eV) ist in Abb. 4.6 für vier Energiebereiche dargestellt. Im Gegensatz zu den übrigen Messungen wurde hierbei der elektrooptische r_{33}-Tensor verwendet, welcher im Vergleich zum r_{13}-Tensor zu einer $\approx$ 10-fach höheren Beugungseffizienz führt [56]. Für Pumpenergien $E_P < 1{,}8\,eV$ (Bereich I) tritt die Summenfrequenz zwischen Pump- und IR-Pulsen auf, welche das gebeugte Signal auf der Diode überdeckt. Ab einer

Pumpenergie $E_P > 1{,}8\,eV$ (Bereich II) steigt die Beugungseffizienz an und erreicht den maximalen Wert $\eta \approx 20\,\%$ bei $2{,}1\,eV < E_P < 2{,}4\,eV$ (Bereich III). Für $E_P > 2{,}4\,eV$ fällt die Beugungseffizienz und geht bei $E_P = 2{,}6\,eV$ gegen null (Bereich IV).

Beugung gepulster Laser:
Abbildung 4.7(a) beschreibt den Aufbau der normierten Beugungsintensität der ersten Ordnung des Pump-Pulses bei $\lambda = 510\,nm$, wobei zum Zeitpunkt $t = 0$ beide IR-Strahlen ($I_{IR} = 1{,}34\,PW/m^2$) zusätzlich zum Pump-Puls ($I_P = 0{,}24\,PW/m^2$) eingeschaltet werden.

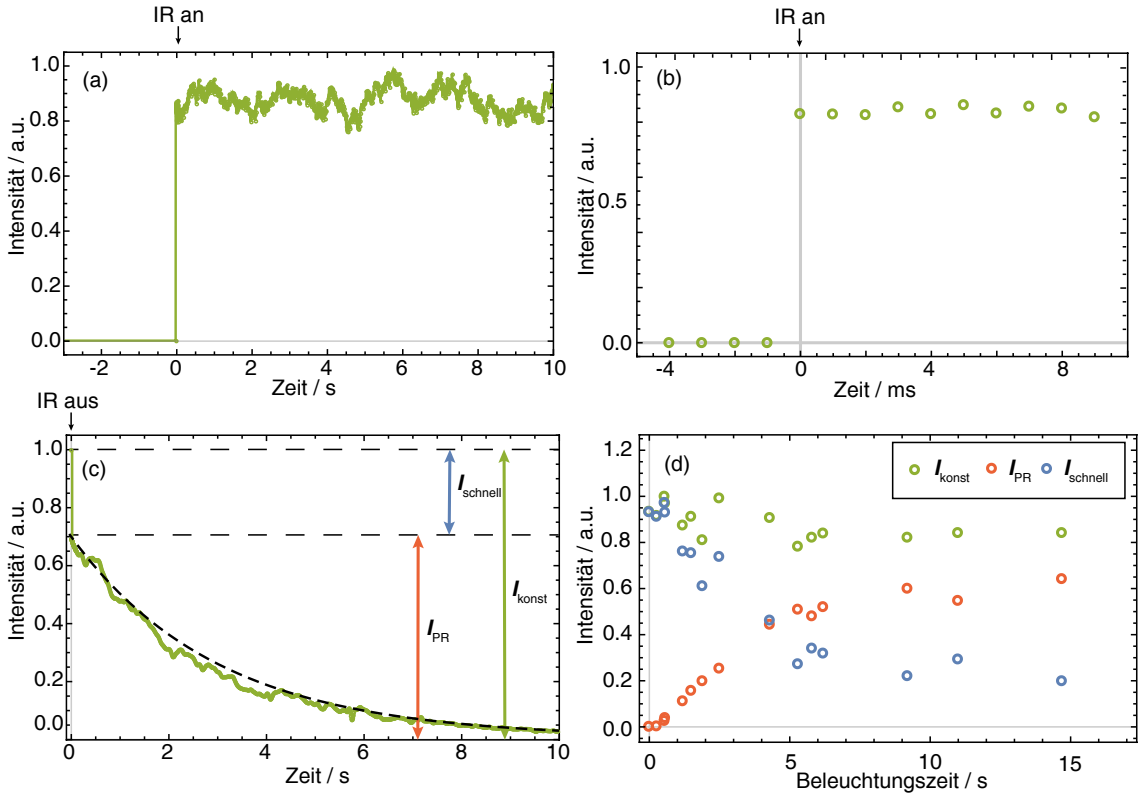

Abbildung 4.7: Beugungsintensität des Pump-Pulses mit $\lambda_P = 510\,nm$, $\lambda_{IR} = 1600\,nm$, $I_P = 0{,}24\,PW/m^2$ und $I_{IR} = 1{,}34\,PW/m^2$ nach Ein-(a,b) und Ausschalten (c) als Funktion der Zeit und für die einzelnen Komponenten ($I_{schnell}(t)$, $I_{PR}(t)$, $I_{konst}(t)$) als Funktion der Belichtungszeit (d). Vielen Dank an Dr. Alexandr Shumelyuk für die Erstellung dieser Messung.

Die Beugungsintensität steigt bei $t = 0\,s$ sprunghaft an und bleibt bei weiterer Beleuchtung auf einem konstanten Niveau. Eine vergrößerte Abbildung des Zeitbereichs um $t = 0$ ist in Abb. 4.7(b) dargestellt. Der Aufbau der Beugung ist kürzer als die Repititionsrate des Lasersystems ($t_{Aufbau} < 1\,ms$), da bereits nach dem ersten IR-Puls die Beugungsintensität auf einen konstanten Wert angestiegen ist. Der Zerfall der Beugungsintensität ist in Abb. 4.7(c) gezeigt und besteht aus einer schnellen $I_{schnell}$ ($\tau_{schnell} < 1\,ms$) und einer langsamen I_{PR} ($\tau_{PR} \gg 1\,s$) Komponente. Die Gesamtbeugungsintensität setzt sich folgend aus $I_{konst} = I_{PR}(t) + I_{schnell}(t)$ zusammen. Die Beugungsintensität der langsamen Komponente ist, wie bei dem Zerfall der Beugung des HeNe-Lichts, durch

Gl. (4.7) anpassbar ($\tau_{\text{Zerfall}} = (3{,}0 \pm 0{,}5)\,\text{s}$, $I_0 = 0{,}7$). Die zeitliche Dynamik und der physikalische Ursprung der schnellen Komponente wird in Kapitel 4.2.4 näher diskutiert. Abbildung 4.7(d) illustriert die Beugungsintensität als Funktion der Beleuchtungszeit der IR-Strahlen, wobei die Intensität auf das Maximum bei einer Beleuchtungszeit normiert wurde. Bei längeren Beleuchtungszeiten prägt sich die langsame Komponente stärker aus, wohingegen die schnelle Komponente abnimmt. Nach einigen Sekunden stellt sich ein konstantes Verhältnis der Komponenten ein.

In Abb. 4.8 ist die Beugungseffizienz des schnellen Gitters bei $\lambda_P = 510\,\text{nm}$ und $\lambda_P = 2400\,\text{nm}$ als Funktion (a) der IR-Intensität ($I_P = 0.35\,\text{PW/m}^2$) und (b) der Pump-Intensität ($I_{IR} = 3{,}91\,\text{PW/m}^2$) dargestellt. Die Intensitätswerte sind nach der Probe bestimmt worden, um Verluste durch Ein- und Zwei-Photonen-Absorption ($\alpha_{510\,\text{nm}}^{\text{gemessen}} = 330\,\text{m}^{-1}$, $\beta_{510\,\text{nm}}^{\text{gemessen}} = 1{,}05 \cdot 10^{-11}\,\text{m/W}$) in der Probe vernachlässigen zu können. Die Daten wurden über die ersten 250 Pulse gemittelt. Bei sehr kurzen Beleuchtungszeiten ist das photorefraktive Gitter nur sehr schwach ausgeprägt (vgl. Abb. 4.7(d)), sodass ausschließlich die Abhängigkeit des schnellen Gitters gemessen wird. Die Beugungseffizienz des schnellen Gitters nimmt für steigende IR-Intensitäten zu und für steigende Pump-Intensitäten ab und beschreibt die Zusammenhänge $\eta \propto I_{IR}^2$ (Abb. 4.8(a)) und $\eta \propto I_{IR}^{-1}$ für $I_P < 0{,}3\,\text{PW/m}^2$ bzw. $\eta \propto I_{IR}^{-6}$ für $I_P > 0{,}3\,\text{PW/m}^2$ (Abb. 4.8(b)).

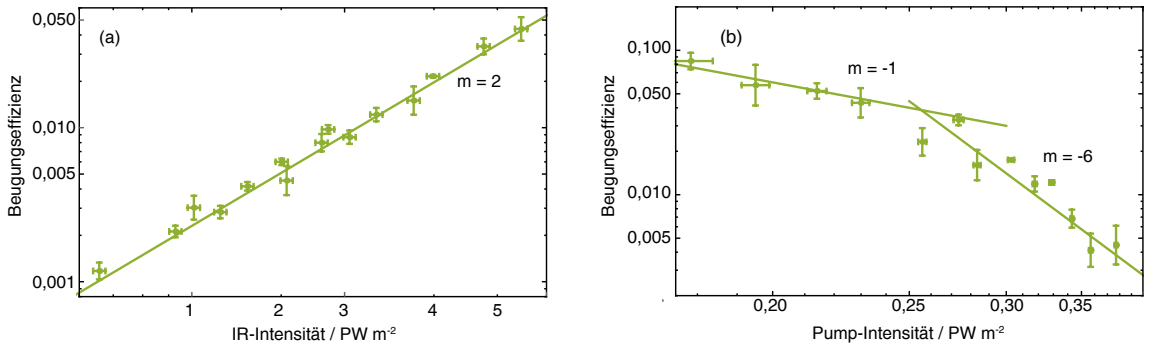

Abbildung 4.8: Die Begungseffizienz des schnellen Gitters als Funktion der (a) IR-Intensität ($I_P = 0.35\,\text{PW/m}^2$) wird durch den Zusammenhang $\eta \propto I_{IR}^2$ beschrieben und (b) Pump-Intensität ($I_{IR} = 3.91\,\text{PW/m}^2$) kann durch die Zusammenhänge $\eta \propto I_{\text{Pump}}^{-1}$ für $I_P < 0{,}3\,\text{PW/m}^2$ bzw. $\eta \propto I_{\text{Pump}}^{-6}$ für $I_P > 0{,}3\,\text{PW/m}^2$ beschrieben werden. Die Skalierung der Achsen ist doppelt-logarithmisch gewählt.

4.2.4 Auswertung - Diskussion

Auswertung und Diskussion der Beugung des Dauerstrich-Lasers:
Aus den oben aufgeführten Messdaten lassen sich für die Beugung des Dauerstrich-Strahls folgende neue Schlüsse ziehen:

(i) Die Zerfalls- und Aufbaucharakteristik entspricht der Charakteristik des PR-Effekts bei Dauerstrich-Ein-Photonen-Anregung [56, 70] (vgl. Abb. 4.4).

(ii) Auch bei $\lambda = 2400\,\text{nm}$ ist es möglich, ein PR-Gitter zu schreiben (vgl. Abb. 4.3).

(iii) Bei $\lambda = 1600\,\text{nm}$ kann sich ein Gitter ausschließlich durch IR-Beleuchtung ausprägen, dessen Anregungsmechanismus auf Drei-Photonen-Absorption beruht.

(iv) Bei $\lambda = 2400\,\text{nm}$ prägt sich bei ausschließlicher IR-Beleuchtung kein Gitter aus.
(v) Die Daten der Beugungsintensität als Funktion der Pumpwellenlänge lassen sich über eine Anregung durch NDTPA erklären.

Zu (iii): Aus den Berechnungen in Abb. 4.2 geht der Zusammenhang der Ladungsträgerdichte $N \propto I_{IR}^3$ hervor. Die Ladungsträgerdichte hängt mit der Änderung des Raumladungsfeldes über die Poissongleichung linear zusammen, wobei ebenfalls das Raumladungsfeld linear über den elektrooptischen Effekt mit der Brechungsindexänderung Δn verknüpft ist. In 1969 folgerte Kogelnik [71] in seiner Theorie zu gekoppelten Wellengleichungen für gemischte Volumenhologramme einen quadratischen Zusammenhang zwischen der Beugungseffizienz und der Änderung der Absorption bzw. des Brechungsindex', welcher auch allgemein für dünne Gitter gilt [72]. Für ein auf der Anregung durch Drei-Photonen-Absorption beruhendes Gitter wird folglich $\eta \propto I_{IR}^6$ erwartet, welches mit der experimentell bestimmten Steigung bei kurzen Belichtungszeiten $m = 5{,}9 \pm 0{,}3$ übereinstimmt (vgl. Abb. 4.5). Die Vermutung, dass die Drei-Photonen-Absorption ursächlich für die Entstehung eines PR-Gitter ist, wurde bei einer Schreibwellenlänge $\lambda = 1500\,\text{nm}$ bereits von Beyer et al. [73] geäußert und kann in dieser Arbeit erstmals für $\lambda = 1600\,\text{nm}$ experimentell bestätigt werden. Die Entstehung eines PR-Gitters durch Drei-Photonen-Absorption widerspricht dabei nicht einem Anregungsmechanismus über nicht degenerierte Zwei-Photonen-Absorption, da zum Einen in dieser Messung nur mit IR-Strahlung beleuchtet wurde und zum Anderen die NDTPA in die Drei-Photonen-Absorption für hohe IR-Intensitäten übergeht (vgl. Abb. 4.2).

Zu (iv): Bei $\lambda = 2400\,\text{nm}$ konnte nur durch IR-Strahlen kein Gitter geschrieben werden, da die Photonenenergie nicht ausreicht, um durch Drei-Photonen-Absorption Elektronen aus Eisenzentren ins Leitungsband anzuregen ($3 \cdot 0{,}51\,\text{eV} \ll 2{,}6\,\text{eV}$) [74], welches sich im Drei-Photonen-Absorptionskoeffizenten $\gamma_{2400} \ll \gamma_{1600}$ widerspiegelt (vgl. Anhang A). Prozesse höherer Ordnung sind daher für die Bildung eines PR-Gitters auszuschließen.

Zu (v): Die vier Bereiche der Beugungseffizienz als Funktion der Photonenenergie des Pumpstrahls (siehe Abb. 4.6) lassen sich über das Anregungsschema in Abb. 4.9 erklären; hierbei wird sowohl die direkte Ein-Photonen-Absorption eines Pump-Photons, die NDTPA, als auch die Drei-Photonen Absorption der Schreibstrahlen berücksichtigt. Die grünen Pfeile entsprechen einer Photonenenergie $E_P = 2{,}43\,\text{eV}$ ($\lambda = 510\,\text{nm}$) und die roten Pfeile $E_{IR} = 0{,}77\,\text{eV}$ ($\lambda = 1600\,\text{nm}$). Die Bandlücke $E_B = 2{,}6\,\text{eV}$ (Halbwertbreite $\Delta E_B \approx 0{,}6\,\text{eV}$) für den Übergang $Fe^{2+} \rightarrow Nb^{5+}$ wurde aus Clark's Studien [74] entnommen. Direkte Übergänge aus dem Valenz- in das Leitungsband werden vernachlässigt, da der Volumen Photovoltaische Effekt bei direkter Anregung verschwindet [61]. Im Bereich I (siehe Abb. 4.6) reicht zwar die Pump-Photonenenergie $E_P < 1{,}8\,\text{eV}$ gerade aus, um Elektronen zusammen mit einem IR-Photon aus einem Teil des Fe^{2+}-Bandes in das untere Ende des Leitungsbandes anzuregen, jedoch dominiert in diesem Bereich die Summenfrequenzbildung zwischen Pump- und IR-Strahl. Die Wechselwirkung tritt auf Grund des Unterschiedes im Phasenanpassungsfehler der beiden IR-Strahlen hauptsächlich nur mit einem IR-Strahl auf, sodass sich das Intensitätsverhältnis der IR-Strahlen ändert. Hierdurch sinkt nach Gl. (4.4) die Modulationstiefe der Energiedichte des IR-Gitters und folglich die Beugungseffizienz.

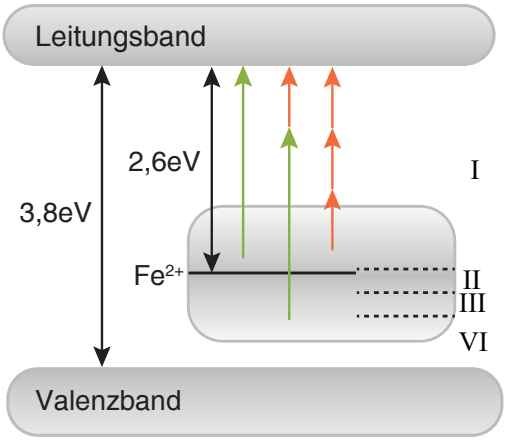

Abbildung 4.9: Anregungsschema in Fe:LN ($E_P = 2{,}43\,\text{eV}$ grün, $E_{IR} = 0{,}77\,\text{eV}$ rot): Über Ein-Photonen-Absorption eines Pump-Photons, NDTPA oder Drei-Photonen Absorption der Schreibstrahlen können Elektronen aus dem Eisenzentrum ins Leitungsband angehoben werden. Die vier Bereiche der Beugungseffizienz (siehe Abb. 4.6): I: $E_{Pump} < 1{,}8\,\text{eV}$, II: $E_{Pump} = (1{,}8 - 2{,}1)\,\text{eV}$, III: $E_{Pump} = (2{,}1 - 2{,}4)\,\text{eV}$, IV: $E_{Pump} > 2{,}4\,\text{eV}$) sind mit I - IV gekennzeichnet.

Die Beugungseffizienz steigt für $E_P > 1{,}8\,\text{eV}$ mit steigender Pump-Photonenenergie an (Bereich II) bis zu einem Plateau (Bereich III), da Elektronenanregungen aus einem größeren Teil bzw. dem gesamten Fe^{2+}-Band erfolgen können, und die Phasenanpassungsbedingung der Summenfrequenzbildung nicht mehr erfüllt werden kann. Für noch größere Pump-Photonenenergien (Bereich IV) dominiert die direkte Anregung über Ein-Photonen-Absorption von Elektronen ins Leitungsband und die Zwei-Photonen-Absorption aus dem Valenzband, da der Zwei-Photonen-Absorptionskoeffizient im UV stark zunimmt [75, 76]. Hierdurch folgt eine räumlich homogene Ladungsträgeranregung, weshalb sich die Modulationstiefe des IR-Gitters reduziert und die Beugungseffizienz sinkt. Diese Messung bestätigt die Vermutung aus der Publikation [49], dass bei gleichzeitiger infraroter und sichtbarer Beleuchtung die nicht degenerierte Zwei-Photonen-Absorption der dominierende Anregungsprozess für den PR-Effekt ist.

Auswertung und Diskussion der Beugung des Femtosekundenpulses:
Im Folgenden soll das Auftreten der Beugung des Pump-Pulses näher betrachtet werden. Aus Abb. 4.7 geht hervor, dass die Beugung des Pump-Pulses durch einen schnellen und einen langsamen Prozess charakterisiert ist. Der langsame Prozess lässt sich wie bei der Beugung des Dauerstrich-Strahls auf den PR-Effekt zurückführen, da sowohl die Bildungs- und Zerfallsdynamiken (vgl. Abb. 4.7 (c,d)) durch die Gleichungen für den Aufbau Gl. (4.6) und Zerfall Gl. (4.7) eines PR-Gitters beschrieben werden können als auch ca. einstündiges Bestrahlen mit einer inkohärenten Weißlichtquelle zu einem Löschen der langsamen Komponente führt. Da im vorherigen Kapitel bereits auf die Charakteristiken des PR-Gitters eingegangen wurde, soll im Weiteren die schnelle Komponente näher betrachtet werden.

Der schnelle Prozess findet innerhalb von $\tau \ll 1\,\text{ms}$ (Abb. 4.7 (a,b)) statt und tritt

nur auf, wenn beide Pulse miteinander überlagern. Die Bildung des schnellen Gitters muss daher, verglichen mit der Ausprägung eines stabilen Gitters durch den PR-Effekt, auf der Zeitskala der Pulsdauer ($\tau_{\mathrm{FWHM}} \approx 100\,\mathrm{fs}$) erfolgen. In [77] ordnen Psaltis, Buse, Sturman et al. den Aufbau eines instantanen Gitters zweier Femtosekundenpulse ($\lambda_{\mathrm{S}} = 388\,\mathrm{nm}$, Fe:LN) der Modulation des Brechungsindex' oder der Absorption über den Kerr-Effekt bzw. der Multi-Photonen-Absorption zu.

Anhand der Abhängigkeit der Beugungseffizienz von der Intensität sollen im Folgenden diese Prozesse unterschieden werden. Der Kerr-Effekt führt wie die NDTPA (vgl. Abb. 4.2) zu einer linearen Abhängigkeit von der IR-Intensität, wobei die Zwei- und Drei-Photonen-Absorption von IR-Photonen zu einem quadratischen bzw. kubischen Zusammenhang führen würde. Im Hinblick auf die Multi-Photonen-Absorption ist bei einer Schreibwellenlänge $\lambda = 2400\,\mathrm{nm}$ die Zwei-Photonen-Absorption und Drei-Photonen-Absorption alleine durch Tastphotonen ebenso zu vernachlässigen (vgl. Drei-Photonenabsorptionskoeffizient Anhang A.3) wie die direkte Anregungen durch zwei Pump-Photonen aus dem Valenzband, da es im Gegensatz zu [77] zu keiner Modulation der Ladungsträgerdichte kommt. Einzig Anregungen über NDTPA aus dem Eisenzentrum führen zu einer Modulation der Ladungsträgerdichte.

Aus Abb. 4.8(a) geht für die Beugungseffizienz des Pump-Pulses η als Funktion der IR-Intensität I_{IR} unter Vernachlässigung der Drei-Photonen-Absorption der experimentelle Zusammenhang $\eta \propto I_{\mathrm{IR}}^2$ hervor. Da ein quadratischer Zusammenhang zwischen der Beugungseffizienz und der Änderung der Absorption bzw. des Brechungsindex' zu erwarten ist [72], ist für die Beugung an dem schnellen Gitter ein Prozess, bei dem α bzw. n linear moduliert werden, ursächlich. Somit sind für die Entstehung des instantanen Gitters sowohl der Kerr-Effekt als auch die NDTPA in Erwägung zu ziehen.

Es gilt festzuhalten, dass für niedrige Pump-Intensitäten die Beugungsintensität unabhängig von der Pump-Intensität ist ($\eta \propto I^{-1}$), welches aus den Berechnungen aus Abb. 4.2 (b) hervorgeht. Bei hohen Pump-Intensitäten kann der erwartete lineare Anstieg (Abb. 4.2 (b)) der Beugungseffizienz jedoch nicht reproduziert werden (Abb. 4.8 (b)). Dieses lässt sich durch die hohe Leitfähigkeit im Material bei hohen Lichtintensitäten begründen, welche die Lebensdauer der Modulation stark reduziert [72], so dass es zu keinem akkumulierenden Effekt bei einer Laser-Repititionsrate von 1 kHz mehr kommen kann.

Die obige Betrachtung geht von einem einstufigen Anregungsmechanismus aus. Im Gegensatz zu dem PR-Effekt, bei dem langlebige Prozesse ($\tau > 1\,\mathrm{s}$) zur Ausprägung des Gitters relevant sind, müssen bei dem schnellen Gitter auch Abläufe auf ultrakurzer Zeitskala innerhalb des Pulses untersucht werden. In Abb. 4.10 ist das Anregungsmodell über einen Zwei-Stufen Prozess dargestellt. Durch Zwei-Photonen-Absorption aus dem Valenzband oder Ein- bzw. Zwei-Photonen-Absorption aus dem Eisenzentrum werden heiße Ladungsträger angeregt, welche entweder mit Löchern in den Grundzustand rekombinieren, Exzitonen bilden oder durch starke Kopplung an das Gitter innerhalb von ca. hundert Femtosekunden Polaronen bilden (vgl. [32, 38, 39]). Die transiente Absorption der Polaronen kann über Ein-Photonen-Absorption des gleichen Pump-Pulses getastet werden, wobei eine Modulation der Zentren nur über die NDTPA erfolgt. Ein Ladungsträgergitter konnte bereits in [62, 77] beobachtet werden, wurde jedoch allgemein den freien Ladungsträgern oder 'shallow traps' zugeordnet.
Um näheren Aufschluss über den konkreten Ladungsträgertyp zu gewinnen (Exzi-

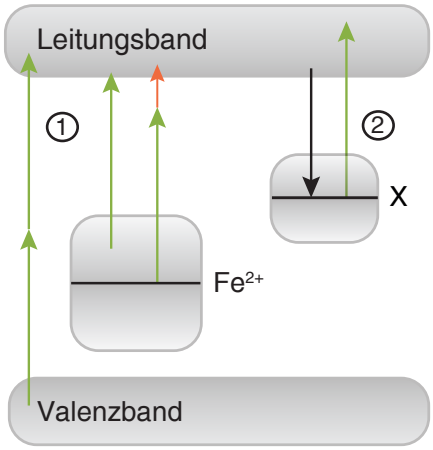

Abbildung 4.10: Zwei-Stufen-Anregungsschema in Fe:LN ($E_{\mathrm{P}} = 2{,}43\,\mathrm{eV}$ grün, $E_{\mathrm{IR}} = 0{,}51\,\mathrm{eV}$ rot): (1) Über Ein-Photonen-Absorption eines Pump-Photons oder NDTPA aus dem Eisenzentrum bzw. Zwei-Photonen-Absorption aus dem Valenzband, werden Elektronen ins Leitungsband angeregt, welche Polaronen oder Exzitonen (X) bilden können. (2) Über Ein-Photonen-Absorption können die metastabilen Zustände innerhalb desselben Pulses direkt wieder angeregt werden.

ton/Polaron), sind Messungen mit einem weiteren Puls erforderlich, welcher gegenüber dem Pump-Puls und den IR-Pulsen verzögert werden kann. Im Gegensatz zu dem bisherigen Experiment kann so der zeitliche Versatz zwischen Pump- und IR-Pulsen zu jedem Tast-Zeitpunkt konstant gehalten werden, welches zu allen Zeiten die NDTPA und Beugung des Tast-Pulses ermöglicht. Dieses würde es ebenfalls ermöglichen, erstmals Ladungsträgergitter im mittleren Infraroten in Magnesium dotierten LN zu untersuchen, da in diesem Spektralbereich nach [32] eine starke transiente Absorption durch freie Polaronen bzw. Ladungsträger vorliegt.

5 Zusammenfassung

In dieser Arbeit werden elektronische und strukturelle Dynamiken durch Femtosekundenpuls *injizierte* kleine Polaronen in Lithiumniobat betrachtet, sowie die Auswirkungen auf die nichtlineare Optik mit Schwerpunkt auf die Holographie und den mittleren infraroten Spektralbereich untersucht. Auf Grund der kumulativen Art dieser Arbeit wurden alle wissenschaftlichen Neuerungen bereits ausführlich innerhalb der Publikationen diskutiert und zusammengefasst. Im Folgenden wird daher eine verkürzte Zusammenfassung präsentiert.

In Kapitel 2 wird die Bildungs- und Transportdynamik von kleinen Polaronen mittels Z-Scan Experiment mit variabler Pulsdauer und durch Kombination von transienten Absorptionsmessungen und Lumineszenzmessungen in einem weiten Temperaturbereich untersucht. Bei Betrachtung der Bildungsdynamiken kann die Polaronen Entstehungszeit in kongruenten LN auf 100 fs bestimmt werden und ein Zeitraum von ca. 80 fs nach Anregung ermittelt werden, indem polaronische Absorption ausgeschlossen werden kann. Das mikroskopische Modell zur Polaronentransport- und Rekombinationsdynamik wird um die Entstehung und den Zerfall von selbstlokalisierenden Exzitonen erweitert, welchen erstmals eine Absorption im ultravioletten/blauen Spektralbereich zugeordnet werden kann.

In Kapitel 3 wird der Nachweis von Gitterverzerrungen kleiner Polaronen in Lithiumniobat erbracht. Es wird eine Methodik entwickelt, welche den Zusammenhang zwischen der Schwingungsbande eines zweiatomigen Moleküls und den strukturellen Veränderungen in der direkten Umgebung dieser lokalen Sonde herstellt. Durch Kombination aus Anreg-Abtast Spektroskopie im mittleren infraroten Spektralbereich und einer Modellierung der Umgebung über Coulomb- und Morsepotential können dynamisch strukturelle Änderungen während der Polaronenbildung und Rekombination ermittelt werden.

In Kapitel 4 werden bisher unbekannte nichtlinear optische Eigenschaften von Polaronen im mittleren infraroten Spektralbereich betrachtet. Der transienten Absorption im Zeitbereich > 1 ps nach Anregung von heißen Ladungsträgern/Exzitonen kann eindeutig den freien Polaronen im Nichtgleichgewichtszustand zugeordnet werden. Erstmals wird die Entstehung eines (nahezu) instantanen und photorefraktiven holographischen Gitters durch nicht degenerative Zwei-Photonen-Absorption bis in den mittleren infraroten Spektralbereich ($\lambda = 2400$ nm) untersucht und der Einfluss von kleinen Polaronen in der Holographie betrachtet. Kleine Polaronen werden als mögliche Ursache für einen retardierten transienten Energietransfer bei der Selbstbeugung oder für einen Mehr-Stufen-Prozess bei der Entstehung eines infraroten holografischen Gitters diskutiert.

Grundlegend stellen die Ergebnisse dieser Studie einen entscheidenden Schritt für die Weiterentwicklung von nichtlinear optischen Materialien dar, in denen Femtosekundenpulse kleine Polaronen *injizieren*. Dabei wurden nicht nur grundlagenphysikalische Fragestellungen wie die Bildungs-, Transport- und Rekombinationsdynamiken von klei-

nen Polaronen in oxidischen Materialien beantwortet, sondern auch Möglichkeiten für die Entwicklung neuer Technologien mit Lithiumniobat als das „Silizium der Photonik“ dargestellt. Beispielsweise beeinflussen die Ergebnisse in der transienten Absorption die Anwendung von Lithiumniobat als Frequenzkonverter in optisch parametrischen Verstärkern/Oszillatoren oder die Realisierung eines Exzitonenlasers. Die Erkenntnisse zum Nachweis von Gitterverzerrungen durch kleine Polaronen schaffen den Weg zu neuen Technologien zum Bestimmen dynamischer lokaler Gitterveränderungen in oxidischen Materialien im Allgemeinen. Durch die Resultate in der Holographie werden Methoden zur Diagnostik und Kontrolle von MIR-Pulsen eingeleitet und die Entwicklung von holographischen Filtern im mittleren infraroten Spektralbereich ermöglicht.

Um auf das eingangs genannte Sprichwort zurückzublicken, liegt die Schönheit bzw. der Erkenntnisgewinn auch in dieser Dissertation im Auge des Betrachters. Je nach Betrachtungsweise konnten verschiedene Eigenschaften kleiner Polaronen untersucht werden. Erst durch die Kombination aus strukturellen, elektronischen und nichtlinear optischen Verfahren (vgl. Fig. 1.1) war es möglich, ein umfassendes Bild von Femtosekundenpuls *injizierten* kleinen Polaronen zu erhalten.

Literaturverzeichnis

[1] L. Germine, R. Russell, P. M.Bronstad, G .A. M. Blokland, J. W. Smoller, H. Kwok, S. E. Anthony, K. Nakayama, G. Rhodes, J. B. Wilmer. *Individual Aesthetic Preferences for Faces Are Shaped Mostly by Environments, Not Genes.* Curr. Biol. **25**, 2684–2689 (2015).

[2] T. H. Maiman. *Stimulated Optical Radiation in Ruby.* Nature **187**, 493–494 (1960).

[3] J. A. Armstrong, N. Bloembergen, J. Ducuing, P. S. Pershan. *Interactions between Light Waves in a Nonlinear Dielectric.* Phys. Rev. **127**, 1918–1939 (1962).

[4] P. A. Franken, A. E. Hill, C. W. Peters, G. Weinreich. *Generation of optical harmonics.* Phys. Rev. Lett. **7**, 118 (1961).

[5] G. Mayer, R. Gires. *The effect of an intense light beam on the index of refraction of liquids.* C.R. Acad. Sci. **258**, 2039 (1963).

[6] P. D. Maker, R. W. Terhune, C. M. Savage. *Intensity-Dependent Changes in the Refractive Index of Liquids.* Phys. Rev. Lett. **12**, 507–509 (1964).

[7] W. Kaiser, C. G. B. Garrett. *Two-Photon Excitation in CaF_2:Eu^{2+}.* Phys. Rev. Lett. **7**, 229–231 (1961).

[8] F. C. Zumsteg, J. D. Bierlein, T. E. Gier. *$K_xRb_{1-x}TiOPO_4$: A new nonlinear optical material.* J. Appl. Phys. **47**, 4980–4985 (1976).

[9] C. Chuangtian, W. Bochang, J. Aidong, Y. Guiming. *A NEW-TYPE ULTRAVIOLET SHG CRYSTAL–β-BaB_2O_4.* Science Chin. Ser. B **28**, 235–243 (1985).

[10] C. Chuangtian, A. Jiang, W. Bochang, Y. Guiming, Rukang L., Shujie L. *New nonlinear-optical crystal: LiB_3O_5.* J. Opt. Soc. Am. B **6**, 616 (1989).

[11] G.D. Boyd, R.C. Miller, K. Nassau, W.L. Bond, A. Savage. *$LiNbO_3$: AN EFFICIENT PHASE MATCHABLE NONLINEAR OPTICAL MATERIAL.* Appl. Phys. Lett. **5**, 234–236 (1964).

[12] L. E. Hargrove, R. L. Fork, M. A. Pollack. *LOCKING OF He–Ne LASER MODES INDUCED BY SYNCHRONOUS INTRACAVITY MODULATION.* Appl. Phys. Lett. **5**, 4–5 (1964).

[13] T.H. Moulton. *Ti-doped sapphire tunable solid-state laser.* Opt. News **8**, 9 (1982).

[14] D. E. Spence, P. N. Kean, W. Sibbett. *60-fsec pulse generation from a self-mode-locked Ti:sapphire laser.* Opt. Lett. **16**, 42 (1991).

[15] W. Peng-Fei, L. Chuang, Z. Chun-Mei, W. Jian-Liang, L. Yu-Xin, L. Ru-Xin. *High-Conversion-Efficiency and Broadband Tunable Femtosecond Noncollinear Optical Parametric Amplifier.* Chin. Phys. Lett. **25**, 2514–2517 (2008).

[16] A. H. Zewail. *Femtochemistry: Atomic-Scale Dynamics of the Chemical Bond.* J. Phys. Chem. A **104**, 5660–5694 (2000).

[17] A. H. Zewail. *Femtochemistry: Atomic-Scale Dynamics of the Chemical Bond Using Ultrafast Lasers (Nobel Lecture).* Angew. Chem. Int. Ed. **39**, 2586–2631 (2000).

[18] W. Hong, L. E. Halliburton, K. T. Stevens, D. Perlov, G. C. Catella, R. K. Route, R. S. Feigelson. *Electron paramagnetic resonance study of electron and hole traps in β-BaB_2O_4 crystals.* J. Appl. Phys. **94**, 2510–2515 (2003).

[19] G. J. Edwards, M. P. Scripsick, L. E. Halliburton, R. F. Belt. *Identification of a radiation-induced hole center in $KTiOPO_4$.* Phys. Rev. B **48**, 6884–6891 (1993).

[20] W. Hong, M. M. Chirila, N. Y. Garces, L. E. Halliburton, D. Lupinski, P. Villeval. *Electron paramagnetic resonance and electron-nuclear double resonance study of trapped-hole centers in LiB_3O_5 crystals.* Phys. Rev. B **68**, 094111 (2003).

[21] R. Grousson, M. Henry, S. Mallick, S. L. Xu. *Measurement of bulk photovoltaic and photorefractive characteristics of iron doped $LiNbO_3$.* J. Appl. Phys. **54**, 3012–3016 (1983).

[22] O. F. Schirmer, M. Imlau, C. Merschjann, B. Schoke. *Electron small polarons and bipolarons in $LiNbO_3$.* J. Phys. Condens. Matter **21**, 123201 (2009).

[23] C. Merschjann, B. Schoke, D. Conradi, M. Imlau, G. Corradi, K. Polgar. *Absorption Cross Sections and Number Densities of Electron and Hole Polarons in Congruently Melting $LiNbO_3$.* J. Phys. Condens. Matter **21**, 015906 (2009).

[24] O. F. Schirmer, M. Imlau, C. Merschjann. *Bulk photovoltaic effect of $LiNbO_3$:Fe and its small-polaron-based microscopic interpretation.* Phys. Rev. B **83**, 165106 (2011).

[25] H. E. Bennett. *Laser Induced Damage in Optical Materials.* Forgotten Books (1980).

[26] T. Volk, N. Rubinina, M. Wöhlecke. *Optical-damage-resistant impurities in lithium niobate.* J. Opt. Soc. Am. B **11**, 1681 (1994).

[27] R. S. Weis, T. K. Gaylord. *Lithium niobate: Summary of physical properties and crystal structure.* Appl. Phys. A **37**, 191–203 (1985).

[28] D. E. Smalley, Q. Y. J. Smithwick, V. M. Bove, J. Barabas, S. Jolly. *Anisotropic leaky-mode modulator for holographic video displays.* Nature **498**, 313–317 (2013).

[29] S. D. Yang, A. M. Weiner, K. R. Parameswaran, M.M. Fejer. *400-photon-per-pulse ultrashort pulse autocorrelation measurement with aperiodically poled lithium niobate waveguides at 1.55 μm.* Opt. Lett. **29**, 2070 (2004).

[30] C. Weiss, G. Torosyan, Y. Avetisyan, R. Beigang. *Generation of tunable narrow-band surface-emitted terahertz radiation in periodically poled lithium niobate.* Opt. Lett. **26**, 563 (2001).

[31] D. Emin. *Polarons.* Cambridge University Press (2013).

[32] F. Freytag, S. Messerschmidt, A. Krampf, G. Corradi, M. Imlau. *Picosecond mid-infrared absorption of pulse-injected small polarons in lithium niobate.* Submitted.

[33] R. Kaufmann, A. Hartmann, R. Hibst. *Cutting and Skin-Ablative Properties of Pulsed Mid-Infrared Laser Surgery.* J. Dermatol. Surg. Oncol. **20**, 112–118 (1994).

[34] T. J. Carrig, A. M. Schober. *Mid-Infrared Lasers.* IEEE Photon. J. **2**, 207–212 (2010).

[35] M. Imlau, H. Badorreck, C. Merschjann. *Optical Nonlinearities of Small Polarons in Lithium Niobate.* Appl. Phys. Rev. **2**, 040606 (2015).

[36] M. Manzo, F. Laurell, V. Pasiskevicius, K. Gallo. *Lithium Niobate: The Silicon of Photonics!* In *NATO Science for Peace and Security Series B: Physics and Biophysics*, Springer Netherlands, 2012.

[37] M. Kösters, B. Sturman, P. Werheit, D. Haertle, K. Buse. *Optical cleaning of congruent lithium niobate crystals.* Nat. Photonics **3**, 510–513 (2009).

[38] H. Badorreck, S. Nolte, F. Freytag, P. Bäune, V. Dieckmann, M. Imlau. *Scanning Nonlinear Absorption in Lithium Niobate over the Time Regime of Small Polaron Formation.* Opt. Mater. Express **5**, 2729 (2015).

[39] S. Messerschmidt, A. Krampf, F. Freytag, M. Imlau, L. Vittadello, M. Bazzan, G. Corradi. *The role of self-trapped excitons in small-polaron recombination in lithium niobate as a function of temperature.* In preperation.

[40] D. M. Eigler, E. K. Schweizer. *Positioning single atoms with a scanning tunnelling microscope.* Nature **344**, 524–526 (1990).

[41] S. C. Abrahams, J. M. Reddy, J. L. Bernstein. *Ferroelectric lithium niobate. 3. Single crystal X-ray diffraction study at 24°C.* J. Phys. Chem. Solids **27**, 997–1012 (1966).

[42] G. Corradi, H. Söthe, J. M. Spaeth, K. Polgár. *Mn^{2+} defects in $LiNbO_3$: an electron nuclear double resonance (ENDOR) investigation of the Mn^{2+} site and the local disorder.* J. Phys. Condens. Matter **2**, 6603–6618 (1990).

[43] V. Grachev, G. Malovichko. *EPR, ENDOR, and optical-absorption study of Cr^{3+} centers substituting for niobium in Li-rich lithium niobate crystals.* Phys. Rev. B **62**, 7779–7790 (2000).

[44] M. Wöhlecke, L. Kovács. *OH^- ions in Oxide Crystals*. Crit. Rev. Solid State Mater. Sci. **26**, 1–86 (2001).

[45] S. Moser, L. Moreschini, J. Jaćimović, O. S. Barišić, H. Berger, A. Magrez, Y. J. Chang, K. S. Kim, A. Bostwick, E. Rotenberg, L. Forró, M. Grioni. *Tunable Polaronic Conduction in Anatase TiO_2*. Phys. Rev. Lett. **110**, 196403 (2013).

[46] F. Freytag, G. Corradi, M. Imlau. *Atomic insight to lattice distortions caused by carrier self-trapping in oxide materials*. Sci. Rep. **6**, 36929 (2016).

[47] S. Nolte, B. Bourdon, F. Freytag, M. Imlau, A. Shumelyuk, S. Odoulov. *Dynamic grating mediated energy transfer between two sub-picosecond pulses in $LiNbO_3$*. J. Phys. Conf. Ser. **867**, 012003 (2017).

[48] S. Nolte, B. Bourdon, F. Freytag, M. Imlau, A. Shumelyuk, S. Odoulov *Transient energy transfer on the femtosecond timescale in lithium niobate*. In *CLEO/Europe-EQEC*, 2017.

[49] B. Bourdon, F. Freytag, M. Imlau, A. Shumelyuk, S. Odoulov. *Mid-Infrared photorefractivity with non-degenerate two-photon absorption*. J. Phys. Conf. Ser. **867**, 012006 (2017).

[50] D. Gabór. *A New Microscopic Principle*. Nature **161**, 777–778 (1948).

[51] E. Hering, R. Martin. *Photonik*. Springer Berlin Heidelberg (2005).

[52] S. Tay, P.-A. Blanche, R. Voorakaranam, A. V. Tunç, W. Lin, S. Rokutanda, T. Gu, D. Flores, P. Wang, G. Li, P. St Hilaire, J. Thomas, R. A. Norwood, M. Yamamoto, N. Peyghambarian. *An updatable holographic three-dimensional display*. Nature **451**, 694–698 (2008).

[53] T. Woike, W. Kirchner, G. Schetter, T. Barthel, K. Hyung-sang, S. Haussühl. *New information storage elements on the basis of metastable electronic states*. Opt. Commun. **106**, 6–10 (1994).

[54] T. Woike, M. Imlau. *Verfahren und Vorrichtung zum Auslesen von holographisch gespeicherten Daten aus einem Kristall*. Patent **DE19912023 C1** (2001).

[55] K. Buse, E. Soergel. *Holographie in Wissenschaft und Technik*. Physik Journal **2**, 3 (2003).

[56] P. Yeh. *Introduction to Photorefractive Nonlinear Optics*. JOHN WILEY & SONS INC (1993).

[57] D. Psaltis, K. Buse, A. Adibi. *Non-volatile holographic storage in doubly doped lithium niobate crystals*. Nature **393**, 665–668 (1998).

[58] K. Buse. *Light-induced charge transport processes in photorefractive crystals I: Models and experimental methods*. Appl. Phys. B **64**, 273–291 (1997).

[59] R. W. Boyd. *Nonlinear Optics*. Elsevier LTD, Oxford (2008).

[60] J.-C. Diels, W. Rudolph. *Ultrashort Laser Pulse Phenomena*. Elsevier LTD, Oxford (2006).

[61] E. Krätzig. *Spectroscopic Investigation of Photovoltaic Effects in Doped $LiNbO_3$*. J. Electrochem. Soc. **124**, 131 (1977).

[62] P. Reckenthaeler, D. Maxein, T. Woike, K. Buse, B. Sturman. *Separation of optical Kerr and free-carrier nonlinear responses with femtosecond light pulses in $LiNbO_3$ crystals*. Phys. Rev. B **76**, 195117 (2007).

[63] S. Sasamoto, J. Hirohashi, S. Ashihara. *Polaron Dynamics in Lithium Niobate upon Femtosecond Pulse Irradiation: Influence of Magnesium Doping and Stoichiometry Control*. J. Appl. Phys. **105**, 083102 (2009).

[64] D. Maxein, S. Kratz, P. Reckenthaeler, J. Bückers, D. Haertle, T. Woike, K. Buse. *Polarons in Magnesium-Doped Lithium Niobate Crystals Induced by Femtosecond Light Pulses*. Appl. Phys. B **92**, 543–547 (2008).

[65] M. Wesner, C. Herden, D. Kip, E. Krätzig, P. Moretti. *Photorefractive steady state solitons up to telecommunication wavelengths in planar SBN waveguides*. Opt. Commun. **188**, 69–76 (2001).

[66] R. Mosimann, P. Marty, T. Bach, F. Juvalta, M. Jazbinsek, P. Günter, A.A. Grabar. *High-speed photorefraction at telecommunication wavelength 1.55 μm in $Sn_2P_2S_6$:Te*. Opt. Lett. **32**, 3230 (2007).

[67] D. A. Fishman, C. M. Cirloganu, S. Webster, L. A. Padilha, M. Monroe, D. J. Hagan, E. W. Van Stryland. *Sensitive mid-infrared detection in wide-bandgap semiconductors using extreme non-degenerate two-photon absorption*. Nat. Photon. **5**, 561–565 (2011).

[68] S. Odoulov, A. Shumelyuk, H. Badorreck, S. Nolte, K. M. Voit, M. Imlau. *Interference and holography with femtosecond laser pulses of different colours*. Nat. Commun. **6**, 5866 (2015).

[69] O. Beyer, D. Maxein, K. Buse, B. Sturman, H.T. Hsieh, D. Psaltis. *Investigation of Nonlinear Absorption Processes with Femtosecond Light Pulses in Lithium Niobate Crystals*. Phys. Rev. E **71** (2005).

[70] M. Imlau. *Der photorefraktive Effekt, holographische Informationsspeicherung und die Entdeckung holographischer Streuung in zentrosymmetrischen Kristallen*. Cuvillier Verlag (1999).

[71] H. Kogelnik. *Coupled Wave Theory for Thick Hologram Gratings*. Bell Syst. Tech. J. **48**, 2909–2947 (1969).

[72] Robert Collier. *Optical Holography*. Elsevier Science (2013).

[73] O. Beyer, I. Breunig, F. Kalkum, K. Buse. *Photorefractive effect in iron-doped lithium niobate crystals induced by femtosecond pulses of 1.5μm wavelength*. Appl. Phys. Lett. **88**, 051120 (2006).

[74] M. G. Clark, F. J. DiSalvo, A. M. Glass, G. E. Peterson. *Electronic structure and optical index damage of iron-doped lithium niobate.* J. Chem. Phys. **59**, 6209–6219 (1973).

[75] O. Beyer, D. Maxein, K. Buse, B. Sturman, H. T. Hsieh, D. Psaltis. *Femtosecond time-resolved absorption processes in lithium niobate crystals.* Opt. Lett. **30**, 1366 (2005).

[76] M. Imlau, V. Dieckmann, H. Badorreck, A. Shumelyuk. *Tin hypothiodiphosphate: nonlinear response in the sub-100 fs time domain.* Opt. Mater. Express **1**, 953 (2011).

[77] H. Hsieh, D. Psaltis, O. Beyer, D. Maxein, C. von K. Schmising, K. Buse, B. Sturman. *Femtosecond holography in lithium niobate crystals.* Opt. Lett. **30**, 2233 (2005).

A Berechnung linearer und nichtlinearer Absorptionskoeffizienten

Im Folgenden werden die linearen- und nichtlinearen Absorptionskoeffizienten für Eisen-dotiertes Lithiumniobat (0,1 % wt., $d = 1\,\mathrm{mm}$) bestimmt. Die Berechnung der nichtlinearen Koeffizienten folgt den Studien von Sutherland (Handbook of Nonlinear Optics (Optical Science and Engineering), CRC Press, 2003). Zur Bestimmung der linearen Absorption bei $\lambda = 510\,\mathrm{nm}$ ($\alpha_{510} = 472\,\mathrm{m}^{-1}$) wird ein Zwei-Strahl-Spektrometer (*Shimadzu*, UV-3600) verwendet (vgl. Fig. A.1(a)). Die lineare Absorption bei $\lambda = 1600\,\mathrm{nm}$ ($\alpha_{1600} = 532\,\mathrm{m}^{-1}$) und $\lambda = 2400\,\mathrm{nm}$ ($\alpha_{2400} = 514\,\mathrm{m}^{-1}$) wird über ein FTIR-Spektrometer (*Buker*, Vertex 70) ermittelt (vgl. Fig. A.1(b)).

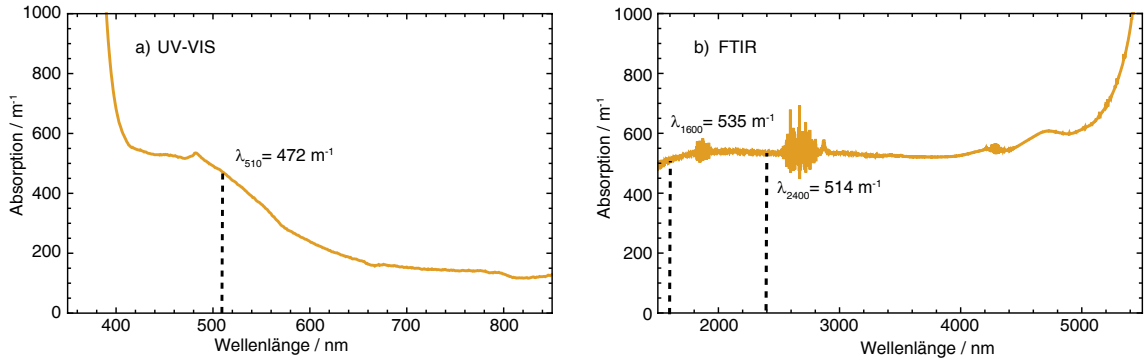

Abbildung A.1: Absorptionsspektrum Fe:LN: (a) Zwei-Strahl-Spektrometer (b) FTIR-Spektrometer.

Der nichtlineare Zwei-Photonen-Absorptions-Koeffizient β wird über Pulsenergiemessung des Pump-Pulses ($\lambda = 510\,\mathrm{nm}$) vor und hinter der Probe bestimmt. Durch Anpassung über:

$$T = \frac{(1-R)^2 \exp(-\alpha L)}{\sqrt{\pi} q_0} \int_{-\infty}^{\infty} \log[1 + q_0 \exp(-x^2)] dx, \text{mit} \tag{A.1}$$

$$q_0 = \beta(1-R) I_0 L_{\mathrm{eff}},\ L_{\mathrm{eff}} = \frac{1 - \exp(-\alpha L)}{\alpha} \tag{A.2}$$

folgt ein Zwei-Photonen-Absorptionskoeffizient $\beta = (1{,}05 \pm 0{,}15) \cdot 10^{-11}\,\mathrm{m/W}$ (vgl. Abb.A.2). T beschreibt die Transmission, α die lineare Absorption, L die Länge des Kristalls, R die Reflexion an der Kristalloberfläche, I_0 die Eingangsintensität und L_{eff} die effektive Länge. Der nichtlineare Drei-Photonen-Absorptionskoeffizient γ wird durch Anpassung über:

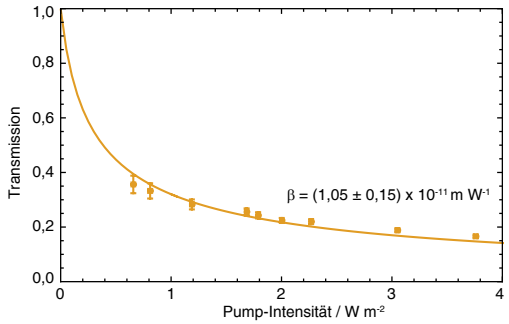

Abbildung A.2: Transmission als Funktion der Pump-Intensität ($\lambda = 510\,\mathrm{nm}$) zur Bestimmung des Zwei-Photonen-Absorptions-Koeffizienten β

$$T = \frac{(1-R)^2 \exp(-\alpha L)}{\sqrt{\pi} p_0} \int_{-\infty}^{\infty} \log[\sqrt{1 + p_0^2 \exp(-2x^2)} + p_0 \exp(-x^2)] dx, \text{mit} \quad \text{(A.3)}$$

$$p_0 = \sqrt{2\gamma(1-R)^2 I_0^2 L'_{\mathrm{eff}}},\ L'_{\mathrm{eff}} = \frac{1 - \exp(-2\alpha L)}{2\alpha} \quad \text{(A.4)}$$

zu $\gamma_{1600} = (2{,}25 \pm 0{,}75) \cdot 10^{-28}\,\mathrm{m/W}$ (Abb. A.3(a)) und $\gamma_{2400} = (0{,}30 \pm 0{,}30) \cdot 10^{-28}\,\mathrm{m/W}$ (Abb. A.3(b)) bestimmt. Der Fehler resultiert aus der im Rahmen des Fehlers maximal (rot) und minimal (schwarz) möglichen Anpassung (vgl. Abb. A.3).

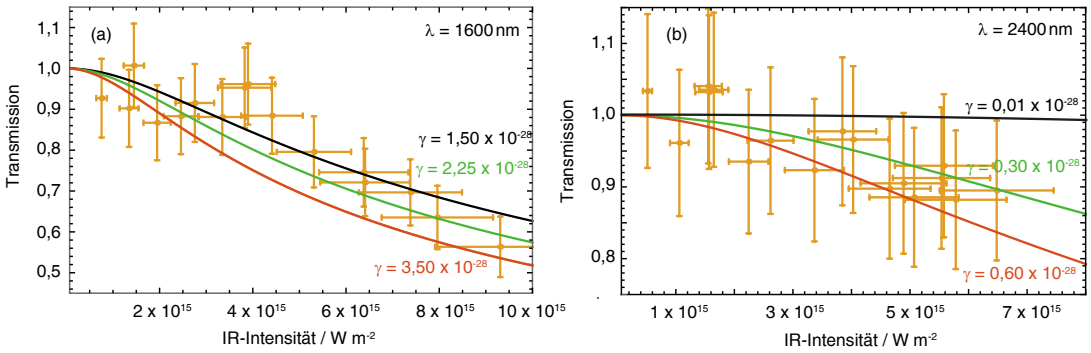

Abbildung A.3: Transmission als Funktion der IR-Intensität zur Bestimmung des Drei-Photonen-Absorptions-Koeffizienten γ: (a) $\lambda = 1600\,\mathrm{nm}$, (b) $\lambda = 2400\,\mathrm{nm}$.

B Publikationen

B.1 Scanning nonlinear absorption in lithium niobate over the time regime of small polaron formation

Scanning nonlinear absorption in lithium niobate over the time regime of small polaron formation

Holger Badorreck, Stefan Nolte, Felix Freytag, Pia Bäune, Volker Dieckmann, and Mirco Imlau*

School of Physics, Osnabrueck University, Barbarastr. 7, 49076 Osnabrueck, Germany
** Corresponding author: mimlau@uos.de*

Abstract: Nonlinear absorption is studied in presence of small polaron formation in lithium niobate using the z-scan technique and ultrashort laser pulses with pulse durations of 70 – 1.000 fs. A model for the analysis of the transmission loss as a function of pulse duration is introduced that considers (i) the individual contributions of two-photon and small polaron absorption, (ii) the small polaron formation time and (iii) an offset time between the optical excitation of free carriers by two-photon absorption and the appearance of small polarons. It is shown that the model allows for the analysis of the experimentally determined z-scan data with high precision over the entire range of pulse durations using a two-photon absorption coefficient of $\beta = (5.6 \pm 0.8)$ mm/GW. A significant contribution by small polaron absorption to the nonlinear absorption is uncovered for pulse durations exceeding the characteristic small polaron formation time of ≈ 100 fs. It can be concluded that the small polaron formation time is as short as $(70 - 110)$ fs and the appearance of small polaron formation is delayed with respect to two-photon absorption by an offset of about 80 fs.

© 2015 Optical Society of America. This work was published in Optical Materials Express and can be found at the URL http://dx.doi.org/10.1364/OME.5.002729. One print or electronic copy may be made for personal use only. Systematic reproduction and distribution, duplication of any material in this paper for a fee or for commercial purposes, or modifications of the content of this paper are prohibited.

1 Introduction

Lithium niobate, $LiNbO_3$ (LN), acts as a reference material in the field of nonlinear optics and experiences increasing attention as frequency converter due to its sound second-order nonlinearity $\chi^{(2)}$, chemical and mechanical stability as well as availability [1]. For efficient conversion, LN is exposed to very intense, short and ultra-short

laser pulses; at high intensities, however, the problem of nonlinear absorption arises due to a predominant contribution of third order nonlinearities $\chi^{(3)}$, in particular two-photon absorption (TPA). Besides limiting the conversion efficiency, TPA plays a major role in irreversible bulk laser-induced damage mechanisms of ferroelectric crystals by heating as well as via the generation of free carriers [2]. In LN the subsequent formation of small polarons from optically excited free carriers must be considered [3], as well, i.e. carriers that become trapped with strong coupling within a self-induced distortion of the surrounding unit cell [4]. The contribution of small polarons to the nonlinear absorption is determined by their broad band ($\approx 1\,\mathrm{eV}$) and pronounced absorption features [5] and characterized by a transient absorption with lifetimes in the regime from µs to ms at room temperature, thus commonly exceeding the pulse duration. Nonlinear interactions of small polarons with short, intense laser pulses in LN have been already addressed by different research groups [6–9]. However, the dependency of nonlinear absorption on incident laser pulses with different pulse durations has not been studied, so far, which is the topic of this work. The pulse duration dependency is of particular interest for nonlinear optical applications using sub-ps laser pulse durations that fall in the time regime of small polaron formation; the latter has been estimated to values much below 400 fs [6, 7, 9–11]). Without this knowledge, nothing is known about the individual contribution of TPA and small polaron absorption to the transmission loss of a propagating (ultra-)short laser pulse. Furthermore, it remains unclear to what extent pulse durations exist where the contribution of small polaron absorption becomes negligible.

In LN, first efforts have been made to separate optically excited carriers from the Kerr third order nonlinearity by means of grating recording [12] or transient absorption [8], demonstrating the impact of carrier dynamics in the time regime subsequent to the incident ultrashort laser pulse (240 fs). Furthermore, the two-photon absorption coefficient β has been determined using various pulse durations in the range of 80 fs – 55 ps yielding values of β between 1.5 and 5.2 mm/GW in the green spectral range (Refs. [7, 13–17], cf. review [11]).

We here study the dependency of nonlinear absorption on the duration of incident (ultra-)short laser pulses in lithium niobate by systematically scanning the transmission loss over the time regime of $70\,\mathrm{fs} < \tau < 1.000\,\mathrm{fs}$ by means of z-scan technique. For analysis, the differential equation for the intensity decrease of a propagating laser pulse along the crystal coordinate is derived. The temporal interplay of non-instantaneous processes with rise/relaxation times in the sub-ps time regime are considered: TPA, free carrier relaxation, small polaron formation and cascaded carrier excitation. The model extensions are motivated by a significant deviation – increasing for longer pulse durations – between experimental data and data analysis based on TPA (cf. original work from Sheik-Bahae [18]), but also TPA with free-carrier absorption [19]. Using our model for analysis, the experimental findings are described over the entire range of pulse durations with high precision. A deconvolution of the individual contributions – particularly of small polaron and two-photon absorption – to nonlinear absorption along the time coordinate becomes possible. We discuss the obtained temporal evolution of the small polaron impact from the viewpoint of a more precise estimate for the small polaron formation time, the existence of an offset of small polaron appearance upon the incident laser pulse as proposed by

Qiu et al. [6] and pulse durations that are insignificantly affected by small polaron formation. It can be concluded, that the pulse duration dependency of nonlinear absorption yields important information for the area of nonlinear applications with intense, (ultra-)short laser pulses of LN, but also of the variety of nonlinear optical materials showing small polaron formation in general.

2 Modeling

2.1 Temporal evolution of optically excited carriers in lithium niobate

For our study, we refer to the potential scheme depicted in Fig. 1, particularly describing the interplay of two-photon and small polaron absorption. In what follows,

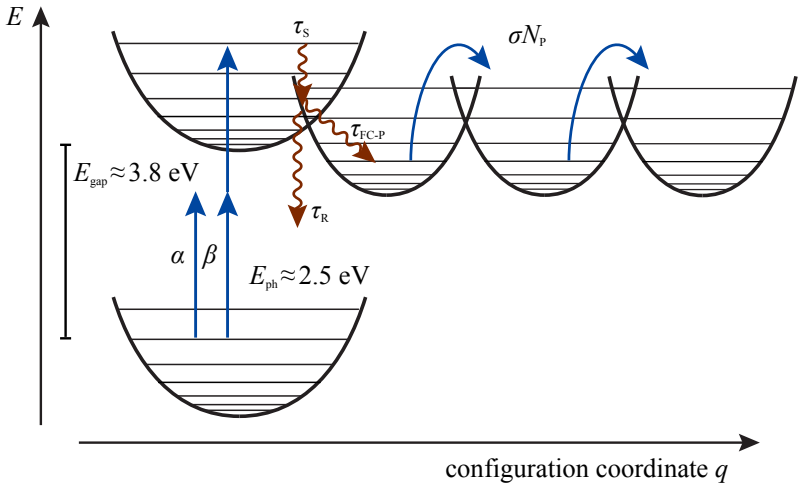

Figure 1: Potential diagram of the band-to-band excitation by one-photon (α) and two-photon (β) absorption with photon energies of $E_{\mathrm{ph}} = 2.5\,\mathrm{eV}$, electron-phonon cooling process with time constant τ_{S}, relaxation to the ground state (τ_{R}) and subsequently formation of small polarons ($\tau_{\mathrm{FC-P}}$) in lithium niobate. Absorption cross section σ and number of polarons N_{P} determine the absorption triggered by optically induced transport of small polarons [11].

the configuration coordinate q will be identified as spatial displacements of carriers in the real crystal lattice in the nanoscopic regime as well as the time axis covering the sub-ps regime.

We focus our considerations on the absorption of incident (ultra-)short sub-ps laser pulses with a photon energy of $E_{\mathrm{ph}} = 2.5\,\mathrm{eV}$ via one-photon and two-photon absorption in a nominally undoped LN crystal. The probability of the former is small because of the large band gap of lithium niobate ($\alpha = 20\,\mathrm{cm}^{-1}$ at $\approx 3.8\,\mathrm{eV}$ [20]), i.e. the LN crystal is transparent for this photon energy at low incident laser intensities. At the contrary, two-photon absorption dominates the nonlinear absorption at elevated intensities. For the regime of sub-ps laser pulses, the TPA coefficient β is reported to values of $\beta = 5.2\,\mathrm{mm/GW}$ (80 fs, 400 nm, Mg-doped LN) [7] and $\beta = 3.5\,\mathrm{mm/GW}$ (240 fs, $\approx$ 480 nm, nominally undoped LN) [17]. The response time of TPA being related to bound electrons is nearly instantaneous; an estimate of $\tau_{\mathrm{TPA}} \approx 5\,\mathrm{fs}$ has been

deduced from degenerate recording of TPA gratings for LN crystals [21], such that $\tau_{\mathrm{TPA}} \ll \tau$ for all pulse durations (70 – 1.000 fs) in our study. The temporal dynamics of TPA will thus be neglected in the differential equations given in the theoretical subsection below.

With TPA, free carriers far from the thermal equilibrium (hot carriers) are generated by means of valence-to-conduction band excitation. Energy relaxation to the lowest levels of the conduction band occurs preliminary via the emission of phonons; for semiconductors, this electron-phonon cooling process is characterized by a relaxation time of $\tau_{\mathrm{S}} \approx 100\,\mathrm{fs}$ [22]. For LN, $\tau_{\mathrm{S}} = 80\,\mathrm{fs}$ has been calculated for relaxation from an energetic level 0.5 eV above the conduction band minimum (T=296 K) [6]. By experimental means, ultrafast pump-probe-spectroscopy with LN did not show indications of an energy relaxation of hot carriers, so far [6, 8], whereas the time-resolved measurement of the reflectivity of a lithium niobate surface reveals a delayed signal with $\tau_{\mathrm{S}} = 600\,\mathrm{fs}$ that has been attributed to free electron generation [23].

In the next step, the carrier may either relax to the ground state by recombination with a hole and a characteristic time constant τ_{R}. Or carrier localization occurs followed by strong vibrational coupling, i.e. a small polaron is formed with characteristic time constant $\tau_{\mathrm{FC-P}}$ (*small polaron formation time*). In LN, $\tau_{\mathrm{FC-P}} \approx 100\,\mathrm{fs}$ for small free $\mathrm{Nb}_{\mathrm{Nb}}^{4+}$ polarons (room temperature) [6, 7] and $\tau_{\mathrm{FC-P}} < 400\,\mathrm{fs}$ for small bound $\mathrm{Nb}_{\mathrm{Li}}^{4+}$ polarons [9].

If the pulse duration exceeds the temporal regime until small polaron formation, the optical excitation from a small polaron must be considered, as well, and the carrier relaxes repeatedly into a small polaron. We assume that this process can be repeated several times over the incident pulse duration, i.e. cascaded excitation occurs [11].

In a similar way, the remaining holes in the valence band become localized as O^{-} hole polarons in the vicinity of lithium vacancies [3, 24, 25]. In the following, however, we will not distinguish between the particular types of small electron and hole polarons [24,26,27], because of probing at a single photon energy and the overlap of the absorption features of small free and bound electron and small hole polarons [5]. All types of small polarons result from the intrinsic defect structure of $\mathrm{LiNbO_3}$ that – although complex – has been modeled from first principles in very recent articles by *Li et al.* [28, 29]. We, thus, use LN crystals grown from the congruently melting composition in our experimental study.

2.2 Transfer to z-scan technique

The starting point for the determination of the nonlinear absorption composed by TPA and small polaron absorption is the z-scan technique. It has been developed originally for the analysis of near-instantaneous third order nonlinearities, particularly of the two-photon coefficient β and the nonlinear index of refraction n_2 [18]. A nonlinear optical sample is shifted (*scanned*) along the z-coordinate through the focus of a laser pulse with spatial and temporal Gaussian profile. The transmission as a function of z is expressed by

$$T(z) = \frac{1}{q(z)\sqrt{\pi}} \int_{-\infty}^{\infty} \ln\left(1 + q(z)\exp(-s^2)\right)\mathrm{d}s \tag{1}$$

with $q(z) = \beta I d_{\mathrm{eff}}/(1+z^2/z_0^2)$, the peak intensity I, the two-photon absorption coefficient β, the effective sample thickness d_{eff} and integration constant s. The additional impact of free-carrier absorption to the transmission was derived in Ref. [19]; Ogusu et al. [30] introduced the appearance of a transient free carrier absorption with silicon as an example. Based on these theoretical concepts, we need to add the characteristic time of electron-phonon relaxation τ_{S}, i.e. a temporal offset prior to small polaron formation, as a particular feature of small polaron dynamics. Then, the change of the pulse intensity through a sample as a function of the propagation depth L and time t is given by:

$$\frac{\partial I(L,t)}{\partial L} = -[\alpha + \beta I(L,t) + \sigma N_{\mathrm{P}}(L,t)]I(L,t). \tag{2}$$

Here, α is the one-photon absorption coefficient, and σ and N_{P} are the absorption cross section and number density of small polarons. The temporal evolution of the latter is modeled according to Fig. 1 by considering the number density of free carriers N_{FC}, the subsequent electron-phonon cooling (τ_{S}), carrier recombination (τ_{R}) and/or small polarons formation ($\tau_{\mathrm{FC-P}}$) during pulse duration (τ) via:

$$\frac{\partial N_{\mathrm{P}}(L,t)}{\partial t} = \frac{N_{\mathrm{FC}}(L,t-\tau_{\mathrm{S}})}{\tau_{\mathrm{FC-P}}} \tag{3}$$

with the temporal evolution of free carriers:

$$\frac{\partial N_{\mathrm{FC}}(L,t)}{\partial t} = \frac{\alpha I(L,t)}{h\nu} + \frac{\beta I^2(L,t)}{2h\nu} - \frac{N_{\mathrm{FC}}(L,t-\tau_{\mathrm{S}})}{\tau_{\mathrm{R}}} - \frac{N_{\mathrm{FC}}(L,t-\tau_{\mathrm{S}})}{\tau_{\mathrm{FC-P}}} \tag{4}$$

Differential equation (2) is solved numerically for data analysis; Figure 2 highlights the impact of pulse duration on the transmission of a z-scan measurement. For numerical

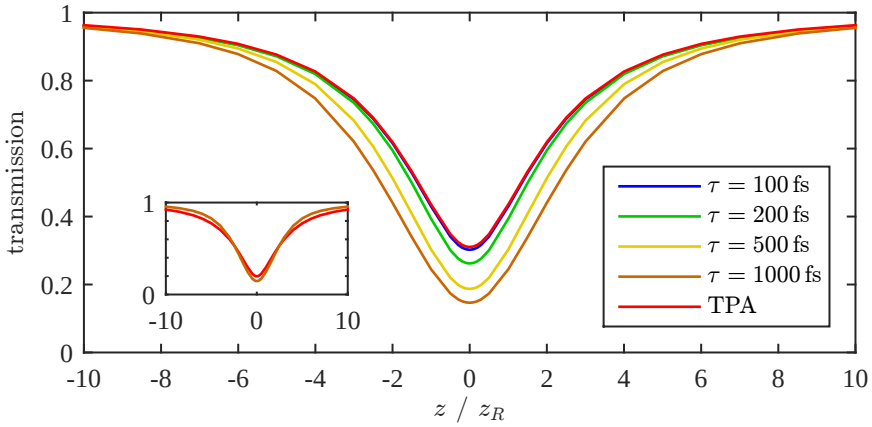

Figure 2: Numerical solution of Eq. (2) as a function of pulse duration (100 fs – 1.000 fs) and the following model parameters: $\alpha = 0\,\mathrm{m}^{-1}$, $\beta = 5\,\mathrm{mm/GW}$, $\tau_{\mathrm{S}} = 100\,\mathrm{fs}$, $\tau_{\mathrm{FC-P}} = 100\,\mathrm{fs}$, $\tau_{\mathrm{R}} = 100\,\mathrm{fs}$, and $I = 8.6\,\mathrm{PW/m^2}$. For comparison the red graph representing Eq. (1) is also shown. The inset highlights the change in the shape of the transmission traces exemplarily for a pulse duration of 1.000 fs and a fitted graph using the original z-scan theory Eq. (1) with an TPA-coefficient increased by a factor of 2.2 in comparison to the main figure.

solution, the following model parameters are used: $\alpha = 0\,\mathrm{m}^{-1}$, $\beta = 5\,\mathrm{mm/GW}$, $\tau_\mathrm{S} = 100\,\mathrm{fs}$, $\tau_\mathrm{FC-P} = 100\,\mathrm{fs}$, $\tau_\mathrm{R} = 100\,\mathrm{fs}$ and the pulse duration is varied from 100 fs to 1.000 fs while the peak intensity I at $z = 0$ is kept constant at $8.6\,\mathrm{PW/m^2}$. The plots show the characteristic drop of the transmission while scanning along the z-coordinate with a minimum transmission at $z = 0$, and are mirror symmetric to $z = 0$. The additional contribution of non-instantaneous absorption processes results in a pronounced increase of the transmission loss in the order of several tens of percentage, i.e. the increase of nonlinear absorption by small polaron formation, with increasing pulse duration is obvious. For comparison, the result of Eq. (1) considering the action of TPA, only, is depicted in addition (red curve). The numerical solution Eq. (2) converges to the result of Eq. (1) for pulse durations equal to the electron-phonon cooling rate, $\tau \simeq \tau_\mathrm{S}$, or below. Thus, it is possible to estimate the characteristic time constants of small polaron formation from z-scan experiments as a function of pulse duration, if τ is in the order of τ_S. It is important to note, that the analysis of nonlinear absorption using Eq. (1) and pulse durations exceeding τ_S will result in an overestimate of the TPA coefficient β. This is due to the fact, that the numerical solutions not only show an increase in the transmission loss, but also a change in the shape of $T(z)$ (cf. inset of Fig. 2). A limit of the numerical analysis is that it is not possible to distinguish between several types of small bound polarons; this, however, may be solved by performing a systematic study at different photon energies of the incident pulse.

3 Experimental section

3.1 Setup and lithium niobate samples

The systematic scan of the nonlinear absorption over the time regime of 70 fs – 1.000 fs has been performed using the common z-scan technique described in Ref. [18] with an incident laser pulse of spatial and temporal Gaussian profile that – as an original feature – has been compressed/stretched to the desired pulse duration. The extended setup, as depicted schematically in Fig. 3, is composed by (i) a prism pulse stretcher/compressor, (ii) a spatial frequency filter, and (iii) the common z-scan configuration. An optical parametric amplifier (Coherent Inc., model: OPerA solo) pumped by a regeneratively amplified Ti^{3+}:Sapphire laser (Coherent Inc., model: Libra-F HE) serves as the source for ultrashort laser pulses (pulse energy maximum: 150 µJ at 2.5 eV, center wavelength: 488 nm). A neutral density filter is used for intensity adjustment. The repetition rate of 250 Hz is reduced to 12.5 Hz using a Chopper wheel, in order to avoid cumulative absorption from pulse to pulse due to long-lived small polarons (maximum characteristic lifetime $\approx 3\,\mathrm{ms}$ at room temperature, see e.g. Ref [11]). The pulses first enter a prism pulse stretcher/compressor that allows for tuning the pulse duration by means of adjustment of prism P2 and mirror M using a linear stage (LS). A spectral width of $\Delta\lambda = 5\,\mathrm{nm}$ is obtained, equal with a bandwidth limited pulse duration of $\tau \approx 70\,\mathrm{fs}$. For the purpose of our study, the pulse duration is varied up to 1.000 fs and characterized by means of a scanning autocorrelator (APE, model pulseCheck 15). After the stretcher/compressor, the pulses enter a spatial frequency filter that consists of two concave mirrors (focal length: 500 mm),

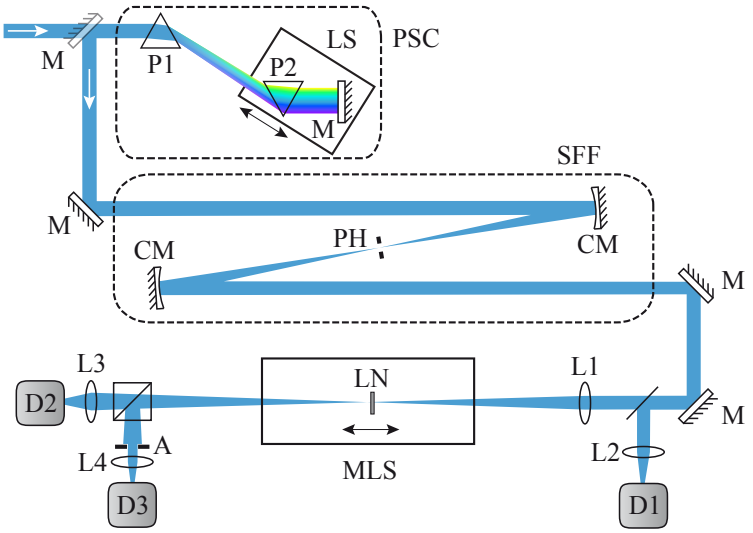

Figure 3: Sketch of the optical setup composed by a prism stretcher/compressor (PSC) (P1; P2 on a linear stage LS), a spatial frequency filter (SFF) (CM: concave mirrors with $f = 500\,\text{mm}$, PH: pinhole with diameter of 100 µm) and a common configuration for z-scan technique: L1: lens (f = 150 mm), LN: lithium niobate crystal, MLS: motorized linear stage, L2-L4: lenses (f = 50 mm), D1-D3: Si-PIN detectors (photosensitive area $\gg$ beam spot), A: aperture with diameter of 4 mm. Incident pulses obey a maximum pulse energy of 150 µJ at 2.5 eV (center wavelength: 488 nm) and are adjusted in intensity by a neutral density filter. The repetition rate of 250 Hz is reduced to 12.5 Hz using a Chopper wheel. The pulse duration can be varied with PSC from 70 fs – 1.000 fs.

avoiding chromatic abberation, and a pinhole (diameter $d = 100\,\mu\text{m}$). Astigmatism is minimized by a small angle of incidence of approximately 2 degree. The pulse spatial radius is determined to $(r = 2.0 \pm 0.1)\,\text{mm}$. Both, M^2 and r, are required for the calculation of beam waist and intensity of each pulse as a function of position z. A nearly spatial ($M^2 = 1.1 \pm 0.1$) and temporal Gaussian beam profile is verified using beam profile measurements and an autocorrelator, thus, fulfilling the experimental conditions of the z-scan technique to a great extent [31]. The as-prepared pulses are focused by lens L1 ($f = 150\,\text{mm}$) and propagate through the lithium niobate crystal LN. The position of LN can be shifted along the direction of pulse propagation (z-coordinate) by means of a motorized linear stage (MLS). Incident and transmitted pulse energies are detected using biased Si-PIN detectors D1-D3 (Thorlabs, *DET10a*). The detectors D2 and D3 are equipped with opened and closed apertures, respectively, thus allowing for the determination of both nonlinear absorption and nonlinear index of refraction. Lenses L2-L4 focus the pulses to a spot size less than the photosensitive area of the detector.

All studies were performed with thin a-cut plates (aperture $8\times6\,\text{mm}^2$, thickness $d = (260 \pm 10)\,\mu\text{m}$) of nominally pure LN grown from a congruently melting composition (CrysTec GmbH). The thickness ensures that the sample is much thinner than the Rayleigh length, avoiding asymmetric z-scan traces and effects of the group velocity dispersion (GVD). Front and back surfaces are carefully polished to optical grade with nearly plan-parallelism (wedge below 5 arcmin). The one-photon absorption coefficient is determined to $\alpha = (0.16 \pm 0.1)\,\text{cm}^{-1}$ for extraordinary ($\mathbf{e} \parallel c$) light polarisation and $\lambda = 488\,\text{nm}$.

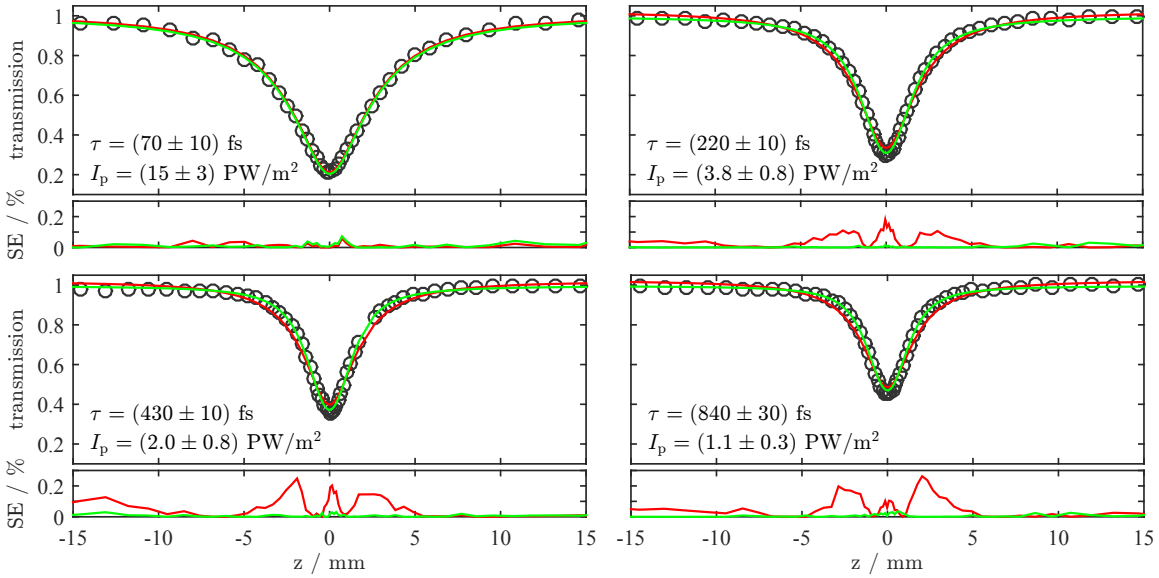

Figure 4: (Upper parts): Experimentally determined transmission as a function of scanning coordinate z for four pulse durations: (a) (70 ± 10) fs, (b) (220 ± 10) fs, (c)(430 ± 10) fs and (d) (840 ± 30) fs, all for a constant pulse energy of (270 ± 30) nJ and at a center wavelength of $\lambda = 488$ nm. The results of our numerical fitting procedure according to Eqs. (2) to (4) are shown as green lines with the following model parameters: a two-photon absorption coefficient of $\beta = (5.6 \pm 0.8)$ mm/GW, a small polaron absorption cross section of $\sigma = (210 \pm 70) \times 10^{-22}\,\mathrm{m}^2$, and characteristic times for electron-phonon relaxation of $\tau_\mathrm{S} = 80$ fs, for interband relaxation of $\tau_\mathrm{R} = 100$ fs and for small polaron formation of $\tau_{\mathrm{FC-P}} = 100$ fs. For comparison, fitting of Eq. (1) to the experimental data is shown as red line. (Lower parts): squared error of the fits with respect to the experimental data as a function of z.

3.2 Experimental results

The experimentally determined z-scan traces are plotted in Fig. 4, exemplarily, for four pulse durations: (a) (70 ± 10) fs, (b) (220 ± 10) fs, (c)(430 ± 10) fs and (d) (840 ± 30) fs, all for a constant pulse energy of (270 ± 30) nJ and at a center wavelength of $\lambda = 488$ nm. The upper parts of the figures show the transmission T obtained from the signal ratio of diodes D2 and D1 as a function of z-coordinate from -15 mm to +15 mm. The travel range is chosen such that one-photon absorption dominates the transmission at ± 15 mm; the transmission is normalized to unity at $|z| > 15$ mm and shows a pronounced drop by scanning over the focus of the incident pulse. The minimum of transmission is used to define the position $z = 0$; all data sets are almost mirror-symmetric to $z = 0$. Qualitatively, the shape of the z-scan traces are comparable with each other for all pulse durations, and are characterized by a very low noise. A closer inspection reveals that the shape becomes narrower with increasing τ, which is a sign of higher order nonlinearities as discussed above (cf. inset of Fig. 2). In addition, and because of the adjustment of a constant pulse energy for all pulse durations, the varying peak intensity yields an increase of the transmission with increasing τ from $T \approx 20\%$ at 70 fs to $T \approx 45\%$ at 840 fs.

The data plots are analyzed by numerical solution of Eqs. (2) to (4). Fitting was performed iteratively by optimizing the squared error between fit and experimental data and the same model parameters for all data sets; the fitting results are shown

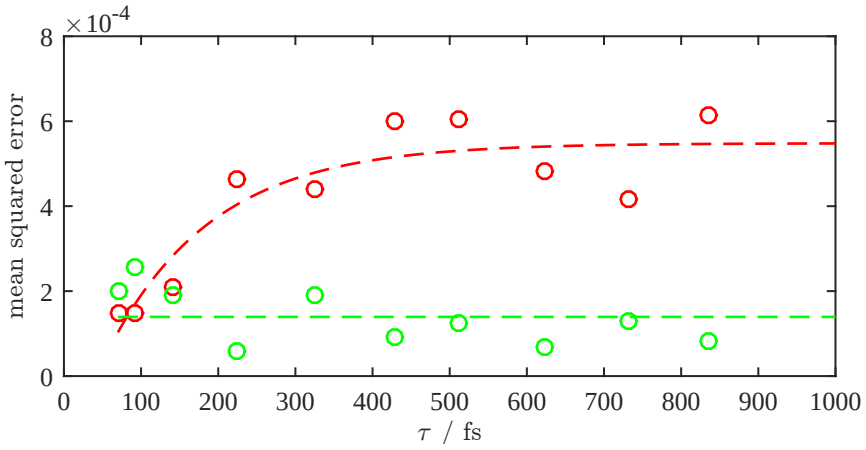

Figure 5: Mean squared error between fit and experimental data for both, the numerical solution of our model approach according to Eqs. (2) to (4) (green), and the original z-scan theory using Eq. (1) (red). The dashed lines represent best fits with constant minimum value of the mean squared error $\mathrm{MSE}_{\mathrm{min}} = (1.5 \pm 0.1) \times 10^{-4}$ (green) and a fit with Eq. (5) to the data points (red) with saturation amplitude $\mathrm{MSE}(t = \infty) = (4 \pm 0.1) \times 10^{-4}$, characteristic time constant $\tau_{\mathrm{exp}} = (137 \pm 8)\,\mathrm{fs}$, temporal offset of $\tau = (86 \pm 5)\,\mathrm{fs}$, and minimum value of mean squared error $\mathrm{MSE}_{\mathrm{min}} = (1.5 \pm 0.1) \times 10^{-4}$.

as green curves in Fig. 4(a)-(d) with the following model parameters: a two-photon absorption coefficient of $\beta = (5.6 \pm 0.8)\,\mathrm{mm/GW}$, a small polaron absorption cross section of $\sigma = (210 \pm 70) \times 10^{-22}\,\mathrm{m}^2$, and characteristic times for electron-phonon relaxation of $\tau_{\mathrm{S}} = 80\,\mathrm{fs}$, for interband relaxation of $\tau_{\mathrm{R}} = 100\,\mathrm{fs}$ and for small polaron formation of $\tau_{\mathrm{FC-P}} = 100\,\mathrm{fs}$. A high degree of agreement is obvious from the inspection by eye over the entire range of scanning. The lower plots of Fig. 4(a)-(d) highlight the squared error of the fits with respect to the experimental data as a function of z with values much below 0.1% throughout the data set, typically below 0.03%. For comparison, the data sets have been also analyzed using Eq. (1), i.e. the z-scan theory considering two-photon absorption, only, yielding the red curves in Fig. 4(a)-(d). For the shortest pulse duration of 70 fs, the data can be modeled by the z-scan theory with very good coincidence, expressed by a squared error of below 0.1%. From this data set, the fit yields a two-photon absorption coefficient of $\beta = (5.8 \pm 0.8)\,\mathrm{mm/GW}$ (for the nonlinear refractive index n_2 we obtained a value of about $5 \times 10^{-20}\,\mathrm{m}^2/\mathrm{W}$). For longer pulse durations, a deviation of the original TPA theory to the experimentally determined traces becomes obvious and is more pronounced with increasing pulse duration (exceeding a squared error of $\approx 0.2\%$). The evolution of *mean* squared errors (MSE) between fit and data set is plotted for both theoretical approaches in Fig. 5 for all measured pulse durations. Again, the plot highlights the excellent agreement of our model approach with the experimental data over the entire regime of pulse durations; a minimum value of mean squared error $\mathrm{MSE}_{\mathrm{min}} = (1.5 \pm 0.1) \times 10^{-4}$ is reached throughout the pulse durations. The original z-scan theory describes the data with high precision in the regime of the shortest pulse durations (below 100 fs), as well. However, a characteristic rise of MSE of Eq. (1) becomes obvious for pulse durations $\geq 100\,\mathrm{fs}$ with a development that can be best described by a single-exponential growth function. We thus have fitted the

function

$$\mathrm{MSE}(t) = \mathrm{MSE}(t=\infty) \times \left[1 - \exp\left(\frac{-(t - t_{\mathrm{offset}})}{\tau_{\mathrm{exp}}}\right)\right] + \mathrm{MSE}_{\mathrm{min}} \tag{5}$$

to the data set yielding the following parameters: saturation amplitude $\mathrm{MSE}(t = \infty) = (4\pm0.1)\times10^{-4}$, characteristic time constant $\tau_{\mathrm{exp}} = (137\pm8)$ fs, temporal offset of $\tau = (86\pm5)$ fs, and minimum value of mean squared error $\mathrm{MSE}_{\mathrm{min}} = (1.5\pm0.1)\times10^{-4}$.

4 Discussion

From the experimental viewpoint, a very high quality of transmission traces are collected using the applied optical setup that represents an extension of the common z-scan technique. In particular, the important conditions of a Gaussian spatial profile is obtained, using a spatial frequency filter, and a Gaussian temporal profile is verified by autocorrelation measurements. A diode-pumped, regeneratively amplified Ti:Sa-laser system obeys an excellent beam profile and pointing stability and, thus, is ideally suited for generation of harmonic, Gaussian pulses by means of an optical parametric amplifier. The RMS noise of the pulse energy at the OPAs' output ($\ll 5\%$) could be reduced successfully by selection of incident pulses with equal pulse energy using diode D1. The disadvantage of this procedure is the extended measurement time, which is further enlarged by the low pulse repetition rate of 12.5 Hz and the two dimensional parameter range (z, τ) of our particular study. However, all these efforts are justified considering the outmost marginal deviations between the model approaches typically of below 0.03% (cf. Fig. 4).

As a superior result, a more detailed insight to the underlying physics of nonlinear absorption in lithium niobate is obtained, and clear evidence for small polaron formation and its contribution to nonlinear absorption is found. From the dependency of the shape of the z-scan trace as a function of pulse duration and its analysis, it is possible to derive a set of important material parameters that will be discussed in the following. First, the two-photon absorption coefficient $\beta = (5.6 \pm 0.8)\,\mathrm{mm/GW}$ is obtained from the complex numerical fitting procedure, that uses a single set of parameters for all pulse durations. Thus, the transmission is described throughout the regime of pulse durations from 70 fs – 1.000 fs with the same TPA coefficient – a result that is to be expected as β is a material parameter independent on τ. Considering the high quality of the numerical fits, a reliable value of β with an error of $\approx 15\%$ occurs for the LN crystal under investigation. Nearly the same value ($\beta = (5.8 \pm 0.8)\,\mathrm{mm/GW}$) is obtained using the original z-scan theory at the shortest pulse duration of (70 ± 10) fs, that underlines the reliability of the obtained value. Moreover, it is an important (first) anchor for proving the action of our model approach as nonlinear absorption persists solely from TPA for pulse durations much below the small polaron formation time. The TPA value itself is much larger than the state-of-the-art knowledge in literature. For comparable pulse durations and photon energies, values of $\beta = 5.2\,\mathrm{mm/GW}$ (80 fs, 400 nm, Mg-doped LN) [7] and $\beta = 3.5\,\mathrm{mm/GW}$ (240 fs, $\approx$ 480 nm, nominally undoped LN) [17] are reported. Besides the possibility, that this difference may be attributed to the impact of small

polaron absorption according to our model approach, we like to emphasize the role of stoichiometry on the TPA coefficient. It is well established, that the position of the band gap energy is strongly dependent on the crystals' stoichiometry. Being an absorption process of higher order, the transition probability for TPA is expected to change in accordance with the linear absorption feature [32]. Therefore, differences in the TPA coefficient may be due to differences in stoichiometry of the studied LN crystals, which seems to be very likely to us.

New insights are revealed to the relaxation dynamics of optically excited free carriers, characterized by τ_S. First evidence for this intermediate process was presented by Qiu et al. [6] performing time-resolved fs-absorption spectroscopy in Mg-doped LN crystals. As a remarkable characteristic of the small polaron formation dynamics, a temporal offset was discovered prior to the rise of small polaron absorption. No change of the transmission was observed during this temporal offset. A similar observation is reported in the work of Beyer et al. [8] using 240 fs laser pulses. Here, we also need to take into account a temporal offset prior to small polaron formation. In advance of the results of Qiu et al. [6], the time of the incident pulse does not need to be determined which is a particular feature of the approach of pulse duration scanning; the time constant τ_S is equal to the pulse duration where the transmission trace starts to alter its shape. Therefore, the temporal offset $\tau_S = 80\,\mathrm{fs}$ can be determined with appealing precision. The lack of free-carrier absorption may be attributed either to the fact that the photon energy of the probing pulse is insensitive to the free-carrier absorption cross section or the carrier-phonon relaxation time τ_S falls much below the pulse duration ($\tau_S \ll (70 \pm 10)\,\mathrm{fs}$ in our case). However, as pointed out in Ref. [22], τ_S exceeds $10^{-13}\,\mathrm{s}$ in most semiconductors and for common optical phonon modes. Further studies, particularly with shorter pulse durations need to be performed for clarification.

From the rise of the nonlinear absorption as a function of pulse duration we further obtain the small polaron formation time of $\tau_{FC-P} = 100\,\mathrm{fs}$ in the numerical modeling procedure. This value is in good coincidence with the formation times obtained by transient absorption measurements [6, 7, 9]. Combining, however, our result on the presence of an offset time of $\tau_S = 80\,\mathrm{fs}$ and the transient data from Sasamoto et al. using also very short, 80 fs pump and probe laser pulses [7], it is possible to conclude an upper limit of $\tau_{FC-P} = 100\,\mathrm{fs}$. It is because the transmission loss due to two-photon absorption and due to small polaron absorption can not be resolved on the temporal axis in pump-probe experiments and overlap with each other.

Another parameter obtained from our study is the small polaron absorption cross section σ that is by more than one order of magnitude higher than the values published by Merschjann et al. [5]. We note that it is not possible to find a converging numerical solution using Merschjann's value as fixed fitting parameter, even by neglecting relaxation of excited carriers to the ground state ($\tau_R = \infty$). One explanation for the striking difference is an oversimplification of our model approach presented in section 2. In particular, the dynamics of holes with the possibility of O^- small hole polaron formation in LN [25] has been disregarded. Such holes obey nearly the same absorption cross section at a photon energy of 2.5 eV as it is the case for small bound Nb_{Li}^{4+} and/or small free Nb_{Nb}^{4+} polarons, although the maxima of the respective absorption features are fairly different (2.5 eV for O^- and 1.6 eV for Nb_{Li}^{4+}). It is thus likely

to assume that half of the contribution to small polaron absorption at 2.5 eV must be attributed to O^- hole polarons. As a consequence, a value reduced by a factor of two will be obtained for the absorption cross section. Nevertheless, as individual types of small polarons are not resolved by our study, further pulse duration dependencies using different photon energies are required for a more quantitative analysis of this aspect. We like to add, that there is a severe difference in the boundary conditions of small polaron absorption between the study of Merschjann et al. [5] and the present one: Merschjann's cross sections were determined using pump-probe experiments, i.e. under the conditions of no light, whereas small polarons are inspected during the presence of a strong pump in our study, i.e. with light. Considering the presence of specific charge transport phenomena in LN, particularly of bulk photovoltaic currents [33], a difference in the absorption features of small polarons with and without light illumination can not be excluded.

It is noteworthy that all parameters discussed above and obtained from the rather complex numerical solution of Eqs. (2) to (4) show a correlation with each other. Particularly, the ratio between $\tau_{\mathrm{FC-P}}$ and τ_{R} is not independent from other model parameters and directly impacts the density numbers N_{FC} and N_{P} as well as the polaron absorption coefficient σ. As a consequence, the characteristic times can be varied in a limited regime, only. The offset time τ_{S} can be varied between 70 fs and 90 fs while the polaron formation time is limited to $70\,\mathrm{fs} < \tau_{\mathrm{FC-P}} < 110\,\mathrm{fs}$. At the same time, it is very reasonable that the increase of the number of fitting parameters in general results in the optimization of fitting functions. However, in the present case, the extension of the original z-scan theory by small polaron absorption is justified by the striking deviation of the transmission traces between theory and experimental data with increasing pulse duration. As this deviation rises after a characteristic offset time, the data plot of Fig. 5 showing the mean squared error as a function of pulse duration, can be applied also for the determination of the offset time τ_{S} yielding $\tau_{\mathrm{S}} = (86 \pm 5)\,\mathrm{fs}$ – in accordance with the numerical results of our model approach.

5 Summary and Conclusion

The pulse duration dependency of nonlinear absorption has been studied in lithium niobate by means of z-scan technique over the time regime of 70 – 1.000 fs and has been analyzed from the viewpoint of small polaron formation using a numerical approach. It is shown, that the transmission loss of (ultra-)short laser pulses propagating through LN crystals can be described with remarkable precision and can be attributed to the complex interplay of near-instantaneous nonlinearities, particularly of two-photon and small-polaron absorption. Surprisingly, very minor alterations in the shape of the well-known transmission traces of the z-scan technique result in severe changes in the set of nonlinear optical coefficients; for instance, using the original z-scan theory, the TPA coefficient β may be overestimated by a factor of three in the regime of long pulse durations.

Besides the precise determination of β or the absorption cross section of small polarons under illumination σ, the amount of information on the underlying photo-

physical processes obtained from our study is unexpectedly high: the proposed offset of transient absorption features during the time regime of electron-phonon cooling has been verified by experimental means and could be determined to (80 ± 10) fs. Furthermore, a more accurate regime of the small polaron formation time of 70 – 110 fs has been obtained.

These results are of utmost importance for the physics and microscopic modeling of the small polaron approach in LN [25, 26] and the further understanding of the small-polaron based bulk photovoltaic effect [33]. But also for the field of applications in nonlinear photonics as frequency converter – particularly in the growing field of ultrafast laser systems. In more general, the presented theoretical model and the experimental approach of pulse duration scanning can be transferred to the wide field of oxide materials showing small polaron formation and can be applied in the area of ultrafast lasers.

Acknowledgments

The authors gratefully acknowledge discussion from G. Corradi, L. Kovács (SZFKI, Hungary), and from A. Büscher. Financial support by the DFG (IM 37/5-2, INST 190/137-1 FUGG, INST 190/165-1) is gratefully acknowledged.

References

[1] M. Fejer, G. Magel, D. H. Jundt, R. Byer. *Quasi-phase-matched second harmonic generation: tuning and tolerances.* IEEE J. Quantum Electron. **28**, 2631–2654 (1992).

[2] O. A. Louchev, H. H. Hatano, N. Saito, S. Wada, K. Kitamura. *Laser-induced breakdown and damage generation by nonlinear frequency conversion in ferroelectric crystals: Experiment and theory.* J. Appl. Phys. **114**, 203101 (2013).

[3] O. F. Schirmer, D. von der Linde. *Two–Photon and X–Ray–Induced Nb^{4+} and O^{-} Small Polarons in $LiNbO_3$.* Appl. Phys. Lett. **33**, 35 (1978).

[4] D. Emin, *Polarons* (Cambridge University Press, Cambridge, 2013).

[5] C. Merschjann, B. Schoke, D. Conradi, M. Imlau, G. Corradi, K. Polgar. *Absorption cross sections and number densities of electron and hole polarons in congruently melting $LiNbO_3$.* J. Phys. Chem. Sol. **21**, 015906 (2009).

[6] Y. Qiu, K. B. Ucer, R. T. Williams. *Formation time of a small electron polaron in $LiNbO_3$: measurements and interpretation.* Phys. Stat. Sol. C **2**, 232 (2005).

[7] S. Sasamoto, J. Hirohashi, S. Ashihara. *Polaron dynamics in lithium niobate upon femtosecond pulse irradiation: Influence of magnesium doping and stoichiometry control.* J. Appl. Phys. **105**, 083102 (2009).

[8] O. Beyer, D. Maxein, K. Buse, B. Sturman, H. T. Hsieh, D. Psaltis. *Investigation of nonlinear absorption processes with femtosecond light pulses in lithium niobate crystals.* Phys. Rev. E **71**, 056603 (2005).

[9] O. Beyer, D. Maxein, T. Woike, K. Buse. *Generation of small bound polarons in lithium niobate crystals on the subpicosecond time scale.* Appl. Phys. B **83**, 527–530 (2006).

[10] H. Yochum, K. Ucer, R. Williams, P. Sheldon, V. Nagirnyi, V. Denks, L. Grigorjeva, D. Millers, E. Kotomin. *Short-pulse excitation and spectroscopy of $KNbO_3$, $LiNbO_3$ and $KTiOPO_4$*. Rad. Eff. Def. Sol. **150**, 271–276 (1999).

[11] M. Imlau, H. Badorreck, C. Merschjann. *Optical nonlinearities of small polarons in lithium niobate*. Appl. Phys. Rev. (in press).

[12] D. Maxein, K. Buse. *Interaction of Femtosecond Laser Pulses with Lithium Niobate Crystals: Transmission Changes and Refractive Index Modulations*. J. Holography Speckle **5**, 1–5 (2009).

[13] A. Seilmeier, W. Kaiser. *Generation of tunable picosecond light pulses covering the frequency range between 2700 and 32,000 cm^{-1}*. Appl. Phys. A **23**, 113 (1980).

[14] R. DeSalvo, A. Said, D. Hagan, E. Van Stryland, M. Sheik-Bahae. *Infrared to ultraviolet measurements of two-photon absorption and n_2 in wide bandgap solids*. IEEE J. Quantum Electron. **32**, 1324 (1996).

[15] H. Li, F. Zhou, X. Zhang, W. Ji. *Picosecond Z-scan study of bound electronic Kerr effect in LiNbO3 crystal associated with two-photon absorption*. Appl. Phys. B **64**, 659 (1997).

[16] R. Ganeev, I. Kulagin, A. Ryasnyansky, R. Tugushev, T. Usmanov. *Characterization of nonlinear optical parameters of KDP, $LiNbO_3$ and BBO crystals*. Opt. Commun. **229**, 403–412 (2004).

[17] O. Beyer, D. Maxein, K. Buse, B. Sturman, H. T. Hsieh, D. Psaltis. *Femtosecond time-resolved absorption process in lithium niobate crystals*. Opt. Lett. **30**, 1366 (2005).

[18] M. Sheik-Bahae, A. A. Said, T. H. Wei, D. J. Hagan, E. W. Van Stryland. *Sensitive Measurement of Optical Nonlinearities Using A Single Beam*. IEEE J. Quantum Electron. **26**, 760 (1990).

[19] A. A. Said, M. Sheik-Bahae, D. J. Hagan, T. H. Wei, J. Wang, J. Young, E. W. Van Stryland. *Determination of Bound-electronic and Free-carrier Nonlinearities In ZnSe, GaAs, CdTe, and ZnTe*. J. Opt. Soc. Am. B **9**, 405 (1992).

[20] S. Redfield, W. J. Burke. *Optical Absorption Edge of $LiNbO_3$*. J. Appl. Phys. **45** (1974).

[21] A. Shumelyuk. Institute of Physics, National Academy of Sciences, 46, Prospekt Nauki, 03 650 Kyiv, Ukraine, H. Badorreck, S. Nolte, M. Imlau, and S. Odoulov are preparing a manuscript to be called *Selfdiffraction from moving gratings recorded in $LiNbO_3$ with ultra-short laser pulses of different colors*.

[22] A. Othonos. *Probing ultrafast carrier and phonon dynamics in semiconductors*. J. Appl. Phys. **83**, 1789–1830 (1998).

[23] M. Garcia-Lechuga, J. Siegel, J. Hernandez-Rueda, J. Solis. *Imaging the ultrafast Kerr effect, free carrier generation, relaxation and ablation dynamics of Lithium Niobate irradiated with femtosecond laser pulses*. J. Appl. Phys. **116**, 113502 (2014).

[24] O. F. Schirmer, O. Thiemann, M. Wöhlecke. *Defects in $LiNbO_3$ — I. Experimental Aspects*. J. Phys. Chem. Solids **52**, 185 (1991).

[25] O. F. Schirmer. *O^- bound small polarons in oxide materials*. J. Phys. Condens. Matter **18**, R667 (2006).

[26] O. F. Schirmer, M. Imlau, C. Merschjann, B. Schoke. *Electron small polarons and bipolarons in $LiNbO_3$*. J. Phys. Condens. Matter **21**, 123201 (2009).

[27] B. Faust, H. Müller, O. F. Schirmer. *Free small polarons in $LiNbO_3$*. Ferroelectrics **153**, 297 (1994).

[28] Y. Li, W. G. Schmidt, S. Sanna. *Intrinsic* $LiNbO_3$ *point defects from hybrid density functional calculations*. Phys. Rev. B **89**, 094111 (2014).

[29] Y. Li, S. Sanna, W. G. Schmidt. *Modeling intrinsic defects in LiNbO3 within the Slater-Janak transition state model*. The Journal of Chemical Physics **140**, 234113 (2014).

[30] K. Ogusu, K. Shinkawa. *Optical nonlinearities in silicon for pulse durations of the order of nanoseconds at 1.06 µm*. Opt. Express **16**, 14780–14791 (2008).

[31] P. B. Chapple, J. Staromlynska, J. A. Hermann, T. J. Mckay, R. G. Mcduff. *Single-Beam Z-Scan: Measurement Techniques and Analysis*. J. Nonlinear Opt. Phys. Mater. **06**, 251–293 (1997).

[32] M. Sheik-Bahae, D. J. Hagan, E. W. Van Stryland. *Dispersion and band-gap scaling of the electronic Kerr effect in solids associated with two-photon absorption*. Phys. Rev. Lett. **65**, 96–99 (1990).

[33] O. F. Schirmer, M. Imlau, C. Merschjann. *Bulk photovoltaic effect of $LiNbO_3$:Fe and its small-polaron-based microscopic interpretation*. Phys. Rev. B **83**, 165106 (2011).

B.2 The role of self-trapped excitons in polaronic recombination processes in lithium niobate

The role of self-trapped excitons in polaronic recombination processes in lithium niobate

Simon Messerschmidt[1,*], Andreas Krampf[1], Felix Freytag[1], Mirco Imlau[1], Laura Vittadello[2], Marco Bazzan[2], Gábor Corradi[3]

[1] *School of Physics, Osnabrueck University, Barbarastr. 7, 49076 Osnabrueck, Germany*
[2] *Dipartimento di Fisica e Astronomia, Universita di Padova, Via Marzolo 8, 35131 Padova, Italy*
[3] *Wigner Research Centre for Physics, Institute for Solid State Physics and Optics, Hungarian Academy of Sciences, Konkoly-Thege u. 29-33, 1121 Budapest, Hungary*
[*] *Corresponding author: smesserschmi@uos.de*

Abstract: Transient absorption and photoluminescence are experimentally investigated in the polaronic reference system lithium niobate, $LiNbO_3$ (LN), with the aim to refine the microscopic model of small polaron dynamics in materials with strong electron-phonon coupling. As a unique feature, our study is performed by using two different spectroscopic methods, in crystals with dopants enhancing photorefraction or damage resistance, and over a broad temperature range from $15 - 400\,\mathrm{K}$. Although being self-consistent for particular experimental conditions, the hitherto used microscopic polaronic models reveal inconsistencies when applied to this larger data set. We show that comprehensive modeling is unlocked by the inclusion of an additional type of polaronic state with the following characteristics: (i) strongly temperature- and dopant-dependent relaxation times, (ii) an absorption feature in the blue-green spectral range, and (iii) a Kohlrausch-Williams-Watts decay shape with a temperature-dependent stretching factor $\beta(T)$ showing a behavior contrary to that of small, strong-coupling polarons. The hypothesis of self-trapped excitons (STEs, i.e., bound electron-hole pairs strongly coupled to Nb^{5+} and O^{2-} within a niobium-oxygen octahedron) and their pinning on defects as the microscopic origin of these characteristics is supported by a spectroscopic linkage of photoluminescence at low ($15\,\mathrm{K}$) and elevated ($300\,\mathrm{K}$) temperatures and explains the long-lifetime components in transient absorption as due to pinned STEs.

This work was published in J.Phys.: Condens. Matter and can be found at doi: 10.1088/1361-648X/aaf4df. As the Version of Record of this article is going to be / has been published on a gold open access basis under a CC BY 3.0 licence, this Accepted Manuscript is available for reuse under a CC BY 3.0 licence immediate. Any further

distribution of this work must maintain attribution to the author(s) and the title of the work, journal citation and DOI. Published under licence by IOP Publishing Ltd.

1 Introduction

The study of charge carrier dynamics with strong-coupling to the lattice, e.g., small polarons and self-trapped excitons (STEs) in lithium niobate, $LiNbO_3$ (LN), triggered widespread attention even in nanosciences since the verification of their decisive role in the microscopic mechanisms of ferroelectric photovoltaics [1,2], of THz wave damping [3] and laser-induced bulk damage mechanisms [4, 5], but also of photocatalysis in other oxide dielectrics like TiO_2, MgO, or ZnO [6–10]. LN is a ferroelectric oxide with excellent photoelectrical and (nonlinear) optical features, exhibits pronounced electron-/hole-phonon coupling, and hosts four different kinds of intrinsic small polarons [1, 4, 11, 12]: the free polaron Nb_{Nb}^{4+}, the bound polaron Nb_{Li}^{4+}, the bipolaron Nb_{Li}^{4+}:Nb_{Nb}^{4+}, and the hole polaron $O^- - V_{Li}$. It should be noted that electrons bound to Fe_{Li}^{3+} [1,13] or $Ti_{Li/Nb}^{4+}$ [14,15] may also be described in the framework of the strong-coupling-polaron picture. Luminescent STEs in LN are bound electron-hole pairs with strong coupling to Nb^{5+} and O^{2-} within a single niobium-oxygen octahedron and reveal different optical properties depending whether the STEs form in stoichiometric materials or in niobium-oxygen octahedra near defect sites [16, 17]. Small polarons can be accessed by transient absorption spectroscopy (TAS) due to their characteristic, broad-band absorption features (for a rough overview of the absorption cross sections of the different polaron species cf. Ref. [18]), whereas time-resolved photoluminescence (TRPL) is applied for STEs, showing broad-band luminescence in the blue-green spectral range (cf. Refs. [11, 16, 19–23]).

To this date, carrier self-trapping and recombination in LN, i.e., polaron formation and decay, is described by microscopic models restricted to certain temperature ranges, stoichiometries and dopings of the particular study [16, 24–27], and appear consistent on their own, i.e., within the framework of given experimental boundary conditions and/or within the focus of a specific physical question. The restrictions of these models naturally contradict to the demand of a comprehensive microscopic model for pulse-induced transient absorption (TA) and luminescence in LN as reflected in detail by the following striking examples of our previous studies: (i) room temperature (RT) TA measurements of Conradi *et al.* [24] in LN doped with Mg above the optical damage resistance threshold (ODRT) showed that neither a slow decay component at $\lambda = 488\,\mathrm{nm}$ nor the spectral form of the TA-signal can be explained by absorption features of hole and free polarons alone. (ii) Comparing the results of Herth *et al.* [25] and Berben *et al.* [26] who investigated the TA in Fe:LN in the blue-green spectral range and at $\lambda = 785\,\mathrm{nm}$, respectively, several inconsistencies regarding the stretching-factor β obtained by fitting a Kohlrausch-Williams-Watts function (KWW) to the data can be found. For Fe_{Li}^{2+} polarons absorbing in the blue-green, Herth *et al.* reveal β values between $0.55 - 1$, depending on the wavelength whereas Berben *et al.* published $\beta \approx 0.35$ at 785 nm for the decay of bound polarons under similar experimental conditions. This is in contrast with the claim of Herth *et al.*, according to which the decrease of the near-infrared signal is due to a direct

transition from Nb_{Li}^{4+} bound polarons to Fe_{Li}^{3+}. In this case, the increasing numbers of Fe_{Li}^{2+} polarons should be described by the same τ and β values as obtained from the bound polaron decay function.

Studies of STEs in LN, generated also by band-to-band excitation, refer to (TR)PL measurements [19,21,22], usually carried out at temperatures below 100 K. At elevated temperatures, in particular at RT, the luminescence signal becomes weak so that STEs have been disregarded in small polaron dynamics, so far. Using intense laser pulses and considering the complex formation paths in the temporal regime from electron-hole-pair generation up to small polaron formation [4], a considerable number density of STEs and their contribution to the transients can per se not be neglected. Only recently, Reichenbach *et al.* showed that photoluminescence (PL) of unknown microscopic origin can be raised in LN by femtosecond pulse illumination at RT [28, 29].

Thus – despite the presence of a sound knowledge on the formation, transport and recombination of small polarons as well as on the luminescence properties of STEs – we need to accept that nearly nothing is known about the possible interplay of STEs with small polarons in LN in different temperature ranges. This interplay may occur at different stages during the various lifetimes of the individual quasi-particles. For instance small polaron and STE formation may be highly competitive in the ultrafast time range upon hot carrier excitation. On longer timescales, transformations of small polaron pairs to STEs may be discussed and may be decisive to explain the variety of optical phenomena being unexplained in TA experiments, so far.

The intention of this work is to fill this gap in knowledge by inspection of the possible role of self-trapped excitons in the polaronic recombination processes in LN in its very details. This topic inherently comprises a large degree of complexity: two different experimental techniques (TAS and PL) have to be applied, and the studies need to be performed with LN crystals with different doping below and above the photorefractive concentration threshold, over a large temperature range from about 15 K up to RT and on timescales up to minutes upon an incident pump event. Furthermore, it is challenging to uncover an appropriate experimental fingerprint to identify STEs within the polaronic recombination process. We address this complex task by stepwise answering the most obvious and driving questions, at first: (i) *are STEs at the origin of PL in LN up to room temperature?*, (ii) *is there a justified need for a revision of the microscopic polaronic recombination processes?*, and (iii) *is there any experimental fingerprint pointing to a role of STEs in the polaronic recombination process*? After (positively) answering these questions, we become able to focus our discussion on the development of a comprehensive picture for polaronic recombination including STEs and, finally, to tackle the revision of the existing microscopic model.

The paper is organized according to this concept: we first present steady state PL data over a large temperature range uncovering STEs as the microscopic origin of PL at RT (cf. question (i)). Then, TA data of Fe- and Mg-doped lithium niobate samples, again obtained over a large temperature and an extended wavelength range, indicate, beyond experimental incertitude, that the dynamics of TA in the red/near-infrared (λ = 633 nm or 1310 nm, λ = 785 nm), and the blue (λ = 445 nm, λ = 488 nm) spectral range cannot be correlated with each other for a number of experimental conditions in the framework of the current model proposed by Herth *et al.* (cf.

question (ii)). Finally TRPL and TA data in Mg:LN are presented and compared over a large temperature range demonstrating some distinct properties of the stretching factor β of STEs deviating from the ones of small polarons, which is used to identify STE-related phenomena in the transient blue absorption in Fe:LN (cf. question (iii)). Based on these results, we discuss that STEs, and mainly *pinned* STEs (STEs bound to a defect), shall be considered in polaronic recombination. We present a revised comprehensive microscopic model, being an extension of the original Herth model [25]. It is capable to explain all inconsistencies in TA and TRPL measurements discussed, so far.

2 Experimental Methods

Three experimental techniques were used in this study.

(i) PL: Photoluminescence spectra under fs-exposure (regeneratively amplified Ti:Sapphire laser, $\tau_{\mathrm{FWHM}} = 35\,\mathrm{fs}$, repetition rate 1 kHz; Coherent Inc., type *Astrella*) were obtained using a spectrograph with an air-cooled back-illuminated CCD-camera (Roper Scientific, type *Isoplane* and *PIXIS-UV*). The frequency doubled pump beam ($\lambda = 400\,\mathrm{nm}$) with an energy of $40\,\mu\mathrm{J}$ per pulse was slightly focused into the sample and the luminescent emission was collected over the duration of a whole second (averaging over 1,000 pump events).

(ii) TAS: Transient absorption spectroscopy using a Q-switched, frequency doubled Nd:YAG pulse laser (Innolas, type *Spitlight 600*) at a center wavelength of $\lambda = 532\,\mathrm{nm}$ (ordinary light polarization) with a pulse duration of $\tau_{\mathrm{FWHM}} = 8\,\mathrm{ns}$ and a maximum pulse energy of $E_{\mathrm{max}} \approx 290\,\mathrm{mJ}$. Pulse-induced changes of the absorption were detected by the dynamic transmission loss of continuous-wave probe lasers at wavelengths: $\lambda = 445\,\mathrm{nm}$, 488 nm, 785 nm, and 633 nm or 1310 nm (ordinary light polarization) via Si-PIN photodiodes and a fast digital storage oscilloscope (LeCroy, type *Waverunner LT584*). The recording took place in a time range from 30 ns after excitation up to the complete recovery of the sample (up to several tens of seconds). As shown by comparisons with as-grown crystals, effects of permanent photorefractive damage can be neglected for the given pulse parameters.

(iii) TRPL: Time-resolved photoluminescence measurements were performed utilizing the above mentioned ns-pulse laser, but now in the frequency tripled configuration with a center wavelength of $\lambda = 355\,\mathrm{nm}$ ($E_{\mathrm{max}} \approx 120\,\mathrm{mJ}$, extraordinary polarization). A combination of a monochromator and a photon counter with a time resolution of 125 ns was used to detect the emitted luminescence in a direction perpendicularly to the pump pulse propagation. In both setups, the measurement was triggered by a diode detecting the scattered pump light and in the case of TRPL the signal to noise ratio was improved by averaging over a total of 1,000 shots.

In all setups, the sample temperature could be tuned in the range from 15 K to 400 K using a closed-cycle cryostat with optical windows.

Samples: Polished plates of thickness 1 mm of congruent lithium niobate, with the c-axis in the plane, with dopant concentrations of 0.1 mol% Fe or 6.5 mol% Mg in the melt were prepared by Czochralski growth at the University of Padova, and the WIGNER Research Centre for Physics Budapest by the high-temperature top-seeded

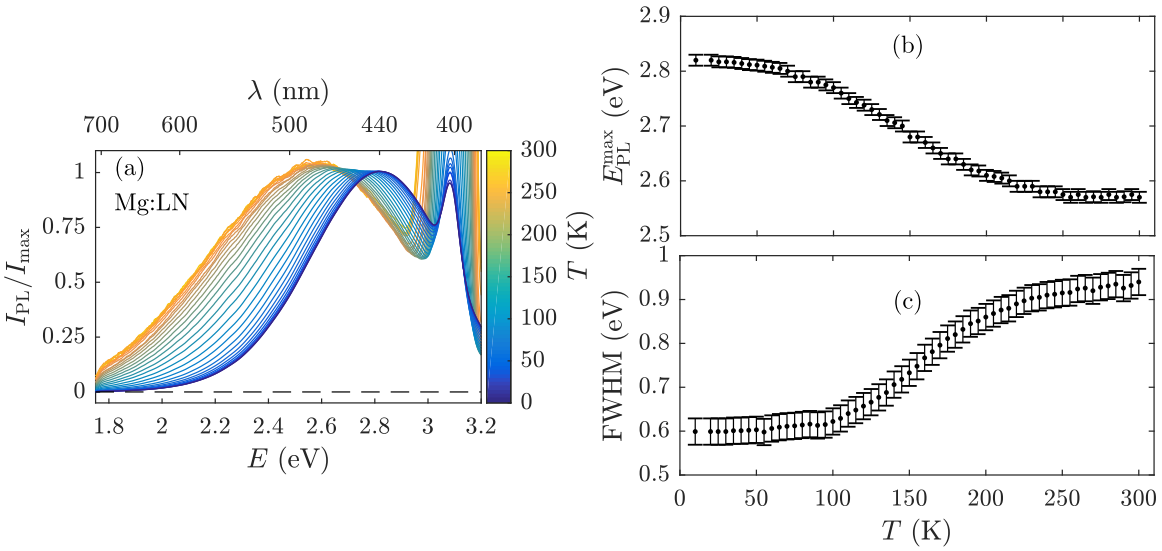

Figure 1: (a) Normalized temperature-dependent emission spectra of Mg:LN following exposure to a fs pump pulse at 400 nm. (b) Emission maximum and (c) full width at half maximum (FWHM) of the emitted luminescence as a function of temperature. A red-shift and a spectral broadening with increasing temperature can be observed.

solution growth method, respectively.

3 Are STE's at the origin of photoluminescence in LN up to room temperature?

The first question to be experimentally answered is whether STEs can be identified unambiguously at the origin of PL up to RT. The anchor for addressing this question is the low temperature luminescence spectrum that already has been attributed to the radiative decay of STEs, i.e., of electron-hole-pairs localized in a Nb-O-octahedron. By temperature-dependent measurements of the steady state PL signal in the temperature range from 15–300 K, we intend to gradually track the evolution of peak position and width of emission as the temperature changes. The results then allow for a clear assignment of the emission to STEs in the entire range. We note that the measurement series is performed with over-threshold Mg:LN (6.5 mol% Mg in the melt) where luminescence can be observed also at elevated temperatures.

Figure 1a shows the spectral fingerprints of the PL of Mg:LN in the temperature range from 15 K to 300 K for the particular case of an exposure to a train of fs-laser pulses with a center wavelength of 400 nm. The spectra, all normalized to their respective peak maxima, feature at 15 K a spectral width of ≈ 0.6 eV (FWHM) at a peak position of 2.82 eV. For the first time, clear evidence for a red-shift of the peak maximum by a total of about 0.2 eV upon heating to RT (cf. figure 1b), together with a spectral broadening to a bandwidth of ≈ 0.95 eV (cf. figure 1c), is found. It should be noted that the total PL intensity decreases by several orders of magnitude at elevated temperatures.

The data are in good agreement with low temperature data published in the liter-

ature [16, 19–21], where the PL signal was mostly assigned to the recombination of STEs, and additionally confirm the results of Reichenbach *et al.* [28, 29] about RT emission in Mg:LN. Up to $T \approx 200\,\mathrm{K}$ the gradual shift of the luminescence peak maximum corresponds to the Varshni equation [30] expected for luminescence also in semiconductors [31], and can be understood, together with the observed broadening as the impact of phonon coupling on the electron-hole pairs bound in the STE [32]. At higher temperatures the flattening of the peak maximum's temperature dependence, accompanied by a decreased broadening rate, may indicate the gradual appearance of a second, weak, slightly blue-shifted luminescence signal reported by Kämpfe *et al.* [19]. The authors attributed it to a recombination process similar to the one at low temperatures, only involving trapping centers at larger distances with respect to the formation area.

It is thus very reasonable to conclude, that (i) up to RT the PL signal must be assigned to the radiative decay of optically generated STEs, and (ii) STEs have to be present within the entire temperature range. The assignment of the luminescence to STEs generated at early stages of pumping is strongly supported by TAS results indicating much slower transport processes for charged electron polarons (up to minutes), compared to PL dynamics, both to be presented and discussed in the forthcoming sections.

4 Is there a justified need for a revision of the microscopic polaronic recombination processes?

Previous experimental studies on polaronic recombination by means of TA already revealed a few inconsistencies in the microscopic models for polaronic recombination that could not be resolved satisfactorily, so far. In particular, inconsistencies were uncovered if the experimental boundary conditions, such as doping concentration or wavelength of inspection were changed significantly (examples are given in the introduction). We here address the question, whether it is possible to clearly demonstrate the failure of the established models under certain experimental conditions. For this purpose, we use the temperature as main tuning parameter, but also extend the spectral range of optical inspection to the ultraviolet-blue spectral range. A particular feature of the previous microscopic models, a relaxation of electrons from $\mathrm{Nb}_{\mathrm{Li}}^{4+}$ to $\mathrm{Fe}_{\mathrm{Li}}^{3+}$, can specifically be inspected in the ultraviolet spectral range. Our results are finally capable to highlight the model failure by severe differences in the relaxation and rise times of the number densities of $\mathrm{Nb}_{\mathrm{Li}}^{4+}$ and $\mathrm{Fe}_{\mathrm{Li}}^{3+}$, respectively, at temperatures below RT. The studies are performed (a) with Fe:LN (0.1 mol% Fe in the melt) in order to connect and compare our findings with the literature data, and (b) with over-threshold Mg:LN in order to foster the presence of STEs, but also to exclude that our findings may mainly be related to the presence of $\mathrm{Fe}_{\mathrm{Li}}$.

4.1 Transient absorption experiments in Fe-doped lithium niobate

In figure 2a, measurements of the transient absorption on the Fe:LN sample are shown at $T = 293\,\mathrm{K}$ at the probing wavelengths 445 nm, 488 nm, 633 nm, and 785 nm.

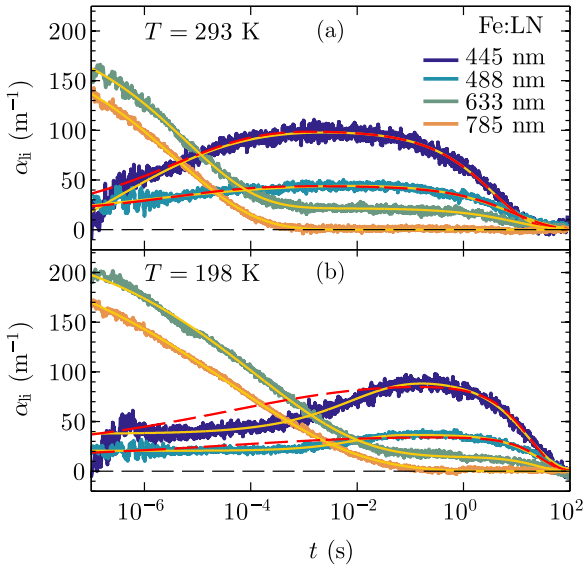

Figure 2: Temporal development of the transient absorption in Fe:LN at (a) $T = 293\,\mathrm{K}$ and (b) $198\,\mathrm{K}$ ($I_\mathrm{P} \approx 133\,\mathrm{MW/cm^2}$). The continuous yellow and dashed red lines represent fits of equation (1) to the data set. A two-term KWW-function ($N = 2$) was used at wavelengths 445 nm, 488 nm, and 633 nm, whereas a one-term function ($N = 1$) for $\lambda = 785\,\mathrm{nm}$. In the case of the continuous lines $\alpha^0_{\mathrm{li},i}(\lambda, T)$, $\tau_i(\lambda, T)$, and $\beta_i(\lambda, T)$ were chosen as free parameters in the fitting procedure, whereas in the case of the dashed red lines the fixed values $\tau_1(785\,\mathrm{nm}, T)$ and $\beta_1(785\,\mathrm{nm}, T)$ obtained in the red region were also used in the blue spectral range. The results are summarized in Table 1.

The first two are monitoring the nearly coinciding $\mathrm{Fe}^{2+}_{\mathrm{Li}}$ and trapped hole absorption bands and the last one roughly corresponding to the maximum of the $\mathrm{Nb}^{4+}_{\mathrm{Li}}$ band, all being strongly overlapping broad asymmetric features characteristic for polarons [18]. Following the incident pump pulse at $t = 0\,\mathrm{s}$, a transient absorption appears in the near-infrared spectral range and vanishes almost completely in the microsecond range at RT. In the blue spectral range (445 nm and 488 nm), the transient absorption increases on a time scale up to several microseconds and vanishes to zero only after a few seconds.

In comparison, at $T = 198\,\mathrm{K}$ (figure 2b), the TA signals show clearly decelerated decay dynamics affecting much stronger the blue than the red spectral range, the maximum for 445 nm and 488 nm being preceded by an almost flat stage up to the millisecond time regime. The blue absorption signal vanishes to zero only after a duration of tens of seconds. This behavior suggests a pronounced time delay between the decaying red and increasing blue transients and can, in fact, be observed for various reduction and oxidation pre-treatments, i.e., for differently adjusted $[\mathrm{Fe}^{2+}]/[\mathrm{Fe}^{3+}]$ ratios between 0.01 and 0.19.

Previously, Berben *et al.* [26] and Herth *et al.* [25] reported that a sum of stretched-exponential functions (Kohlrausch-Williams-Watts function, KWW)

$$\alpha_{\mathrm{li}}(t, \lambda, T) = \sum_{i=1}^{N} \alpha^0_{\mathrm{li},i}(\lambda, T) \cdot \exp\left[-\left(\frac{t}{\tau_i(\lambda, T)}\right)^{\beta_i(\lambda,T)}\right], \tag{1}$$

is a reasonable ansatz for the description of the temporal behavior of the transient absorption in Fe:LN. Accordingly, equation (1) has been fitted to the entire exper-

imental data set as represented in figure 2 by the continuous yellow lines. For the absorption at 785 nm a single KWW-function is used to describe the data ($N = 1$), while $N = 2$ is chosen for all other wavelengths. The obtained values of the fitting parameters providing a fair description of the results are presented in Table 1 for both temperatures and all four probe wavelengths. The mean relaxation and build-up times for the various components defined by

$$\begin{aligned}\langle \tau_i(\lambda, T) \rangle &= \int_0^\infty \exp\left[-(t/\tau_i(\lambda, T))^{\beta_i(\lambda,T)}\right] dt \\ &= \tau_i(\lambda, T)\Gamma\left(\frac{1}{\beta_i(\lambda, T)} + 1\right) \end{aligned} \tag{2}$$

are also included in Table 1. Here, Γ denotes the gamma function. It should be noted that the error intervals for $\langle \tau_i(\lambda, T) \rangle$ can be close to the order of the calculated value itself due to the combined error of β and τ. Still, the activation energies given in section 5 can be estimated very well, as we deal with different orders of magnitude of the decay time $\langle \tau_i(\lambda, T) \rangle$ at different temperatures. Furthermore, a large number of separate measurements over a broad temperature range is available.

	293 K											
	445 nm			488 nm			633 nm			785 nm		
$\alpha^0_{\mathrm{li},1}$ (m^{-1})	−72	±	10	−25	±	5	184	±	10	191	±	10
τ_1 (μs)	5	±	3	2	±	1	6	±	2	4	±	2
β_1	0.39	±	0.04	0.30	±	0.03	0.32	±	0.03	0.29	±	0.03
$\langle\tau_1\rangle$ (μs)	18	±	16	19	±	17	42	±	30	43	±	42
$\alpha^0_{\mathrm{li},2}$ (m^{-1})	99	±	10	41	±	5	21	±	5		−	
τ_2 (s)	4	±	2	7	±	4	9	±	4		−	
β_2	0.61	±	0.06	0.64	±	0.06	0.62	±	0.06		−	
$\langle\tau_2\rangle$ (s)	5.9	±	3.0	9.7	±	6.0	13	±	6.5		−	
	198 K											
	445 nm			488 nm			633 nm			785 nm		
$\alpha^0_{\mathrm{li},1}$ (m^{-1})	−41	±	10	−16	±	5	227	±	10	238	±	10
τ_1 (μs)	(20	±	10) $\cdot 10^3$	(9	±	4) $\cdot 10^3$	121	±	30	40	±	10
β_1	0.52	±	0.05	0.69	±	0.07	0.22	±	0.02	0.18	±	0.01
$\langle\tau_1\rangle$ (μs)	(37	±	3) $\cdot 10^3$	(12	±	6) $\cdot 10^3$	(68	±	62) $\cdot 10^3$	(13	±	10) $\cdot 10^3$
$\alpha^0_{\mathrm{li},2}$ (m^{-1})	82	±	10	37	±	5	14	±	5		−	
τ_2 (s)	20	±	10	26	±	10	25	±	10		−	
β_2	0.9	±	0.1	0.9	±	0.1	0.8	±	0.08		−	
$\langle\tau_2\rangle$ (s)	21	±	11	27	±	11	28	±	15		−	

Table 1: Parameters of the KWW-function used to describe the TA of the 0.1 mol% Fe:LN sample at $T = 293$ K and 198 K exemplarily for the data set depicted in figure 2.

At RT, all transients seem to be in accordance with the model proposed by Herth *et al* [25]. In the red spectral range, the initial absorption change α^0_{li} is attributed to the formation of $\mathrm{Nb}^{4+}_{\mathrm{Li}}$ bound electron polarons excited either from the valence band or $\mathrm{Fe}^{2+}_{\mathrm{Li}}$ to the conduction band by a two-photon or one-photon process, respectively. The initial absorption change in the blue spectral range can be assumed to originate from various sources. There is a negative contribution, i.e., induced transparency due to the transformation of the $\mathrm{Fe}^{2+}_{\mathrm{Li}}$ (part or all) into non-absorbing $\mathrm{Fe}^{3+}_{\mathrm{Li}}$ centers [1,18]. A positive contribution comes from valence band holes trapped next to Li vacancies as $\mathrm{O}^- - \mathrm{V}_{\mathrm{Li}}$ hole polarons together with a much smaller positive contribution coming from the overlapping absorption tail of the $\mathrm{Nb}^{4+}_{\mathrm{Li}}$ bound electron polarons formed during the parallel electron trapping event.

According to the Herth model, the hopping motion of electron polarons may lead to the formation of stable or intermediate Fe_{Li}^{2+} centers, resulting in the decrease of red absorption and to the simultaneous appearance of the rising component in the blue on the microsecond timescale, which is in agreement with the coincidence of the values τ_1, β_1 and $\langle\tau_1\rangle$ measured at RT for different wavelengths simultaneously. Some of the Fe_{Li}^{2+} centers might be metastable (e.g. due to their specific charge compensation), whereby electron trapping and release at such iron centers could occur repeatedly while electrons recombine with all available pump-induced trapped-hole centers; this process could lead to a decrease of the blue absorption of both trapped holes and metastable Fe_{Li}^{2+} centers, contributing to some (rather) long TA component. This model neglects the formation of Nb_{Li}^{4+} electron polarons between possible repeated trapping events on iron which can be justified by Nb_{Li}^{4+} lifetimes shorter by several orders of magnitude than those of metastable Fe_{Li}^{2+} centers (a similar argument explains the neglect of Nb_{Nb}^{4+} free polarons compared to Nb_{Li}^{4+} bound ones at faster stages).

In contrast, cooling the sample by $\approx 100\,\mathrm{K}$ (figure 2b) results in clear changes that are no longer consistent with Herth's model assuming the same τ_1 and β_1 for all probe wavelengths. In particular significant deviations appear in the first few milliseconds in this low temperature regime (dashed red lines in figure 2). The non-zero blue absorption remains remarkably constant during most of the Nb_{Li}^{4+} decay, prior to its rise to an interim maximum value. Adopting for $\tau_1(445/488\,\mathrm{nm}, 198\,\mathrm{K})$ and $\beta_1(445/488\,\mathrm{nm}, 198\,\mathrm{K})$ the values $\tau_1(785\,\mathrm{nm}, 198\,\mathrm{K})$ and $\beta_1(785\,\mathrm{nm}, 198\,\mathrm{K})$ obtained at 785 nm as fixed parameters, i.e., applying the Herth model, the data set cannot be reconstructed by a converging fit. The only way to reach a very good fit quality is by treating the τ_1 and β_1 parameters at various wavelengths as independent free parameters in the fitting procedures (cf. yellow lines in figure 2). The decay time in the near-infrared and the rise time in the blue deviate by a factor of 100 and only the mean relaxation/build-up times $\langle\tau_1(\lambda, 198\,\mathrm{K})\rangle$ have approximately the same values. The bound polarons thus seem to disappear without having recombined simultaneously with holes or having promptly filled $Fe_{Li}^{3+/2+}$ traps, and reappear only later as Fe_{Li}^{2+} centers. This trend is already indicated for temperatures below $\approx 250\,\mathrm{K}$.

The considerable displacement of the TA signal towards longer times and its changed shape at low temperatures have to be described by strongly increased τ_1 and β_1 values in the blue ($\lambda = 445/488\,\mathrm{nm}$) compared to a moderately rising τ_1 and decreasing β_1 in the red region. The increased stretching factor $\beta_1(488\,\mathrm{nm}, 198\,\mathrm{K}) = 0.69$ in the blue has to be contrasted with its decreased value $\beta_1(785\,\mathrm{nm}, 198\,\mathrm{K}) = 0.18$ in the red (Table 1). The slow decreasing component shows an even larger β value in the blue: $\beta_2(445/488\,\mathrm{nm}, 198\,\mathrm{K}) = 0.9$. The weakly defined mean values $\langle\tau\rangle$ show much less variation which is also due to the fact that different combinations of τ and β can, by coincidence, lead to the same value of $\langle\tau\rangle$.

Taking into account the widely accepted interpretation of β [33–35] including the attempt of Merschjann *et al.* [36] to relate τ and β directly to characteristic parameters of the hopping transport (time of a single hopping event, number of hopping events, etc.), means that the blue transients have a much weaker dependence on hopping history before annihilation than the respective transients in the red. While the electron polaron decay for lower temperatures is increasingly characterized by slow hopping, the blue transients become nearly mono-exponential.

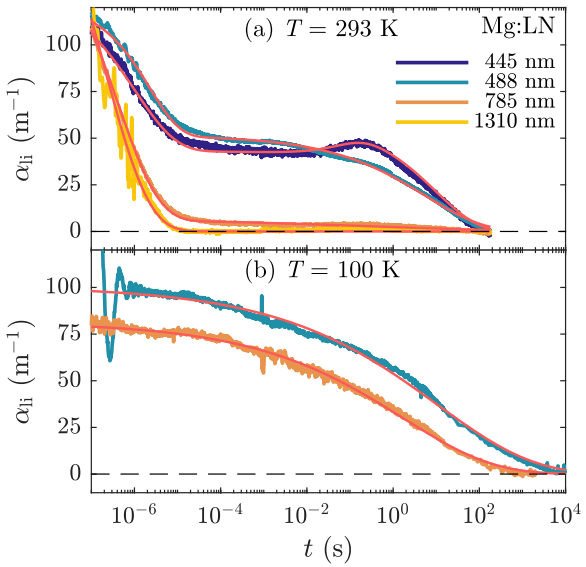

Figure 3: Temporal development of the light-induced absorption in Mg:LN at (a) $T = 293\,\mathrm{K}$ and (b) $T = 100\,\mathrm{K}$ for a pump pulse intensity of $I_\mathrm{P} \approx 130\,\mathrm{MW/cm^2}$. The red lines represent fits of equation (1) to the experimental data. Fitting results are summarized in Table 2.

These data point to a clear failure of the Herth model and support the previous reports on inconsistencies in Fe:LN crystals under rather different conditions. In particular at low temperatures and with probing wavelengths in the blue and near-infrared spectrum, we are faced by two striking experimental observations: (i) the decay of bound polaron absorption in the near-infrared is not correlated with the increase of the $\mathrm{Fe}_{\mathrm{Li}}^{2+}$ absorption anymore, and (ii) there is a strong discrepancy of the determined β value with the state-of-the-art knowledge for small, strong-coupling polaron dynamics in LN [26, 35, 37] to be further discussed in section 5. At the same time, these data are not sufficient to conclude a general failure of the Herth model, i.e., that Herths' model also fails for the description of TA in LN crystals of different stoichiometry and/or with/without different dopants (including non-photorefractive defect centers). In what follows, we intend to exclude that the failure is solely related to the dominating existence of $\mathrm{Fe}_{\mathrm{Li}}^{2+/3+}$ by means of equivalent TAS studies with over-threshold Mg:LN.

4.2 Transient absorption experiments in Mg-doped lithium niobate

The dynamics of the transient absorption in Mg:LN at 445 nm, 488 nm, 785 nm, and 1310 nm at RT (the latter approximately centered on the broad absorption band of $\mathrm{Nb}_{\mathrm{Nb}}^{4+}$ free polarons) is depicted in figure 3, showing, in addition to a fast decreasing transient on the same time scale for all wavelengths, a long-lived transient blue absorption as previously reported by Conradi *et al.* [24]. However, in comparison to former studies a new probe at 445 nm was applied and we were able to observe an unexpected feature, i.e., a clear increase in the absorption at surprisingly long timescales. The newly measured transient local maximum for 445 nm is observed

after a significant period (few milliseconds) of constant absorption that resembles the dominant feature of the low-temperature TA dynamics of Fe:LN. This corresponds to a small rising component (denoted by the index 1b) with a time constant $\tau_{1b}(445\,\mathrm{nm}, 293\,\mathrm{K}) = (70 \pm 20)\,\mathrm{ms}$. The fitting parameters derived for all KWW components in Mg:LN are summarized in Table 2, essentially coinciding at RT with those reported in Ref. [24]. The fast component on the microsecond timescale (denoted by the index 1a) is decreasing in the blue region at variance from the case of Fe:LN. The slow component extends to hundreds of seconds in the visible and is absent in the infrared as in Fe:LN.

The dynamics in Mg:LN at RT should be compared to scenarios in Fe:LN taking into account the changed defect structure of Mg:LN: i) $\mathrm{Nb_{Li}}$ antisites and most $\mathrm{Fe_{Li}}$ centers are missing as indicated by the vanishing photorefractive effect in over-threshold crystals [38], ii) a portion of $\mathrm{Mg^{2+}}$ dopant ions and some of the background Fe impurities on the ppm level are incorporated on Nb sites [39,40], where their charge state remains fixed.

The lack of $\mathrm{Nb_{Li}}$ antisites results in an increase of the electron polaron hopping frequency, now occurring in the regular Nb sublattice, leading to a shortening of τ_1 by nearly an order of magnitude, compared to Fe:LN, so that $\tau_1(785/1310\,\mathrm{nm}, \mathrm{RT}) \approx 0.3\,\mu\mathrm{s}$. Accordingly, there are even longer delays (compared to Fe:LN) between this fast decay of free polarons and the slower components in the blue. Due to the small number of $\mathrm{Fe_{Li}^{2+}}$ centers, a significant influence on the TA can be excluded as supported also by the monotonous decrease of the 488 nm TA signal in the entire observed temporal region. Only the small rising component τ_{1b} at 445 nm extending into the 70 millisecond range has to be attributed to background Fe impurities, based on the analogy with component τ_1 in Fe:LN. The fast blue TA component in Mg:LN, temporarily locked with polaron decay monitored in the near-infrared, can be attributed to a direct process of polaron recombination with trapped-hole centers. For $T < 100\,\mathrm{K}$, TA signals in Mg:LN extend to several minutes both in the near-infrared and the blue region due to the slow hopping of polarons and delays in the recombination processes. Therefore, the three KWW-components in the blue spectral range cannot be satisfactorily distinguished anymore due to similar decay times of several overlapping TA components. A single-component fit at $T = 100\,\mathrm{K}$ and $\lambda = 488\,\mathrm{nm}$ yields $\tau \approx 10\,\mathrm{s}$ and $\beta \approx 0.19$, and therefore $\langle\tau\rangle \approx 1.9 \cdot 10^3\,\mathrm{s}$. The latter is much longer in comparison to the value determined in the near-infrared, thus indicating the presence of the RT processes at low temperatures, as well. The values obtained for 785 nm and 488 nm are summarized in Table 2.

Apart from the latter process, the RT TA-data in Mg:LN thus clearly resemble the findings in Fe:LN, and further stress the failure of the original microscopic model for polaronic recombination. Similarly to the case of Fe:LN the model cannot be corrected by simply considering some process of more complex type but involving only single-electron transfers. Instead, a more complex electronic center, the STE, having clear fingerprints for its identification, will be discussed in more detail below.

	293 K				100 K	
	445 nm	488 nm	785 nm	1310 nm	488 nm	785 nm
$\alpha^0_{\mathrm{li,1a}}$ (m^{-1})	90 ± 10	71 ± 10	177 ± 10	248 ± 20	100 ± 5	81 ± 10
τ_{1a} (μs)	1.0 ± 0.2	2.3 ± 0.5	0.4 ± 0.1	0.2 ± 0.1	(10 ± 5) $\cdot 10^6$	(1.7 ± 1) $\cdot 10^6$
β_{1a}	0.45 ± 0.1	0.62 ± 0.1	0.44 ± 0.1	0.45 ± 0.1	0.19 ± 0.01	0.19 ± 0.01
$\langle\tau_{\mathrm{1a}}\rangle$ (μs)	2.5 ± 1.5	3.3 ± 1.1	1.0 ± 0.6	0.5 ± 0.3	(1890 ± 1200) $\cdot 10^6$	(321 ± 200) $\cdot 10^6$
$\alpha^0_{\mathrm{li,1b}}$ (m^{-1})	−15 ± 5	–	–	–	–	–
τ_{1b} (ms)	70 ± 20	–	–	–	–	–
β_{1b}	0.8 ± 0.2	–	–	–	–	–
$\langle\tau_{\mathrm{1b}}\rangle$ (ms)	79 ± 40	–	–	–	–	–
$\alpha^0_{\mathrm{li,2}}$ (m^{-1})	58 ± 10	51 ± 5	6 ± 2	–	–	–
τ_2 (s)	10 ± 3	6 ± 2	5 ± 3	–	–	–
β_2	0.45 ± 0.05	0.32 ± 0.04	0.25 ± 0.1	–	–	–
$\langle\tau_2\rangle$ (s)	25 ± 10	42 ± 24	120 ± 110	–	–	–

Table 2: Parameters of the KWW-function used to describe the TA of the 6.5 mol% Mg:LN sample at $T = 293\,\mathrm{K}$ and $T = 100\,\mathrm{K}$ (figure 3).

5 Is there any experimental fingerprint pointing to a role of STE's in the polaronic recombination process?

The PL spectra presented in section 3 clearly indicate the presence of STEs over the temperature range 15–300 K suggesting that STEs should not be neglected in non-radiative recombination processes either. In order to find the various transient manifestations of STEs, in this section temperature-dependent TRPL measurements are presented and combined with corresponding TA results. The temperature dependence of the stretching coefficient $\beta(T)$ will be shown to be an unambiguous fingerprint for a clear separation between STE-related phenomena on the one hand and processes determined by the hopping of electron polarons on the other hand. This distinction is also supported by the different Arrhenius-type activation energies obtained from the respective time constants. First we use Mg:LN in order to benefit from the comparison with the characteristic blue PL feature, then turn to the peculiarities offered by Fe:LN.

5.1 Stretching-factors and activation energies in the photoluminescence and transient absorption of Mg:LN

Figure 4a shows the TRPL of Mg:LN upon ns-pulse exposure at 355 nm ($I_{\mathrm{P}} \approx 100\,\mathrm{GW/m^2}$, extraordinary polarization) for the emission wavelength of 460 nm for a series of temperatures in the broad range from 15 K to 200 K in a semi-logarithmic plot. For comparison, all data have been normalized to the maximum luminescence signal at $t = 10^{-7}\,\mathrm{s}$. With increasing temperature the luminescence decay time is found to decrease from the milli- to the microsecond time range as expected from the studies of Powell and Freed, and Fischer *et al.* [21, 23]. For a quantitative analysis, and according to Zatryb *et al.* [41], the evolution rate of excited emitters has to be considered, so that the first time derivative of the stretched-exponential KWW

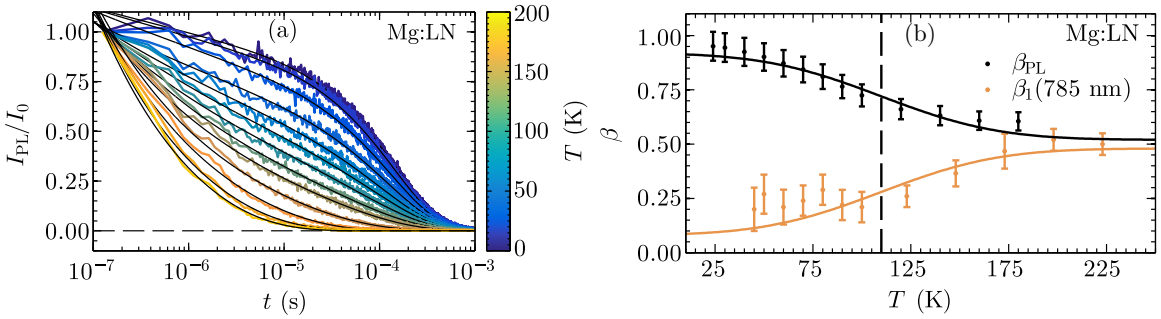

Figure 4: (a) Temporal decay of the PL intensity at 460 nm Mg:LN following exposure to a single ns laser pulse for temperatures given by the color code. The signal is normalized to the value determined at $t = 10^{-7}$ s; the black lines represent fits to the experimental data using equation (3). (b) Temperature dependence of the stretching-factors: β_{PL} (black) obtained from fitting equation (3) to the luminescence decay data and $\beta_1(785\,\text{nm})$ (orange) obtained from fitting equation (1) to TA results in Mg:LN. The solid lines are phenomenological descriptions of the $\beta(T)$ behavior with an error-function. The dashed line represents a common inflection point at $T_\beta^{Mg} = (110 \pm 10)$ K.

function is used for the fitting procedure:

$$I(t,T) = I_0(T) \cdot t^{(\beta_{PL}(T)-1)} \cdot \exp\left[-\left(\frac{t}{\tau_{PL}(T)}\right)^{\beta_{PL}(T)}\right]. \tag{3}$$

As shown by the black lines in figure 4a, very good correspondence could be achieved between equation (3) and the experimental data using only a single KWW component with two independent fitting parameters, the stretching coefficient $\beta_{PL}(T)$ and the decay time $\tau_{PL}(T)$, giving further support to the unambiguous (STE-related) origin of the PL observed. The dependence $\beta_{PL}(T)$ depicted in figure 4b is in full accordance with a trend recently recognized in a smaller temperature interval by Kämpfe *et al.* [19]. The change of $\beta_{PL}(T)$ is very significant and represents a transition from unity for a mono-exponential function at $T \approx 25$ K to the stretched case $\beta_{PL} \approx 0.6$ at $T \approx 180$ K (cf. figure 4b). The decay time $\tau_{PL}(T)$ remains nearly constant for temperatures below 100 K with a value of $\tau \approx 10^{-4}$ s whereas an Arrhenius-like behavior with an activation energy $E_A \approx 0.09$ eV is found for $T \gg 100$ K.

We interpret both findings by assuming that at low T the decay time of the luminescence is defined by a localized process where hopping is suppressed leading to a single exponential decay ($\beta_{PL} = 1$). As the temperature is increased above 100 K, the steep decrease of both τ and the stretching exponent β suggests that a hopping process becomes dominant. To explain the extremely low activation energy for luminescence decay, we assume that hopping of the STE as a whole is involved. In comparison, for free polaron hopping a clearly larger activation energy $E_A \approx 0.26$ eV can be derived from the observed temperature dependence of the mean relaxation time $\langle\tau_1(785\,\text{nm}, T)\rangle$ which also follows an Arrhenius behavior for $T > 100$ K in our Mg:LN sample; practically the same value has been estimated earlier as one fourth of the optical excitation energy ≈ 1 eV of Nb_{Nb}^{4+} [12, 42]. Accordingly the temperature dependence of β_{PL} has to be attributed to the hopping of STEs and their subsequent localized recombination.

Comparing $\beta_{PL}(T)$ with TA measurements of $\beta_1(785\,\text{nm}, T)$ on Mg:LN displaying the behavior expected for polaron hopping (cf. figure 4b), it is immediately clear

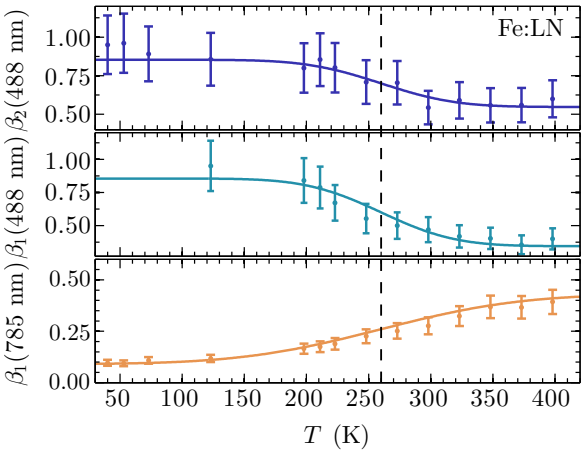

Figure 5: Temperature dependence of the stretching-factors $\beta_1(785\,\mathrm{nm}, T)$, $\beta_1(488\,\mathrm{nm}, T)$, and $\beta_2(488\,\mathrm{nm}, T)$ in Fe:LN. The solid lines are qualitative descriptions of the $\beta(T)$ behavior with an error-function. The dashed line represents a common inflection point at $T_\beta^{\mathrm{Fe}} = (260 \pm 10)\,\mathrm{K}$.

that $\beta_{\mathrm{PL}}(T)$ exhibits a reversed temperature dependence. We chose $\lambda = 785\,\mathrm{nm}$ as a probe wavelength where the largest contribution, in the absence of antisites, can be attributed to $\mathrm{Nb}_{\mathrm{Nb}}^{4+}$ free polarons. Both types (TRPL and TA) of temperature behavior in figure 4b can be described phenomenologically, e.g., by an error-function with a common inflection point at $T_\beta^{\mathrm{Mg}} = (110 \pm 10)\,\mathrm{K}$ indicating the temperature where the processes due to hopping become dominant. Thus, the given reverse type of $\beta_{\mathrm{PL}}(T)$ dependence, can be regarded as a fingerprint of STEs, in contrast to the $\beta(T)$ behavior observed for small electron polarons; this is supported by the fact that the activation energies obtained for luminescence and red/near-infrared absorption decay are different requiring a second hopping entity, STEs. Note, that even though the transients in luminescence and absorption are on different timescales, a comparison between the $\beta(T)$ behaviors may be justified as the stretching-factor is a good indicator for the type of transport and annihilation processes involved.

5.2 Stretching-factors and activation energies in the transient absorption of Fe:LN

In this section detailed temperature-dependent measurements of the red and blue TA on Fe:LN are presented with the goal to uncover similar fingerprints. The obtained behavior of the various stretching-factors $\beta_i(\lambda, T)$ is shown in figure 5. Results in the red and blue spectral range differ in two major points: (i) with decreasing temperatures $\beta_1(T)$ is observed to decrease in the red spectral range, compared to the opposite behavior of both $\beta_1(T)$ and $\beta_2(T)$ in the blue (see figure 5, but also Table 1). Both types of temperature behavior in figure 5, again, can be described by an error-function (orange and blue lines in figure 5) where $T_\beta^{\mathrm{Fe}} = (260 \pm 10)\,\mathrm{K}$ is discovered as a common inflection point. (ii) At higher temperatures, the mean decay times $\langle \tau_i(\lambda, T) \rangle$ follow an Arrhenius behavior, however, for temperatures $T < T_\beta^{\mathrm{Fe}}$ the mean decay times in the blue range become nearly temperature-independent. The obtained activation energy $E_{\mathrm{A}}^1(785\,\mathrm{nm}) \approx 0.37\,\mathrm{eV}$ apparently corresponds to polaron hopping

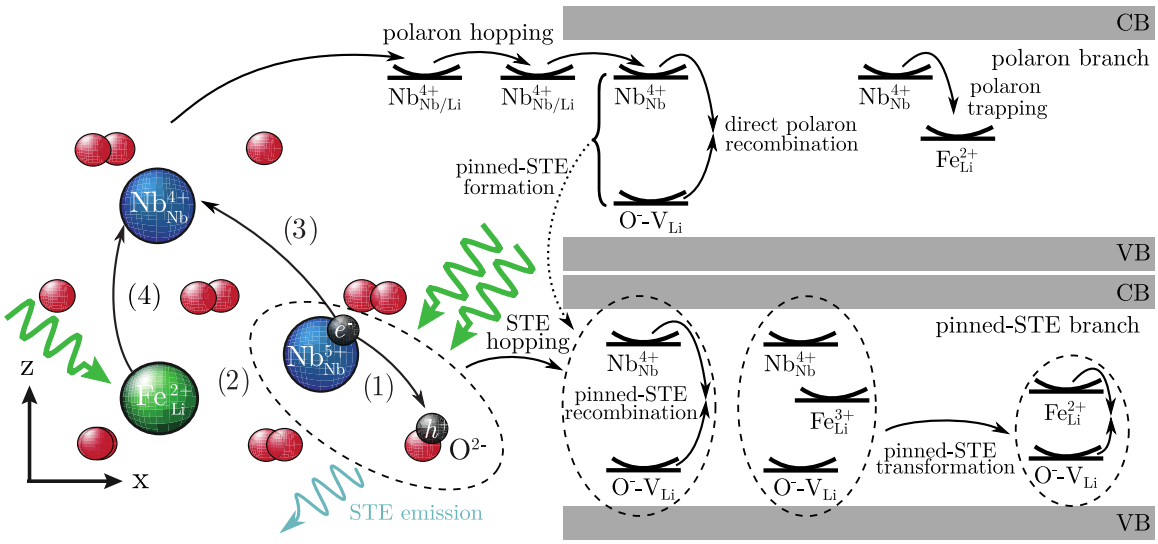

Figure 6: Excitation and recombination model after pulse exposure (green thick arrows) in LN. Hot electron-hole pairs created by the pump pulse in a two-photon process either recombine directly (1), form STEs within NbO_6 octahedra (2), or dissociate to form separate oppositely charged small polarons (3), as a further option, electrons from Fe^{2+}_{Li} may be excited to form additional small polarons leaving back Fe^{3+}_{Li} (4). The recombination paths are divided into a polaron and an exciton branch, for more detail see text.

in the presence of antisites (to be compared to one fourth of the optical excitation energy $\approx 1.6\,\mathrm{eV}$ of Nb^{4+}_{Li} [12]). It should be added that the most recent value of the polaron stabilization energy was determined to $\approx 0.75\,\mathrm{eV}$ [37]. The activation energies derived for the blue region, $E^1_A(488\,\mathrm{nm}) \approx 0.71\,\mathrm{eV}$ and $E^2_A(488\,\mathrm{nm}) \approx 0.78\,\mathrm{eV}$ are correspondingly higher and will be discussed in section 6.

The temperature dependence of the stretching exponents $\beta_1(T)$ and $\beta_2(T)$ in the blue of the TA of Fe:LN (figure 5) qualitatively shows the same fingerprint behavior as $\beta_{PL}(T)$ obtained from time-resolved luminescence measurements on Mg:LN (figure 4b). The similar dynamics of the considered blue transients in emission and absorption strongly suggests their common origin, namely STEs. In Mg:LN the temperature $T^{Mg}_\beta \approx 110\,\mathrm{K}$ equally characterizes the onset of polaronic and excitonic hopping processes observed in transient absorption and luminescence decay, respectively. In Fe:LN, the $T^{Fe}_\beta \approx 260\,\mathrm{K}$ value reflects the smaller mobility of the polarons and a parallel change in electron-phonon coupling due to the presence of antisite Nb defects, as compared to Mg:LN where antisites are absent. These findings will be used in the following section to reconsider the microscopic polaronic recombination model in LN.

6 Extension of the microscopic model by STE's and pinned STE's

So far, our analysis was able to answer the most striking questions related to the role of STEs in the polaronic recombination processes in LN. First, it is clearly demonstrated, that the observed, pulse-induced blue-green luminescence in LN can be attributed to

the decay of STEs up to RT. Second, the failure of the microscopic model comprising solely small electron and hole polarons is highlighted and evident as soon as the temperature is reduced or the doping is changed. Third, the stretching factors and activation energies are recognized to yield sensitive information on the dynamics of both PL and TA indicating the presence of STEs.

As a result, it becomes necessary to extend the microscopic picture by including the additional electronic states of STEs and STEs pinned on defects, as schematically depicted in figure 6. As a matter of fact, such pinned STEs (i) may be long-lived, (ii) should absorb in the blue spectral range, and (iii) decay preferably non-radiatively and, thus, considerably contribute to the blue TA in LN crystals. We like to note that the alternative consideration of an interim formation of bipolarons, that are strongly absorbing in the blue region (see e.g. [11,18]), would not explain the delayed appearance of the blue component in Fe:LN. The same holds for Mg:LN due to the lack of antisites. We will thus disregard the presence of bipolarons in our model approach, though it may be included if thermally reduced LN is considered.

As seen on the left-hand side of figure 6, the starting situation can be summarized as follows: immediately (on the ps scale) after the pump pulse, a given concentration of free or bound electron polarons and holes is created, together with a certain amount of emptied Fe_{Li}^{3+} traps [4, 42]. Small electron polarons forming the polaron branch (upper right-hand part of figure 6) move through the lattice by thermally activated hopping [43, 44] which terminates in deep traps like Fe_{Li}^{3+} converting to Fe_{Li}^{2+} or they annihilate with trapped holes. However, depending on conditions of temperature and composition, a considerable concentration of STEs, disregarded in earlier TA studies, may be present as well, as indicated by luminescence. Since this radiative recombination is observed to be orders of magnitude faster than the small polaron decay time measured by TA (cf. our measurements), we can assume that it stems from STEs formed directly after light exposure forming a second relaxation channel parallel to the polaron recombination. Besides the possibility to recombine radiatively, the STE is the starting point of a pinned-STE branch (lower right-hand part of figure 6) which will be described in more detail in the following.

6.1 (Pinned) STEs in LN

STEs may be assumed to have a significant hopping mobility as confirmed by the presence of a thermally activated process ($E_A \approx 0.09\,\mathrm{eV}$) of the luminescence decay. At higher temperatures and in defective materials, STEs formed at early stages of pumping are expected to get pinned on defects, similarly to the formation and trapping of single-site small polarons. Resonant excitonic/energy transfer can be discarded due to the large Stokes shifts. In particular, STEs may be captured, among others, by the same defects as free holes (e.g. by lithium vacancies or Mg_{Nb}^{2+} defects). The final recombination site should play a decisive role, especially at lower temperatures, when localization sets in and τ gets nearly temperature-independent. The exact optical properties depend on the presence and type of defects adjacent to the niobium-oxygen octahedron containing the STE as shown by luminescence studies in LN with various stoichiometric compositions [16] including also crystals with ilmenite type cationic stacking order [17]. While the presence of Mg up to the $\approx 5\,\mathrm{mol\%}$ threshold,

i.e., the elimination of antisites, leads to increased emission [21], Fe doping seems to lead to luminescence quenching comparable to the case of Cr doping [23], indicating that both intrinsic defects and Fe form pinning centers for STEs where luminescence is suppressed. Non-radiative decay should be strongly preferred for STEs pinned on defects with high pinning/stabilizing energies leading to the longer absorption decay times and higher activation energies as observed for TA in the blue. In this case, the decreasing $\beta_{\mathrm{PL}}(T)$ function characterizes the temperature dependent pinning history of the STE influencing its decay. The existence of a second, slow component, with activation energies slightly larger than in our case (0.14 eV and 0.11 eV) valid above somewhat higher temperatures 140 K and 160 K for the respective luminescence components, obtained in 7.5 mol% Mg-doped samples by Kämpfe *et al.* [19], may then be attributed to minor deviations from the crystal structure optimal for luminescence. It should be noted that pinned STEs might also be formed as interim states during the recombination of electron polarons with trapped-hole centers.

6.2 Absorption properties of (pinned) STEs

STEs, which have been established in various materials, e.g., alkali halides, beside their capability to decay radiatively, have absorption bands similar to those of small polarons as demonstrated by Williams *et al.* [5, 45]. As pointed out by these authors, the hole and electron, which a STE consists of, can be excited optically and show a near ultraviolet and a near-infrared absorption, respectively, corresponding to optically triggered jumps of the respective constituent to equivalent neighboring sites. In LN, due to the transfer of the hole constituent to an equivalent or non-equivalent neighboring oxygen site, STEs are also expected to have an absorption in the blue/near-ultraviolet region. However, a separate contribution of the radiatively decaying STEs to the TA at the measured wavelengths was not observed even in Mg:LN at low temperatures although the luminescence and TA decay times deviate by a factor of at least 1,000 from each other and a TA of such STEs – if present – should have been clearly visible. Furthermore, to the best of our knowledge, evidence for the presence of excitonic infrared/ultraviolet absorption in LN is not reported in literature, so far.

Concerning the absorption properties of pinned STEs, we have no experimental indication for the presence of a near-infrared absorption. The "quenching" of infrared-absorption may be understood by taking into account proposed dynamic or static models of trapped hole O^- centers containing a unique Nb neighbor in a strongly preferred position for electron trapping [46, 47]. In such cases electron hopping may be hampered or requires much higher energy. The blue/ultraviolet absorption of pinned STEs, though present, might be nearly indistinguishable from the absorption of an O^- trapped hole.

6.3 Two-step recombination model of STEs pinned on Fe^{3+} centers

STEs should also be capable to get pinned on iron centers. Most Fe^{3+}_{Li} centers in LN may be assumed to have a nearest neighbor charge-compensating lithium vacancy

(V_{Li}) suggesting the following scenario: the constituents of a nearby STE are attracted by the constituents of the $Fe_{Li}^{3+} - V_{Li}$ dipole leading to an STE pinned on $Fe_{Li}^{3+} - V_{Li}$ with the Nb^{4+} and O^- sites at nearest neighbor positions of the Fe_{Li}^{3+} and V_{Li} sites, respectively. A single jump of the electron from Nb_{Nb}^{4+} to the Fe site (along the c axis) transfers the complex into a new state, which is a coupled $Fe_{Li}^{2+} - O(V_{Li})^-$ defect. Both Fe_{Li}^{2+} and the hole constituent absorb in the blue, their aggregate causing a net increase of the total blue TA with respect to the pinned STE absorption, thus providing a rising TA component. However, this new defect state again has a metastable excitonic character and tends to recombine, restoring the original $Fe_{Li}^{3+} - V_{Li}$ defect having no absorption at all. Thus we consider a strongly localized two-step STE recombination process where the electron constituent, starting from a Nb_{Nb}^{4+} state, proceeds to a lower Fe_{Li}^{2+} level before rejoining its O^- partner. Since both the pinned STE and the intermediary $Fe_{Li}^{2+} - O(V_{Li})^-$ complex can be assumed to have metastable ground states with differently relaxed lattice environments, both jumps have to be phonon-induced/assisted, and may involve significant, separate temperature dependent time delays. This two-step STE recombination path, leading to an interim TA maximum with a subsequent steep decay clearly explains the most conspicuous features of the TA at 445 nm, while it seems to be much less pronounced at 488 nm. As the second jump seems to take significantly longer than the first, a description in terms of two separate KWW-functions has to be a good approximation.

The derived activation energies support the two-step relaxation model of the STE pinned on $Fe_{Li}^{3+} - V_{Li}$ yielding $E_A^1 \approx 0.71$ eV for the first and a larger $E_A^2 \approx 0.78$ eV for the second step, the latter corresponding to the decay of the strongly distorted $Fe_{Li}^{2+} - O(V_{Li})^-$- state, and roughly equaling one fourth of the strong absorption measured at 445 nm (2.79 eV). A similar ratio may hold for the STE pinned on $Fe_{Li}^{3+} - V_{Li}$ in the first step as well, confirming $\propto E_{opt}/4$ as the activation energy characterizing the hopping of a polaron from a given site to an adjacent one [12]. Negligible differences between 488 nm and 445 nm data (τ, β) in Fe:LN indicate small superpositions from other recombination centers not containing Fe.

At low temperatures the proposed two-step relaxation of the STE pinned on $Fe_{Li}^{3+} - V_{Li}$ clearly dominates the 445 nm TA spectrum in Fe:LN for $t > 10$ ms (see figure 2b). While these two steps seem to explain both the rising and decreasing 445 nm components in Fe:LN, an important contribution to the long decreasing component in Mg:LN may come from STEs pinned on hole-trap defects like (V_{Li})-pinned STEs. Contributions from such pinned STEs correspond to centers with observed lifetimes in the minute range and have been attributed to O^--type centers in 5 mol% Mg-doped LN by Xin *et al.* [40]. In fact, our probe wavelengths are in the central part of the $O(V_{Li})^-$ and on the very wing of a TA band attributed to $O^-(Mg_{Nb}^{2+})$ centers in Ref. [40].

Accordingly the first-step lifetime of the ($Fe_{Li}^{3+} - V_{Li}$)-pinned STE state recombination may correspond to the lifetimes of the rising components τ_1 and τ_{1b} observed at 445 nm in Fe:LN at low temperatures and in Mg:LN at RT, respectively. In contrast, much longer second-step lifetime may correspond to τ_2 of the long decreasing component at 445 nm in Fe:LN. The separation of time domains of polaron and pinned-STE decay is rather large in Mg:LN (figure 3). However, there may be a considerable overlap in Fe:LN at RT which resulted in the earlier misinterpretation of the blue TA

components discussed above.

7 Summary and conclusion

In this paper the question is answered whether STEs play a role in polaronic recombination processes in LN. In a first step it was shown that STEs can be optically generated in Mg:LN in the whole temperature range from 15–300 K. In particular, our data, collected for the first time continuously up to 300 K, demonstrate that the PL signal can clearly be assigned to similar STEs in the entire temperature range.

In the next step shortcomings of earlier microscopic polaronic recombination models were demonstrated. Transient absorption measurements in an extended temperature and spectral range on Fe:LN and Mg:LN reveal inconsistencies when Herth's model is applied on these new data sets: (i) the decay of bound polarons absorbing in the near-infrared is not correlated with the increase of blue absorption, (ii) the fact that the β coefficient in the blue spectral range is larger for lower temperatures is in contrast to the state-of-the-art knowledge for small, strong-coupling polaron dynamics in LN.

Third, the temperature-dependent TA was compared with the corresponding TRPL data to check whether features in TA could also be attributed to STEs. The striking increase of the stretching factor β with decreasing temperature attributed to STEs in TRPL, but present also in TA in the blue spectral range, was found to be such a fingerprint. In fact, this is in contrast to the usual $\beta(T)$ behavior which is expected for small polarons in LN.

Based on these results, we propose and discuss for the first time an excitation and recombination model by including a STE branch in addition to the established polaron recombination branch. Both together are capable to describe in a comprehensive model TA and PL over a broad temperature-range. Here, STEs and pinned STEs formed during or immediately after pumping were found to be important transporters of negative charges towards deep Fe^{3+} traps. The presence of long-lived perturbed O^- centers containing an adjacent lithium vacancy in their clusters have to be assumed in both LN systems, while a second distinct group of STE hosts can be attributed to doping (Mg_{Nb} or Fe_{Li}). The varying accessibility of these centers and/or the different stability of the corresponding pinned STEs can be ascribed to different clustering with intrinsic and extrinsic defects, taking into account that clustering not only results in various levels of charge compensation but may also result in different restrictions for polaron and exciton hopping. However, further investigations are required regarding the absorption of the emitting STEs on even shorter timescales and the type of centers at which pinned STEs are formed. We further assume that the concept of both the polaron and (pinned) STE branch in LN could also be transferred to other materials with perovskite structure such as $KNbO_3$, $LiTaO_3$, etc., since all these materials may host similar kinds of defects. Furthermore, we expect that our approach may also serve as a basis for new models and insights to describe related phenomena such as photocatalysis in TiO_2, MgO and/or ZnO.

Acknowledgements

The authors are indebted to O. F. Schirmer and T. Nörenberg for fruitful discussions as well as L. Kovács and coworkers at the Wigner Research Centre for Physics, Budapest, for crystals and crystal preparation. Financial support from the Deutsche Forschungsgemeinschaft (DFG) via projects IM37/5-2, IM37/11-1, INST 190/137-1 FUGG and INST 190/165-1 FUGG is kindly acknowledged.

References

[1] O. F. Schirmer, M. Imlau, C. Merschjann. *Bulk photovoltaic effect of $LiNbO_3$:Fe and its small-polaron-based microscopic interpretation.* Phys. Rev. B **83**, 165106 (2011).

[2] Jiangang He, Cesare Franchini, James M. Rondinelli. *Lithium Niobate-Type Oxides as Visible Light Photovoltaic Materials.* Chem. Mater. **28**, 25–29 (2016).

[3] K. Lengyel, Á. Péter, L. Kovács, G. Corradi, L. Pálfalvi, J. Hebling, M. Unferdorben, G. Dravecz, I. Hajdara, Zs. Szaller, K. Polgár. *Growth, defect structure, and THz application of stoichiometric lithium niobate.* Appl. Phys. Rev. **2**, 040601 (2015).

[4] M. Imlau, H. Badorreck, C. Merschjann. *Optical nonlinearities of small polarons in lithium niobate.* Appl. Phys. Rev. **2**, 040606 (2015).

[5] R. T. Williams, K. S. Song. *The self-trapped exciton.* J. Phys. Chem. Solids **51**, 679–716 (1990).

[6] Michael Nolan. *First-Principles Prediction of New Photocatalyst Materials with Visible-Light Absorption and Improved Charge Separation: Surface Modification of Rutile TiO_2 with Nanoclusters of MgO and Ga_2O_3.* ACS Appl. Mater. Interfaces **4**, 5863–5871 (2012).

[7] Annapaola Migani, Lluís Blancafort. *Excitonic Interfacial Proton-Coupled Electron Transfer Mechanism in the Photocatalytic Oxidation of Methanol to Formaldehyde on TiO_2(110).* J. Am. Chem. Soc. **138**, 16165–16173 (2016).

[8] Hikmet Sezen, Honghui Shang, Fabian Bebensee, Chengwu Yang, Maria Buchholz, Alexei Nefedov, Stefan Heissler, Christian Carbogno, Matthias Scheffler, Patrick Rinke, Christof Wöll. *Evidence for photogenerated intermediate hole polarons in ZnO.* Nat. Commun. **6**, 6901 apr 2015.

[9] Z. Liu, Z. Yin, C. Cox, M. Bosman, X. Qian, N. Li, H. Zhao, Y. Du, J. Li, D. G. Nocera. *Room temperature stable CO_x-free H_2 production from methanol with magnesium oxide nanophotocatalysts.* Sci. Adv. **2** (2016).

[10] Sharifah Bee Abdul Hamid, Swe Jyan Teh, Chin Wei Lai. *Photocatalytic Water Oxidation on ZnO: A Review.* Catalysts **7**, 93 (2017).

[11] O. F. Schirmer, O. Thiemann, M. Wöhlecke. *Defects in $LiNbO_3$—I. experimental aspects.* J. Phys. Chem. Solids **52**, 185–200 (1991).

[12] O. F. Schirmer, M. Imlau, C. Merschjann, B. Schoke. *Electron small polarons and bipolarons in $LiNbO_3$.* J. Phys.: Condens. Matter **21**, 123201 (2009).

[13] A. Sanson, A. Zaltron, N. Argiolas, C. Sada, M. Bazzan, W. G. Schmidt, S. Sanna. *Polaronic deformation at the $Fe^{2+/3+}$ impurity site in Fe:$LiNbO_3$ crystals.* Phys. Rev. B **91**, 094109 (2015).

[14] S. Juppe, O. F. Schirmer. *ESR of Ti^{3+} in $LiNbO_3$.* Physics Letters A **117**, 150–152 (1986).

[15] G. Corradi, I. M. Zaritskii, A. Hofstaetter, K. Polgár, L. G. Rakitina. *Ti^{3+} on Nb site: A paramagnetic Jahn-Teller center in vacuum-reduced $LiNbO_3$:Mg:Ti single crystals.* Phys. Rev. B **58**, 8329–8337 (1998).

[16] D. M. Krol, G. Blasse, R. C. Powell. *The influence of the Li/Nb ratio on the luminescence properties of $LiNbO_3$.* J. Chem. Phys. **73**, 163 (1980).

[17] M. Wiegel, G. Blasse, A. Navrotsky, A. Mehta, N. Kumada, N. Kinomura. *Luminescence of the Ilmenite Phase of $LiNbO_3$.* Journal of Solid State Chemistry **109**, 413–415 (1994).

[18] C. Merschjann, B. Schoke, D. Conradi, M. Imlau, G. Corradi, K. Polgár. *Absorption cross sections and number densities of electron and hole polarons in congruently melting $LiNbO_3$.* J. Phys.: Condens. Matter **21**, 015906 (2008).

[19] T. Kämpfe, A. Haußmann, L. M. Eng, P. Reichenbach, A. Thiessen, T. Woike, R. Steudtner. *Time-resolved photoluminescence spectroscopy of Nb_{Nb}^{4+} and O^- polarons in $LiNbO_3$ single crystals.* Phys. Rev. B **93**, 174116 (2016).

[20] G. Blasse. *Fluorescence of Niobium-Activated Antimonates and an Empirical Criterion for the Occurrence of Luminescence.* J. Chem. Phys. **48**, 3108–3114 (1968).

[21] C. Fischer, M. Wöhlecke, T. Volk, N. Rubinina. *Influence of the Damage Resistant Impurities Zn and Mg on the UV-Excited Luminescence in $LiNbO_3$.* Phys. Status Solidi A **137**, 247–255 (1993).

[22] F. Klose, M. Wöhlecke, S. Kapphan. *Uv-excited luminescence of $LiNbO_3$ and $LiNbO_3$:Mg.* Ferroelectrics **92**, 181–187 (1989).

[23] Richard C. Powell, Edwin E. Freed. *Laser time-resolved studies of exciton migration in doped lithium niobate.* J. Chem. Phys. **70**, 4681–4685 may 1979.

[24] D. Conradi, C. Merschjann, B. Schoke, M. Imlau, G. Corradi, K. Polgár. *Influence of Mg doping on the behaviour of polaronic light-induced absorption in $LiNbO_3$.* Phys. Status Solidi (RRL) **2**, 284–286 (2008).

[25] P. Herth, T. Granzow, D. Schaniel, Th. Woike, M. Imlau, E. Krätzig. *Evidence for Light-Induced Hole Polarons in $LiNbO_3$.* Phys. Rev. Lett. **95**, 067404 (2005).

[26] D. Berben, K. Buse, S. Wevering, P. Herth, M. Imlau, Th. Woike. *Lifetime of small polarons in iron-doped lithium–niobate crystals.* J. Appl. Phys. **87**, 1034 (2000).

[27] P. Herth, D. Schaniel, Th. Woike, T. Granzow, M. Imlau, E. Krätzig. *Polarons generated by laser pulses in doped $LiNbO_3$.* Phys. Rev. B **71**, 125128 mar 2005.

[28] P. Reichenbach, T. Kämpfe, A. Thiessen, A. Haußmann, T. Woike, L. M. Eng. *Multiphoton photoluminescence contrast in switched Mg:$LiNbO_3$ and Mg:$LiTaO_3$ single crystals.* Appl. Phys. Lett. **105**, 122906 (2014).

[29] P. Reichenbach, T. Kämpfe, A. Thiessen, M. Schröder, A. Haußmann, T. Woike, L. M. Eng. *Multiphoton-induced luminescence contrast between antiparallel ferroelectric domains in Mg-doped $LiNbO_3$.* J. Appl. Phys. **115**, 213509 (2014).

[30] Y.P. Varshni. *Temperature dependence of the energy gap in semiconductors.* Physica **34**, 149–154 (1967).

[31] J.R Botha, A. W. R. Leitch. *Temperature dependence of the photoluminescence properties and band gap energy of InxGa1-xAs/GaAs quantum wells.* Journal of Electronic Materials **29**, 1362–1371 (2000).

[32] Yutaka Toyozawa. *Optical Processes in Solids.* Cambridge University Press (2003).

[33] J. Klafter, M. F. Shlesinger. *On the relationship among three theories of relaxation in disordered systems.* Proceedings of the National Academy of Sciences **83**, 848–851 (1986).

[34] B. Sturman, E. Podivilov, M. Gorkunov. *Origin of Stretched Exponential Relaxation for Hopping-Transport Models.* Phys. Rev. Lett. **91**, 176602 (2003).

[35] I. Mhaouech, L. Guilbert. *Temperature dependence of small polaron population decays in iron-doped lithium niobate by Monte Carlo simulations.* Solid State Sci. **60**, 28–36 oct 2016.

[36] C. Merschjann, M. Imlau, H. Brüning, B. Schoke, S. Torbrügge. *Nonexponential relaxation dynamics of localized carrier densities in oxide crystals without structural or energetic disorder.* Phys. Rev. B **84**, 052302 (2011).

[37] Laurent Guilbert, Laura Vittadello, Marco Bazzan, Imed Mhaouech, Simon Messerschmidt, Mirco Imlau. *The elusive role of Nb_{Li} bound polaron energy in hopping charge transport in Fe:$LiNbO_3$.* J. Phys.: Condens. Matter **30**, 125701 (2018).

[38] Tatyana Volk, Manfred Wöhlecke. *Lithium Niobate.* Springer (2010).

[39] G. I. Malovichko, V. G. Grachov, E. P. Kokanyan. *Low-symmetry Fe-Mg complexes in $LiNbO_3$:Mg.* Ferroelectrics **125**, 289–294 (1992).

[40] Feifei Xin, Zhaohui Zhai, Xiaojie Wang, Yongfa Kong, Jingjun Xu, Guoquan Zhang. *Threshold behavior of the Einstein oscillator, electron-phonon interaction, band-edge absorption, and small hole polarons in $LiNbO_3$:Mg crystals.* Phys. Rev. B **86**, 165132 (2012).

[41] G Zatryb, A Podhorodecki, J Misiewicz, J Cardin, F Gourbilleau. *On the nature of the stretched exponential photoluminescence decay for silicon nanocrystals.* Nanoscale Res. Lett. **6**, 106 (2011).

[42] Felix Freytag, Phillip Booker, Gábor Corradi, Simon Messerschmidt, Andreas Krampf, Mirco Imlau. *Picosecond near-to-mid-infrared absorption of pulse-injected small polarons in magnesium doped lithium niobate.* Opt. Mater. Express **8**, 1505–1514 (2018).

[43] David Emin. *Phonon-assisted transition rates I. Optical-phonon-assisted hopping in solids.* Adv. Phys. **24**, 305–348 (1975).

[44] David Emin. *Polarons.* Cambridge University Press (2012).

[45] K. S. Song, Richard T. Williams. *Self-Trapped Excitons.* Springer Berlin Heidelberg (1993).

[46] T. Miki, M. R. Hantehzadeh, L. E. Halliburton. *A new trapped-hole center in irradiated $LiNbO_3$.* Journal of Physics and Chemistry of Solids **50**, 1003–1007 (1989).

[47] I. M. Zaritskii, L. G. Rakitina, G. Corradi, K. Polgar, A. A. Bugai. *A new trapped-hole radiation defect in heavily Mg-doped $LiNbO_3$.* J. Phys.: Condens. Matter **3**, 8457–8465 (1991).

B.3 Atomic insight to lattice distortions caused by carrier self-trapping in oxide materials

Atomic insight to lattice distortions caused by carrier self-trapping in oxide materials

Felix Freytag[1,*], Gábor Corradi[2], and Mirco Imlau[1]

[1] *School of Physics, Osnabrueck University, Barbarastr. 7, 49076 Osnabrueck, Germany*
[2] *Wigner Research Centre for Physics, Institute for Solid State Physics and Optics, Hungarian Academy of Sciences, Konkoly-Thege u. 29-33, 1121 Budapest, Hungary*
[*] *Corresponding author: felix.freytag@uos.de*

Abstract: We gain hitherto missing access to the spatio-temporal evolution of lattice distortions caused by carrier self-trapping in the class of oxide materials - and beyond. The joint experimental/theoretical tool introduced combines femtosecond mid-infrared probe spectroscopy with potential landscape modeling and is based on the original approach that the vibration mode of a biatomic molecule is capable to probe strongly localized, short-lived lattice distortions in its neighborhood. Optically generated, small, strong-coupling polarons in lithium niobate, mediated by OH^- ions present as ubiquitous impurities, serve as a prominent example. Polaron trapping is found to result in an experimentally determined redshift of the OH^- stretching mode amounting to $\Delta\nu_{\mathrm{vib}} = -3\,\mathrm{cm}^{-1}$, that is successfully modeled by a static Morse potential modified by Coulomb potential changes due to the displacements of the surrounding ions and the trapped charge carrier. The evolution of the trapping process can also be highlighted by monitoring the dynamics of the vibrational shift making the method an important tool for studying various systems and applications.

This work was published in Scientific Reports and can be found at doi: 10.1038/srep36929. This work is licensed under a Creative Commons Attribution 4.0 International License. The images or other third party material in this article are included in the article's Creative Commons license, unless indicated otherwise in the credit line; if the material is not included under the Creative Commons license, users will need to obtain permission from the license holder to reproduce the material. To view a copy of this license, visit http://creativecommons.org/licenses/by/4.0/

1 Introduction

Self-trapping by electron- or hole-phonon-coupling, commonly described as small polaron formation [1], is increasingly considered in the modeling of transport phenomena

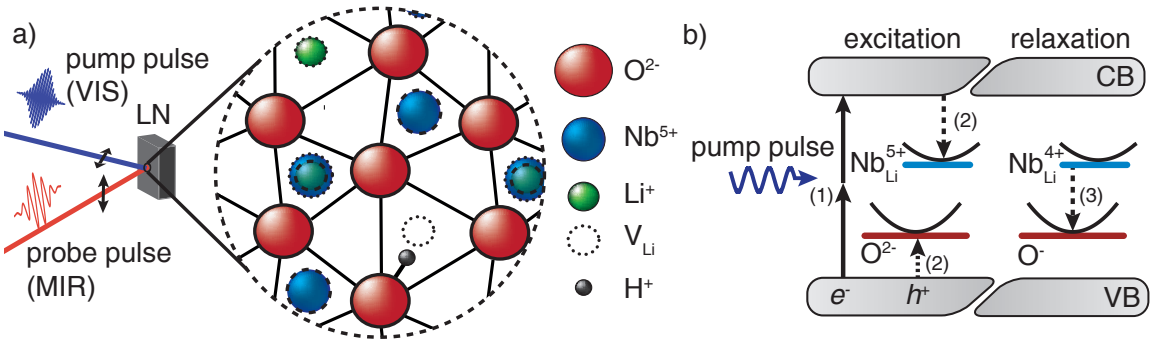

Figure 1: (a) Structure of the oxygen plane of $LiNbO_3$ [10] (dotted: cations above plane, dashed: below plane) and schematic setup. (b) Electronic transition: (1) two-photon-absorption, (2) generation of small Nb_{Li}^{4+} electron and O^- hole polarons ($\tau < 1$ ps) [17], (3) recombination ($\tau \approx 1$ s) (Tab. 1)

in oxide materials such as superconductivity in cuprates [2], semiconduction in transition metal oxides [3], colossal magnetoresistance in manganites [4, 5], and also for the mechanism of photocatalysis in TiO_2 [6]. In this connection, a detailed knowledge on the lattice distortions related to self-trapping, and in particular on the respective dynamics at elevated temperatures, are of major importance; however, no adequate experimental tools have been described in the literature, so far. Only recently, first attempts for a direct view on small polarons on the surface of TiO_2 have been reported by Setvin et al. based on a combination of scanning tunneling microscopy/spectroscopy and density functional theory [7]. In turn, Sezen et al. applied infrared reflection-absorption spectroscopy at low temperatures to study photoexcited polarons in zinc oxide (ZnO) [8]. By contrast, in this article, we intend to access optically generated, small polarons in the crystal bulk at room temperature and propose a time-resolved vibrational method to experimentally achieve local information on small polarons at this temperature.

Our study is performed with nominally undoped, near stoichiometric lithium niobate ($LiNbO_3$, LN) as a prototypical oxide material that allows for the optical generation of various kinds of short-lived small, strong-coupling electron and hole polarons [9], i.e., self-trapped carriers with associated distortions strongly confined to a single lattice site [1]. A multitude of knowledge based on a variety of experimental techniques has been gathered to access small polarons in LN in the past decades. Structural (steady-state) parameters are obtained using a combination of X-ray diffraction Electron Paramagnetic Resonance (EPR)/ Electron Nuclear Double Resonance (ENDOR)/ Angle-resolved Photoemission Spectroscopy (APRES) measurements [10–14], which, however, are limited to low temperatures and systems having appropriate spin. Information on the electronic structure is best modeled by ab initio techniques [15], or, from the experimental viewpoint, using optical pump-probe techniques in the visible spectral range [9]. Access to the dynamics of lattice distortions due to the self-trapping of optically excited carriers, is of importance in LN to foster the understanding of the bulk photovoltaic effect and its small polaron based microscopic modeling [16].

Our original approach makes use of a molecular ligand in direct vicinity of the small

polaron site such that its vibrational spectroscopic fingerprint $E_{\mathrm{vib}} = h\nu_{\mathrm{vib}}$ changes by $\Delta\nu_{\mathrm{vib}}$ due to a modified electrostatic potential in the presence of a short-range lattice displacement. With knowledge on the lattice position of both the molecular ligand and the small polaron site, the structural distortion can be reconstructed from the measurement of $\Delta\nu_{\mathrm{vib}}$. Thus, a variety of small polaron features like the associated displacements of atomic equilibrium positions or the electron-phonon coupling strength can be obtained. A particular strength of the approach is the possibility to study the temporal evolution of localized atomic displacements if dynamic measurements for the detection of $\Delta\nu_{\mathrm{vib}}(t)$ are applied. Here we use a femtosecond visible pump, mid-infrared (MIR) probe absorption spectrometer (cf. e.g. [18]) with a remarkable shot-to-shot sensitivity below 10^{-3} OD (Optical Density) at a spectral and temporal resolution of $\delta\nu_{\mathrm{vib}}(t)/\nu_{\mathrm{vib}} \approx 9\cdot10^{-4}$, and $\delta t = 1$ ms, respectively. It is shown that the transient absorption spectrum $\Delta A(\nu,t) = A(\nu,t)_{\mathrm{pumped}} - A(\nu,t)$ reveals a frequency shift of $\Delta\nu_{\mathrm{vib}}(\mathrm{OH}^-)$ upon light exposure that can be related to the formation of short-lived, small O^- hole polarons. Furthermore, the dynamic features from ms to seconds in the dark resemble the well-known stretched-exponential behavior that is characteristic for hopping-transport [19]. The main purpose of this article is (i) to verify the underlying experimental approach, i.e., to demonstrate and explain the small polaron access using changes in a vibrational fingerprint, (ii) to sketch the physical relation between experimentally determined frequency shifts and the structural properties of small, strong-coupling polarons, and (iii) to show-up the possibility for dynamic measurements with small polaron hopping-transport as an example.

2 Fundamentals

2.1 Carrier self trapping in lithium niobate

In what follows, we will focus on small, strong-coupling O^- hole polarons (HP) [20] in direct vicinity to a $\mathrm{V_{Li}}$ vacancy as well as on $\mathrm{Nb_{Li}^{4+}}$ electron polarons (GP) [21]. Structural details of the oxygen plane of LN are depicted in Fig. 1a. In both cases the trapped charge can be transferred by light to a neighboring equivalent or nearly equivalent site, thereby stripping the trapped charge of its polarization halo [19, 20]. This results in broad absorption features playing a central role in the study and application of dynamic properties of small polarons in LN [9]. The absorption maxima are reported in the visible region (VIS, 2.5 eV; $\approx$ 20,000 cm^{-1}) for HP and in the near infrared (NIR, 1.6 eV; $\approx$ 13,000 cm^{-1}) for GP. In nominally undoped LN, pairs of HP and GP can be generated via two-photon excitation at 2.5 eV (cf. Fig. 1b, left part), i.e., with photon energies much below the band edge energy ($\mathrm{E_{gap}} \approx 4.1$ eV [22]). To raise signal changes in the MIR range ($\approx$ 10 mOD, see below), it is necessary to generate a large number density $\mathrm{N_{sp}} > 10^{18}$ cm^{-3} of small polarons. This is realized by using intense laser pulses ($I_{\mathrm{pump}} = (500 \pm 100)$ TW/m^2, extraordinary light polarization) with sub-ps pulse duration ($\tau_{\mathrm{pump}} = (120 \pm 10)$ fs), as N_{sp} depends quadratically on the intensity of the pump-pulse, $N_{\mathrm{sp}} = \mathrm{const.} \cdot I_{\mathrm{pump}}^2$ [23], but also on the pulse duration τ_{pump} [24]. Furthermore, repetitive fs-pulse exposure ($f_{\mathrm{rep}} = 1$ kHz) is applied, which leads, after a few seconds of illumination, to a saturation of the

MIR effect. The average small polaron lifetimes $\tau_{GP} \approx \tau_{HP} \approx (1.1 \pm 0.3)$ s $\gg 1/f_{rep}$ accord with the mutual HP-GP-recombination path, as shown in Fig. 1b, right part.

2.2 Hydroxide ions as a molecular probe

Hydroxide ions, OH^- [13], inevitably introduced during crystal growth are used as molecular probes. Real position and vibrational properties have been studied in LN crystals comprehensively (for reviews, cf. [25] and [26]), showing that H^+ is bound to one of the O^{2-} neighbors of a V_{Li} [27–29] (note that $c_{V_{Li}} \gg c_{H^+}$ [27]). Due to the dipolar character of this defect complex it may be assumed that light-induced, small polarons are formed or get temporarily trapped in its direct vicinity. We consider an O^- hole polaron localized at an oxygen ion next to the same V_{Li} (see Fig. 1a). It is already established that the energy of the OH^--stretching vibration depends on the surroundings of the particular OH^--site resulting in several components of its MIR absorption feature. In as-grown, near stoichiometric LN up to five distinct bands have been observed [30,31]; the most prominent bands appear at $3,466$ cm^{-1}, $3,480$ cm^{-1}, and $3,490$ cm^{-1} (see Fig. 2a) with the lowest vibrational energy related to the O^{2-} sites closest to V_{Li} [27]. To observe pump-induced frequency changes of the OH^--stretching bond, we use probe pulses with a spectral width of $\Delta\tilde{\nu} \approx 200$ cm^{-1} at a center wavenumber of $\tilde{\nu} = 3,484$ cm^{-1} ($I = 0.03$ TW/m^2, $\tau_{probe} = (230 \pm 20)$ fs, $f_{rep} = 1$ kHz, ordinary light polarization). All studies were performed with an X-cut sample (aperture 10×9 mm^2, thickness 2 mm) with a [Li]/[Nb] ratio of 0.992 [32] and a hydrogen concentration [33] of $\approx 3 \cdot 10^{18}$ cm^{-3}.

3 Results

3.1 Experiment

The time dependent change of the absorption feature $\Delta A(\tilde{\nu}, t)$ in the region of $\nu_{vib}(OH^-)$ is plotted as a function of wavenumber $\tilde{\nu}$ in Fig. 2b using the color coding: red for $\Delta A(\tilde{\nu}, t) > 0$ and blue for $\Delta A(\tilde{\nu}, t) < 0$. In the time regime $t < t_{on}$, i.e., without the presence of the pump-pulse, we detect a weak background signal that is applied for signal correction. At t_{on}, the repetitive pump-pulse exposure is switched on and induces spectral changes $\Delta A(\tilde{\nu}, t)$ well above the noise limit. The temporal evolution resembles a mono-exponential behavior with a characteristic time constant in the order of 100 ms. The spectral evolution shows changes in the shape of all three MIR absorption bands with maximum values of about -14 mOD at 3,466 cm^{-1} and about $+10$ mOD at 3,463 cm^{-1}. Pump-induced changes at 3,480 cm^{-1} and 3,490 cm^{-1} are also observed but do not exceed 2 mOD; accordingly we will focus in the following on the strongest absorption band. Switching off the pump-pulse exposure ($t > t_{off}$), the absorption change decays to nearly zero and the process can be repeated from the beginning. Exemplarily, the spectrum $\Delta A(\tilde{\nu}, t = t_{off})$ is extracted and plotted in Fig. 2c. The remarkable shape, in particular in the region of the strongest absorption band, can be understood as a shift of the OH^- absorption frequency by -3 cm^{-1} to 3,463 cm^{-1}.

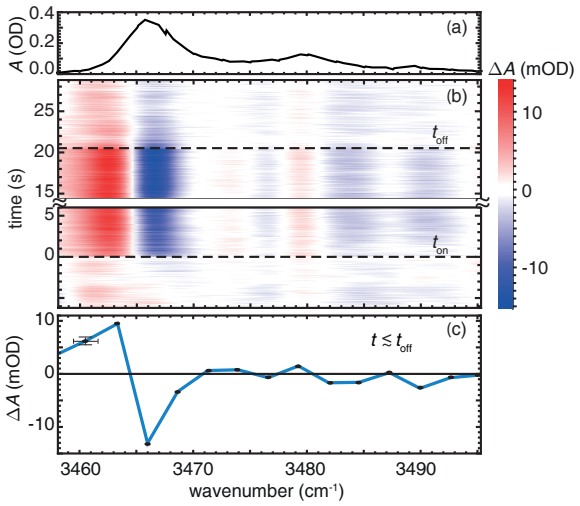

Figure 2: (a) Steady state spectrum of the OH^--stretching absorption feature in nearly stoichiometric lithium niobate. (b) Time dependent change of the absorption $\Delta A(\tilde{\nu}, t)$ of the OH^-- stretching vibration. t_{on} and t_{off} denote the times where repetitive pump-pulse exposure is switched on and off. (c) Spectrum of the absorption change at $t = t_{off}$ (black data points). The blue line is a guide to the eye; its shape indicates a frequency shift of the prominent absorption feature by -3 cm^{-1}.

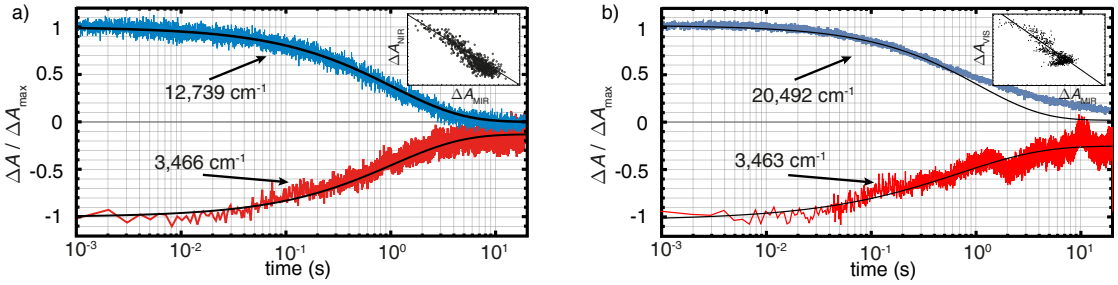

Figure 3: Relaxation dynamics probed at (a) 3,466 cm^{-1} (MIR) and 12,739 cm^{-1} (λ = 785 nm, NIR) and (b) at 3,463 cm^{-1} (MIR, inverted) and 20,492 cm^{-1} (λ = 488 nm, VIS). The solid lines indicate the results of fitting stretched exponential functions to the data sets. Insert: Plot of the absorbance change (a) ΔA_{NIR},(b) ΔA_{VIS} as a function of ΔA_{MIR}; a linear dependence is revealed over the entire data range.

The next step is to verify the relation of this shift to the presence of small, strong-coupling polarons. For this purpose, the temporal relaxation dynamics in the mid-infrared spectral range is highlighted in a semi-logarithmic plot in Fig. 3 (red data points) and compared with the temporal decay dynamics of the light-induced absorption detected in the near-infrared and visible spectral range (blue data points) close to the maximum of the GP and HP absorption features. It is evident from Fig. 3 that the temporal behavior of the absorption changes in the MIR and NIR spectral ranges are strongly correlated, despite the difference in the sign of ΔA. As shown in the insert of Fig. 3 , the $\Delta A_{\mathrm{NIR}}(\Delta A_{\mathrm{MIR}})$ plot is essentially linear. For a quantitative comparison, a stretched-exponential function

$$\Delta \mathrm{A(t)} = \mathrm{A(0)} \cdot \exp[-(t/\tau)^{\beta}] + \mathrm{const.} \tag{1}$$

Probed effect	Range	ν_{probe} / cm^{-1}	τ/ s	β
molecular vibration	MIR	3,463	0.7(4)	0.55(10)
		3,466	1.0(4)	0.65(10)
electronic transition	NIR	12,739	1.1(3)	0.65(10)
	VIS	20,492	1.1(3)	0.70(10)

Table 1: Results of fitting a stretched-exponential function to the temporal dynamics in the VIS, NIR and MIR spectral range (cf. straight lines in Fig. 3).

with time constant τ and stretching exponent β is fitted to both data sets. The values (τ, β) obtained from fitting the experimental data are listed in Table 1 and are comparable within the error margins. These findings are particularly remarkable since the absorption in the NIR and VIS region is related to changes in the electronic structure, whereas the absorption in the MIR is characteristic for the molecular vibration of OH^-. The linear relation between the signals of different origin, thus, gives clear evidence for their common physical background which is the hopping transport of GP and HP leading to their recombination (cf. Fig. 1b). We note that the absorption dynamics at 3,463 cm^{-1} in Fig. 3b shows a reduced signal-to-noise ratio in comparison with data at 3,466 cm^{-1}, that is due to the lower signal level at this wavenumber. Concerning the dynamics at 20,492 cm^{-1}, a slight variation to long decay times in comparison to the stretched-exponential decay is observed, that may be attributed to the presence of Fe_{Li}^{3+} impurities, always present in the ppm regime in nominally undoped lithium niobate and acting as deep electron traps. At the same time, the frequency shift cannot be explained by other defect centers such as extrinsic dopants, as a change in the cation environment, caused, e.g., by doping, leads to a blue shift of the MIR absorption spectrum (e.g. magnesium, indium or neodymium shift the frequency by a few +10 cm^{-1} [26,34]). Electron polarons bound to Nb_{Li}^{5+} antisites can be discarded in this respect as protons are not expected to associate with antisites due to the huge surplus positive charge of the latter. Small, free polarons on a nearby regular Nb_{Nb}^{5+}-site would have much shorter relaxation times ($\tau \approx 1$ μs) [35] and can also be excluded.

3.2 Theory

In the final part of this letter, based on the experimental findings, we give an estimate of the local lattice distortion induced by small hole polarons, using a simple point charge approximation for the change of the crystal field and a static Morse potential [36] along the OH^--bond with the anharmonicity constant $\omega_e x_e$:

$$\begin{aligned} V(r)^{\mathrm{Morse}} &= D_e \cdot (\mathrm{e}^{-2\mathrm{a}(\mathrm{r}-\mathrm{r}_0)} - 2\mathrm{e}^{-\mathrm{a}(\mathrm{r}-\mathrm{r}_0)}) \\ \omega_e &= \frac{a}{2\pi c}\sqrt{\frac{2D_e}{\mu}}, \\ x_e &= hc\frac{\omega_e}{4D_e} \end{aligned}$$

with D_e being the dissociation energy, a the stretching constant, r_0 the O-H distance with the lowest potential energy and $\mu = \frac{m_\mathrm{p} m_\mathrm{O}}{m_\mathrm{O}+m_\mathrm{p}}$ the reduced proton mass. In the absence of polarons the values of D_e and a can be found using measured frequencies ($\nu_{0,1} = \omega_e - 2\omega_e x_e = 3,466$ cm^{-1}, $\nu_{0,2} = 6,745$ cm^{-1}) of the OH$^-$-stretching vibration [37]. A hole polaron is added at another oxygen neighbor of the lithium vacancy out of the three nearest ones. The potential change seen by the proton is accounted for by the Coulomb potential due to the added point charge on its host ion *and* by the changes of the Coulomb potentials due to the displacements of all neighboring ions with the exception of the oxygen in OH$^-$. For simplicity the displacements are assumed to be radial (with respect to the polaron host) and scaled by the factor $q_\mathrm{i}/d_\mathrm{i}$ where q_i is the charge and d_i the distance (to the host) of the ith neighbor (see Fig. 4). This scaling corresponds to considering only long range electron-phonon

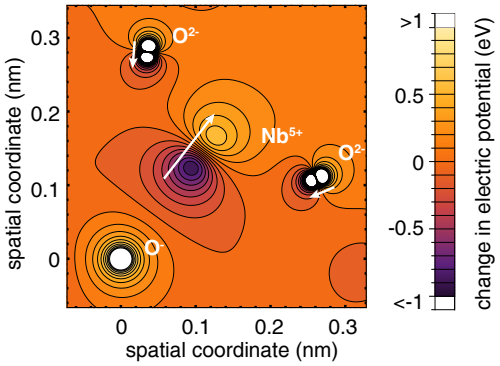

Figure 4: Electrostatic potential change in the oxygen plane of $LiNbO_3$ calculated for a polaronic distortion corresponding to a redshift of -3 cm^{-1} of the OH$^-$-stretching vibration. Arrows (enlarged) indicate amplitudes and directions of displacements (projected to the oxygen plane) of close Nb^{5+} and O$^-$ neighbors of the polaron host that is positioned in the origin. Note that the Nb^{5+} site is ≈ 0.088 nm below the oxygen plane.

interaction characterized by the static dielectric constant ϵ_0 having a large value in comparison to the optical dielectric constant ϵ_∞ ($\epsilon_{0,11}/\epsilon_\infty = 57.6$, $\epsilon_{0,33}/\epsilon_\infty = 19.0$ [38], with $\epsilon_\infty \approx 1.47 \cdot \epsilon_\mathrm{vacuum}$ [39]) in LN. Choosing the displacement δd_Nb of the nearest Nb neighbor ($d_{\mathrm{Nb}^{5+}-\mathrm{O}^{2-}} = 0.188$ nm) as a numerical scaling parameter and neglecting possible changes of the OH$^-$-direction, the resulting potential along the bond can be approximated by a new Morse potential of the same type.

The three dimensional Coulomb potential is calculated for a $5\times5\times2$ hexagonal unit cell (1588 atoms), using the structural data of the $LiNbO_3$ lattice [10] with a lithium and an adjacent oxygen ion at the center of the cell replaced by an OH$^-$-molecular-ion represented by a static Morse potential. The site of the proton substituting V_Li, is assumed to be in the bisecting plane of the largest oxygen triangle (O-O distance 336 pm) [29] with an O-H bond length of 98.8 pm and an out-of-plane angle of 4.3 degrees towards V_Li [28]. We note that a OH$^- - V_\mathrm{Li}$-complex causes only negligible distortions of the lattice as calculated by Lengyel et al. [26,28]. Cation charges in the boundary area of the cell are reduced to secure an overall neutral charge. The changes of the potential along the direction of the O-H bond resulting from the presence of a hole polaron are added to the Morse potential, neglecting the difference between the

center of mass of OH^- and the corresponding oxygen site. The hole polaron state is modeled by an additional positive charge localized at one of the oxygen atoms in closest vicinity to the V_{Li}-site and by scaled displacements of the surrounding atoms within a radius of 5 Å.

For $\delta d_{Nb} = 0.024$ nm the modified Morse potential returns the shifted fundamental frequency 3,463 cm^{-1} found by our experiments. Taking into account only the point charge of the polaron without lattice relaxation, a blue shift of +5 cm^{-1} is obtained which stresses the importance of the polaronic relaxation. The obtained $\approx 12.5\%$ increase of the smallest O-Nb distance corresponds to a $\approx 1.7\%$ increase of the closest O-Li distance ($d_{Li^+-O^{2-}} = 0.245$ nm), and an average $\approx 2.1\%$ decrease of the various O-O distances (between 0.272 nm and 0.336 nm), taking into account the adopted q_i/d_i scaling (see Fig. 4). Considering this scaling our calculations are consistent with recent ab initio studies of the polaronic deformation at the impurity site in Fe:$LiNbO_3$ by Sanson et al. [40] who found a $\approx 4.7\%$ decrease of the Fe-O distance ($d_{Fe^{2+}-O^{2-}} = 0.2124$ nm) upon hole capture by Fe^{2+}, thus, supporting our model assumptions. The estimates derived from our simplified model may already serve as useful input parameters for more complex model calculations and/or as a crosscheck of the validity of various small polaron model approaches. Appropriate calculations may be used straightforwardly for the determination of further small polaron parameters, like the electron phonon coupling strength.

4 Summary and conclusions

Summarizing the results, a pump-induced -3 cm^{-1} shift of the frequency of the OH^--stretching vibration is experimentally verified and attributed to the presence of small, strong-coupling O^- hole polarons next to the OH^- ion. Sign and magnitude of the shift can only be explained by taking into account, in addition to the polaronic charge, also the distortion of the lattice in the imminent neighborhood - a very striking result that supports the microscopic approach for the bulk photovoltaic effect based on small, strong-coupling polarons in LN [16] and will foster its advances. The measured shift can be reconstructed by modeling the change of the three-dimensional Coulomb potential caused by the polaron, leading to reasonable values of the ligand displacements. The measured frequency shift may also provide a stringent test for ab initio/DFT calculations desirable for a deeper understanding of the properties of polarons interacting with molecular defects, and vice versa. It should be stressed that the presented experimental approach for determining local lattice deformation, although introduced with small, strong-coupling polarons, can also be applied for the detection of small, weak-coupling and large polarons [1]. It is furthermore neither limited to the chosen molecular hydoxide group nor to lithium niobate as a host material, and may be adopted, e.g., to further oxides like TiO_2, ZnO or MgO, but also to probe localized atomic distortions in DNA [41]. As its most important aspect, however, the approach enables dynamic studies at room temperature and, thus, general physical questions about polaron formation, hopping-transport and recombination phenomena, encompassing time scales from sub-ps to seconds, become accessible. If necessary, the time resolution can be increased to the sub-ps time regime by using up-

conversion MIR-spectroscopy; this enables a larger signal-to-noise ratio accompanied with a better time resolution.

References

[1] D. Emin. *Polarons*. Cambridge University Press (2013).

[2] K. A. Müller. *The Unique Properties of Superconductivity in Cuprates*. J. Supercond. Novel Magn. **27**, 2163–2179 (2014).

[3] S. Lany. *Semiconducting transition metal oxides*. J. Phys.: Condens. Matter **27**, 283203 (2015).

[4] M. B. Salamon, M. Jaime. *The physics of manganites: Structure and transport*. Rev. Mod. Phys. **73**, 583–628 (2001).

[5] C. Hartinger, F. Mayr, A. Loidl, T. Kopp. *Polaronic excitations in colossal magnetoresistance manganite films*. Phys. Rev. B **73**, 024408 (2006).

[6] A. L. Linsebigler, G.. Lu, J. T. Yates. *Photocatalysis on TiO_2 Surfaces: Principles, Mechanisms, and Selected Results*. Chem. Rev. **95**, 735–758 (1995).

[7] M. Setvin, C. Franchini, X. Hao, A. Schmid, M.and Janotti, M. Kaltak, C. G. Van de Walle, G. Kresse, U. Diebold. *Direct View at Excess Electrons in TiO_2 Rutile and Anatase*. Phys. Rev. Lett. **113**, 086402 (2014).

[8] H. Sezen et al. *Evidence for photogenerated intermediate hole polarons in ZnO*. Nat. Commun. **6**, 6901 (2015).

[9] M. Imlau, H. Badorreck, C. Merschjann. *Optical nonlinearities of small polarons in lithium niobate*. Appl. Phys. Rev. **2**, 040606 (2015).

[10] S. C. Abrahams, J. M. Reddy, J. L. Bernstein. *Ferroelectric lithium niobate. 3. Single crystal X-ray diffraction study at 24°C*. J. Phys. Chem. Solids **27**, 997–1012 (1966).

[11] G. Corradi, H. Söthe, J. M. Spaeth, K. Polgár. *Mn^{2+} defects in $LiNbO_3$: an electron nuclear double resonance (ENDOR) investigation of the Mn^{2+} site and the local disorder*. J. Phys.: Condens. Matter **2**, 6603–6618 (1990).

[12] V. Grachev, G. Malovichko. *EPR, ENDOR, and optical-absorption study of Cr^{3+} centers substituting for niobium in Li-rich lithium niobate crystals*. Phys. Rev. B **62**, 7779–7790 (2000).

[13] M. Wöhlecke, L. Kovács. *OH^- ions in Oxide Crystals*. Crit. Rev. Solid State Mater. Sci. **26**, 1–86 (2001).

[14] S. et al. Moser. *Tunable Polaronic Conduction in Anatase TiO_2*. Phys. Rev. Lett. **110**, 19 (2013).

[15] H. H. Nahm, C. H. Park. *First-principles study of microscopic properties of the Nb antisite in $LiNbO_3$: Comparison to phenomenological polaron theory*. Phys. Rev. B **78**, 184108 (2008).

[16] O. F. Schirmer, M. Imlau, C. Merschjann. *Bulk photovoltaic effect of $LiNbO_3$:Fe and its small-polaron-based microscopic interpretation*. Phys. Rev. B **83**, 165106 (2011).

[17] H. M. Yochum, K. B. Ucer, R. T. Williams, P. A. Sheldon, V. Nagirnyi, V. Denks, L. Grigorjeva, D. Millers, E. A. Kotomin. *Short-pulse excitation and spectroscopy of $KNbO_3$, $LiNbO_3$ and $KTiOPO_4$*. Radiat. Eff. Defect S. **150**, 271–276 (1999).

[18] M. Rini, A. Kummrow, E. T. J. Dreyer, J.and Nibbering, T. Elsaesser. *Femtosecond mid-infrared spectroscopy of condensed phase hydrogen-bonded systems as a probe of structural dynamics.* Faraday Discuss. **122**, 27–40 (2002).

[19] D. Berben, K. Buse, S. Wevering, P. Herth, M. Imlau, Th. Woike. *Lifetime of small polarons in iron-doped lithiumniobate crystals.* J. Appl. Phys. **87**, 1034 (2000).

[20] O. F. Schirmer. *O^- bound small polarons in oxide materials.* J. Phys. Condens. Matter **18**, R667 – R704 (2006).

[21] O. F. Schirmer, M. Imlau, C. Merschjann, B. Schoke. *Electron small polarons and bipolarons in $LiNbO_3$.* J. Phys. Condens. Matter **21**, 123201 (2009).

[22] L. Kovács, G. Ruschhaupt, K. Polgár, G. Corradi, M. Wöhlecke. *Composition dependence of the ultraviolet absorption edge in lithium niobate.* Appl. Phys. Lett. **70**, 2801 (1997).

[23] C. Merschjann, B. Schoke, D. Conradi, M. Imlau, G. Corradi, K. Polgár. *Absorption cross sections and number densities of electron and hole polarons in congruently melting $LiNbO_3$.* J. Phys. Condens. Matter **21**, 015906 (2009).

[24] H. Badorreck, S. Nolte, F. Freytag, V. Bäune, P.and Dieckmann, M. Imlau. *Scanning nonlinear absorption in lithium niobate over the time regime of small polaron formation.* Opt. Mater. Express **5**, 2729 (2015).

[25] J. M. Cabrera, J. Olivares, M. Carrascosa, J. Rams, R. Müller, E. Diéguez. *Hydrogen in lithium niobate.* Adv. Phys. **45**, 342–392 (1996).

[26] K. Lengyel et al. *Growth, defect structure, and THz application of stoichiometric lithium niobate.* Appl. Phys. Rev. **2**, 040601 (2015).

[27] W. Yan, Y. Kong, L. Shi, J. Yao, S. Chen, L. Sun, D. Zhao, J. Xu, G. Zhang. *The H^+ related defects involved in domain reversal for both near-stoichiometric and heavily Mg-doped lithium niobate crystals.* Eur. Phys. J. B **43**, 347–353 (2005).

[28] K. Lengyel, V. Timon, A. Hernandez-Laguna, V. Szalay, L. Kovács. *Structure of OH^- defects in $LiNbO_3$.* IOP Conf. Ser.: Mater. Sci. Eng. **15**, 012015 (2010).

[29] H. H. Nahm, C. H. Park. *Microscopic structure of hydrogen impurity in $LiNbO_3$.* Appl. Phys. Lett. **78**, 3812 (2001).

[30] L. Kovács, V. Szalay, R. Capelletti. *Stoichiometry dependence of the OH^- absorption band in $LiNbO_3$ crystals.* Solid State Commun. **52**, 1029–1031 (1984).

[31] C. Hong-Jian, S. Li-Hong, Y. Wen-Bo, C. Gui-Feng, S. Jun, L. Yang-Xian. *OH^- absorption bands of $LiNbO_3$ with varying composition.* Chin. Phys. B **18**, 2372–2376 (2009).

[32] G. Dravecz, L. Kovács. *Determination of the crystal composition from the OH- vibrational spectrum in lithium niobate.* Appl. Phys. B **88**, 305–307 (2007).

[33] S. Klauer, M. Wöhlecke, S. Kapphan. *Influence of H-D isotopic substitution on the protonic conductivity of $LiNbO_3$.* Phys. Rev. B **45**, 2786–2799 (1992).

[34] L. Kovács, L. Rebouta, J.C. Soares, M.F. da Silva, M. Hage-Ali, J.P. Stoquert, P. Siffert, C. Zaldo, Zs. Szaller, K. Polgár. *Lattice site of trivalent impurities in Mg-doped lithium niobate crystals.* Mater. Sci. Eng. B **9**, 505–508 (1991).

[35] C. Merschjann, D. Berben, M. Imlau, M. Wöhlecke. *Evidence for Two-Path Recombination of Photoinduced Small Polarons in Reduced $LiNbO_3$*. Phys. Rev. Lett. **96**, 186404 (2006).

[36] P. M. Morse. *Diatomic Molecules According to the Wave Mechanics. II. Vibrational Levels*. Phys. Rev. **34**, 57–64 (1929).

[37] A. Gröne, S. Kapphan. *Sharp, temperature dependent OH/OD IR-absorption bands in nearly stoichiometric (VTE) $LiNbO_3$*. J. Phys. Chem. Solids **56**, 687–701 (1995).

[38] R. T. Smith. *Temperature Dependence of the Elastic, Piezoelectric, and Dielectric Constants of Lithium Tantalate and Lithium Niobate*. J. Appl. Phys. **42**, 2219 (1971).

[39] U. Schlarb, K. Betzler. *Refractive indices of lithium niobate as a function of temperature, wavelength, and composition: A generalized fit*. Phys. Rev. B **48**, 15613–15620 (1993).

[40] A. Sanson, A. Zaltron, N. Argiolas, C. Sada, M. Bazzan, W. G. Schmidt, S. Sanna. *Polaronic deformation at the Fe 2+/3+ impurity site in Fe:$LiNbO_3$ crystals*. Phys. Rev. B **91**, 094109 (2015).

[41] S. S. Alexandre, E. Artacho, J. M. Soler, H. Chacham. *Small Polarons in Dry DNA*. Phys. Rev. Lett. **91**, 108105 (2003).

Acknowledgements

The authors gratefully acknowledge suggestions of K. Lengyel and crystal preparation by K.Polgár and coworkers at the Wigner Research Centre for Physics, Budapest as well as discussions with S. Sanna and S. Messerschmidt. Financial support from a bilateral DAAD-MÖB project (No. 57139940 from the German and No. 65056 from the Hungarian side) and the Deutsche Forschungsgemeinschaft (DFG) via projects IM37/5-2, INST 190/137-1 FUUG and INST 190/165-1 is kindly acknowledged.

Author contributions statement

M.I. had the original idea and directed the experiments. F.F. measured and analyzed the data and drafted the text of the paper. G.C. contributed to the analysis of the data and revised the paper. All authors read and approved the final version of the manuscript.

Additional information

Supplementary information accompanies this paper at http://www.nature.com/srep
Competing financial interests: The authors declare no competing financial interests.

B.4 Mid-Infrared photorefractivity with non-degenerate two-photon absorption

Mid-Infrared photorefractivity with non-degenerate two-photon absorption

Björn Bourdon[1,*], Felix Freytag[1], Mirco Imlau[1], Alexander Shumelyuk[2], and Serguey Odoulov[2]

[1] *Department of Physics, Osnabrueck University, Barbarastrasse 7, D-49076 Osnabrueck, Germany*
[2] *Institute of Physics, Science Ave. 46, 03650 Kyiv, Ukraine*
[*] *Corresponding author: bjbourdon@uni-osnabrueck.de*

Abstract: Photorefractive grating recording with mid-infrared subpicosecond light pulses (1.6 μm and longer wavelengths) might be possible in $LiNbO_3$ crystals if the interaction area is illuminated additionally with pulses of visible light. Two processes can enable the experimentally observed MIR recording: One is related to the direct photoexcitation of a free electron via nonlinear absorption of two photons with different frequencies, one in the MIR and one in the visible range. The alternative possibility consists in an enhancement, caused by the diffraction of a visible pulse, of a very weak space-charge grating seeded solely by MIR radiation.

This work was published in IOP Conf. Series: Journal of Physics: Conf. Series and can be found at doi: 10.1088/1742-6596/867/1/012006. Content from this work may be used under the terms of the Creative Commons Attribution 3.0 licence. Any further distribution of this work must maintain attribution to the author(s) and the title of the work, journal citation and DOI. Published under licence by IOP Publishing Ltd.

1 Introduction

Until now the recording of photorefractive gratings with infrared laser light was reported with wavelengths not exceeding 1.55 μm [1–3]. We show in this contribution that - profiting from strongly non-degenerate two-photon or multiphoton absorption (see for example [4]) of a train of subpicosecond pulses - it becomes possible to imprint the fringes of infrared (IR) light as a space-charge grating, when simultaneously illuminating the crystal homogeneously with a visible pulse. This new excitation scheme opens the era of MIR dynamic holography and may potentially be applied for MIR-pulse-characterization or even MIR-pulse-control in medical surgery.

2 Experimental Setup

A 1-mm thick y-cut crystal of $LiNbO_3$:Fe (0.1 wt. %) with optically finished input/output faces is illuminated by two IR beams with $\lambda = 1.6\,\mu$m that impinge upon the sample (see figure 1a). These beams are generated by one of two tuneable OPA's each generating a pulse train with a 1 kHz repetition rate and a pulse duration of $\tau \approx 100$ fs, polarized perpendicular to the optical c-axis. The IR pulses with energies $E_{\mathrm{IR}} \leq 25\,\mu$J are loosely focused ($r \approx 180\,\mu$m) into the sample and superposed in time as well as in space. In addition, a train of visible pulses is synchronized with the IR pulses within the same crystal area; this beam is loosely focused, too, to cover completely the intersection area of the IR pulses. Finally, a cw beam of a He-Ne laser is sent to the intersection area of the subpicosecond pulses at an angle that matches the Bragg diffraction condition from the inertial space charge grating that might be recorded by the IR beams in presence of the visible pulse. Both, the visible pulse train and the red beam are polarized normal to the $LiNbO_3$ c-axis in order to reduce the wavefront distortions because of optical damage. By adjusting the Bragg angle of incidence for the train of ultrashort visible pulses we get an extra tool for directly detecting the instantaneous twophoton absorption grating within every single pulse.

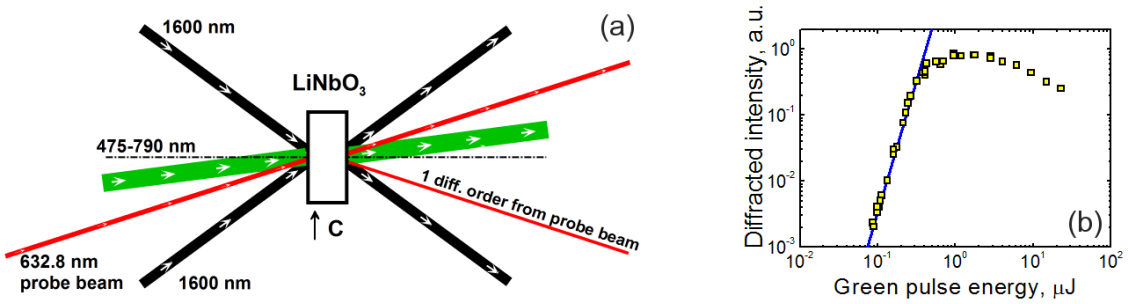

Figure 1: (a) Experimental geometry. Two infrared beams produce the fringes in $LiNbO_3$ sample ($2\Theta_{IR} = 7.7°$) that are superposed to homogeneous illumination by a visible beam; altogether they produce an instantaneous two-photon absorption grating and trigger the formation of a long-living photorefractive grating. A Bragg-matched red beam ($\Theta_r = 3°$) allows for monitoring the build-up of the photorefractive grating. (b) Saturated intensity of the diffracted red beam as a function of visible (510 nm) pulse energy (total energy of two recording IR pulses 25 μJ, repetition rate 1 kHz).

3 Results & Discussion

If two IR pulses and one visible pulse are present in the $LiNbO_3$ sample simultaneously, the diffracted red beam appears as it is shown in figure 1(a). The intensity of the diffracted beam increases with time and typically saturates within twenty seconds for an IR pulse energy of $E_{IR} \approx 10\mu$J. No diffraction is detected if the visible beam is absent or very weak. Figure 1(b) shows the saturated intensity of the diffracted red beam I versus the visible pulse energy EVIS for repetition rate recording, indicating a pronounced nonlinear behavior for moderate energies: $I \propto E_{VIS}^4$; the dependence

versus the IR pulse energy is also nonlinear. Thus we conclude that a photorefractive grating is recorded by common action of IR and visible light.

The temporal delay of the green pulse with respect to the MIR pulses (advanced and retarded, whatever) prevents from formation of both, instantaneous and long-lasting gratings. This allows for excluding possible two-step excitation of free carriers from impurity or defect energy levels within the band gap. In other experiments it was established that the absorption of a MIR pulse increases in presence of a visible pulse and vice versa, the visible pulse absorption becomes larger in presence of MIR pulse. In such a manner the existence of strongly non-degenerate two photon absorption with MIR involved is supported.

Acknowledgements
We gratefully acknowledge financial support from the Deutsche Forschungsgemeinschaft (DFG) via projects IM37/5-2, INST 190/137-1 FUGG and INST 190/165-1 FUGG.

References

[1] M. Wesner, C. Herden, D. Kip, E. Krätzig, P. Moretti. *Photorefractive steady state solitons up to telecommunication wavelengths in planar SBN waveguides.* Opt. Commun. **188**, 69–76 (2001).

[2] R. Mosimann, P. Marty, T. Bach, F. Juvalta, M. Jazbinsek, P. Günter, A.A. Grabar. *High-speed photorefraction at telecommunication wavelength 1.55 μm in $Sn_2P_2S_6$:Te.* Opt. Lett. **32**, 3230 (2007).

[3] O. Beyer, I. Breunig, F. Kalkum, K. Buse. *Photorefractive effect in iron-doped lithium niobate crystals induced by femtosecond pulses of 1.5μm wavelength.* Appl. Phys. Lett. **88**, 051120 (2006).

[4] D. A. Fishman, C. M. Cirloganu, S. Webster, L. A. Padilha, M. Monroe, D. J. Hagan, E. W. Van Stryland. *Sensitive mid-infrared detection in wide-bandgap semiconductors using extreme non-degenerate two-photon absorption.* Nat. Photon. **5**, 561–565 (2011).

B.5 Dynamic grating mediated energy transfer between two sub-picosecond pulses in $LiNbO_3$

Dynamic grating mediated energy transfer between two subpicosecond pulses in $LiNbO_3$

Stefan Nolte[1,*], Björn Bourdon[1], Felix Freytag[1], Mirco Imlau[1], Alexander Shumelyuk[2], and Serguey Odoulov[2]

[1] *Department of Physics, Osnabrueck University, Barbarastrasse 7, D-49076 Osnabrueck, Germany*
[2] *Institute of Physics, Science Ave. 46, 03650 Kyiv, Ukraine*
[*] *Corresponding author: stenolte@uni-osnabrueck.de*

Abstract: Two ultrashort pulses that interact in a nonlinear medium can excite a grating of the nonlinear absorption and refraction and their characteristics can be modified as a result of selfdiffraction from this grating. In this work, we adress an energy transfer between pulses of different energies and/or different frequencies within the visible spectral range in congruent, nominally undoped $LiNbO_3$ aiming to reveal new features that distinguish this process from the known transient and steady-state coupling of cw laser beams.

This work was published in IOP Conf. Series: Journal of Physics: Conf. Series and can be found at doi: 10.1088/1742-6596/867/1/012003. Content from this work may be used under the terms of the Creative Commons Attribution 3.0 licence. Any further distribution of this work must maintain attribution to the author(s) and the title of the work, journal citation and DOI. Published under licence by IOP Publishing Ltd.

1 Introduction

In this presentation we describe a study of the direct energy exchange between ultrashort femtosecond pulses in $LiNbO_3$, the crystal which possesses multiple quite pronounced optical nonlinearities. Apart from the instanteneous high-frequency Kerr nonlinearity and two-photon absorbtion nonlinearity [1], several inertial nonlinear responses have been revealed including those which are due to photoexcitation of free carriers and formation of various kinds of polarons [2].This crystal was the first in which a photorefractive nonlinearity and grating-assisted intensity redistribution of the recording waves has been discovered, see, e.g., [3]. We undertake this study to estimate how strong the coupling of subpicosecond pulses can be in $LiNbO_3$ and to establish the underlying wave mixing process(es) that is(are) responsible for energy redistribution between the interacting pulses.

2 Experimental Setup

The femtosecond laser system consists of a Ti:Sapphire oscillator with amplifier as a pump source for two independent tunable Optical Parametric Amplifiers (OPAs) [cf. [1]]. For the study of frequency degenerate interaction, the output of a single OPA was divided by a beamsplitter, while the use of two OPAs allowed for introducing any desirable frequency detuning between the recording pulses. In the experiment, the two light pulses impinge upon the sample in a plane normal to the axis of spontaneous polarization and are polarized along this axis to avoid possible contribution of spacecharge (photorefractive) gratings in investigated coupling processes. The angle of the beam intersection in air was chosen to be less than 5° to ensure a good spatial overlap of two 100 fs-long pulses. With the help of an optical delay line in one of two intersecting light beams the recording pulses could be perfectly well adjusted in time or deliberately mismatched with a controllable time delay. A double grating setup was used as a compressor/stretcher to change the chirp. This pulse chirp opens the possibility to introduce a frequency difference by changing the temporal mismatch, even in the case of the recording pulses with identical spectra.

3 Results & Discussion

Figure 1a shows the relative sample transmission T for different pulse delays Δt for two interacting pulses with identical pulse durations, pulse energies, chirp coefficients and spectra (centred at 590 nm). The upper and lower graphs differ in the sign of chirp (and pulse energy). In both graphs, pronounced energy redistribution ($\pm$ 20 %) is observed at Δt close to FWHM of the pulses themselves. Within the time interval where pulses interact a red-shifted portion of one pulse is always amplified in expense of the blue-shifted portion of the other pulse. Thus, for a fixed Δt the direction of energy flow is inverted if the sign of the chirp becomes opposite. This type of pulse energy coupling via diffraction from a moving grating is already well known (see, e.g., for plasma gratings in gases [4]). To confirm that it is just a frequency difference that governs this particular energy coupling process we used two pulses with 5 nm difference in wavelength. Instead of two, well separated in Δt energy coupling areas (Figure 1a) we obtained only one high coupling area centered at $\Delta t = 0$.

The next set of experiments consisted in gain measurement of a low signal probe pulse in presence of a strong pump pulse with tunable frequency. Figure 1b shows that nonzero coupling gain of a weak probe exists also in case of strict degeneracy, when both, the pump and probe pulse have identical spectra centered at 488 nm. This confirms the presence of another coupling process that is sensitive not to the detuning in pulse frequencies but to pulse difference in intensity. We believe this is a manifestation of a transient energy transfer (TET) [5] known for coupling of long pulses in media with inertial nonlinearities but never considered before for femtosecond pulses. Thus the detuning dependence of Figure 1b consists of two contributions, a δ-symmetric (odd function) dependence from TET and δ-anti-symmetric (even function) contribution from coupling of frequency nondegenerate pulses. The physical processes that are causing these optical nonlinearities are not yet established, but we know that for

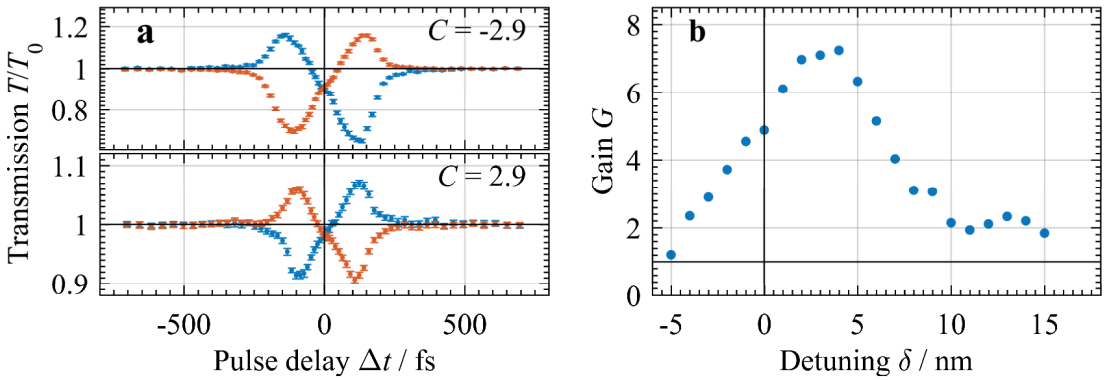

Figure 1: (a) Pulse delay dependence of transmission $T(\Delta t)$ for two identical interacting pulses (see text) with pulse durations $\tau = 200\,\mathrm{fs}$ (FWHM) and opposite chirp parameters C. (b) Wavelength detuning $\delta = \lambda_{\mathrm{probe}} - \lambda_{\mathrm{pump}}$ dependence of the gain G for a weak probe pulse.

observing TET the decay time of the nonlinearity should be longer comparing to the pulse duration. However, for efficient coupling of frequency nondegenerate pulses, on the opposite, this time should be comparable or shorter than the pulse duration.

Acknowledgements
The financial support of the Deutsche Forschungs Gemeinschaft (DFG) via projects IM37/5-2, INST 190/137-1 FUGG and INST 190/165-1 FUGG is gratefully acknowledged.

References

[1] H. Badorreck, S. Nolte, F. Freytag, P. Bäune, V. Dieckmann, M. Imlau. *Scanning nonlinear absorption in lithium niobate over the time regime of small polaron formation.* Opt. Mat. Express **5**, 2729 (2015).

[2] M. Imlau, H. Badorrec, C. Merschjann. *Optical nonlinearities of small polarons in lithium niobate.* Appl. Phys. Rev. **2**, 040606 (2015).

[3] P. Günter, J.-P. Huignard. *Photorefractive materials and their applications.* Springer series in Optical Science, Springer (2007).

[4] Y. Liu, M. Durand, S. Chen, A. Houdard, B. Prade, B. Forrestier, A Mysyrowicz. *Energy exchange between femtosecond laser filaments in air.* Phys. Rev. Lett. **105**, 055003 (2010).

[5] N. Kukhtarev, V. Markov, S. Odoulov. *Transient energy transfer during hologram formation in $LiNbO_3$ in external electric field.* Opt. Commun. **23**, 338 (1977).

B.6 Transient energy transfer on the femtosecond timescale in lithium niobate

Transient energy transfer on the femtosecond timescale in lithium niobate

Stefan Nolte[1,*], Björn Bourdon[1], Felix Freytag[1], Mirco Imlau[1], Alexander Shumelyuk[2], and Serguey Odoulov[2]

[1] *Department of Physics, Osnabrueck University, Barbarastrasse 7, D-49076 Osnabrueck, Germany*
[2] *Institute of Physics, Science Ave. 46, 03650 Kyiv, Ukraine*
[*] *Corresponding author: stenolte@uni-osnabrueck.de*

© 2017 IEEE. Reprinted, with permission, from Stefan Nolte, Transient energy transfer on the femtosecond timescale in lithium niobate, Europe European Quantum Electronics Conference (CLEO/Europe-EQEC, 2017 Conference on), 06/2017

Amplification of a weak signal pulse on expense of a strong pump pulse is a commonly used phenomenon in nonlinear optics. When applying a non-collinear interaction geometry of two ultrashort laser pulses an interference pattern can be observed that might give rise to a grating inside a nonlinear optical crystal. As recently reported, even pulses with different central frequencies can form an interference pattern with sufficient modulation that is favourable to be the origin of the amplification of a weak signal pulse [1]. We aim to reveal the process of amplification of a weak signal pulse in the context of transient energy transfer at a self-recorded grating in the frequency degenerated case of two femtosecond laser pulses. Inside the undoped, congruent sample of lithium niobate the light pattern gives rise to a mixed phase and amplitude grating, due to the instantaneous material response from two-photon absorption (TPA) and nonlinear refraction (optical Kerr effect). Additionally the sample shows an inertial material response from the formation of free charge carrier and small polarons [2]. Self-diffraction from this grating can be observed up to several additional non-Bragg diffraction orders, which can be used to characterize the pulses themselves [3]. Based on transient energy transfer in local response media an energy transfer is observed only for phase gratings in the non-steady-state where the time range is shorter or comparable to the relaxation time τ_r [4]. Additionally for getting unidirectional intensity transfer, thus amplification, a spatial symmetry break is prerequisite that is achieved by asymmetric experimental conditions such as different peak intensities. Two pulses from one Optical Parametric Amplifier (OPA) with a central wavelength of $\lambda = 488\,\mathrm{nm}$ are focussed in a thin sample of congruent nominally undoped lithium niobate with a variable delay Δt between them. When investigating the transmitted energies of the two frequency-degenerated pulses a pronounced increase of a weak signal can be noticed in presence of a strong pump pulse (Fig. 1(a)). The interference fringes are suppressed if the two polarization vectors are oriented perpendicular and no gain is observed. The possibility of switching on and

off the gain is used to extract the gain from the underlying absorption. The basic dependences of the gain from total peak intensity and peak intensity ratio confirm qualitatively the analogy to transient energy transfer: (i) always the weak pulse gains energy (Fig. 1(b)), (ii) the gain increases superlinear with the peak intensity. The generation of free charge carrier and small polarons is very likely to be responsible for the modulation of the refractive index. In the case of small polarons the well investigated light induced absorption can also lead to a change of refraction, both interrelated by Kramers-Kronig relations.

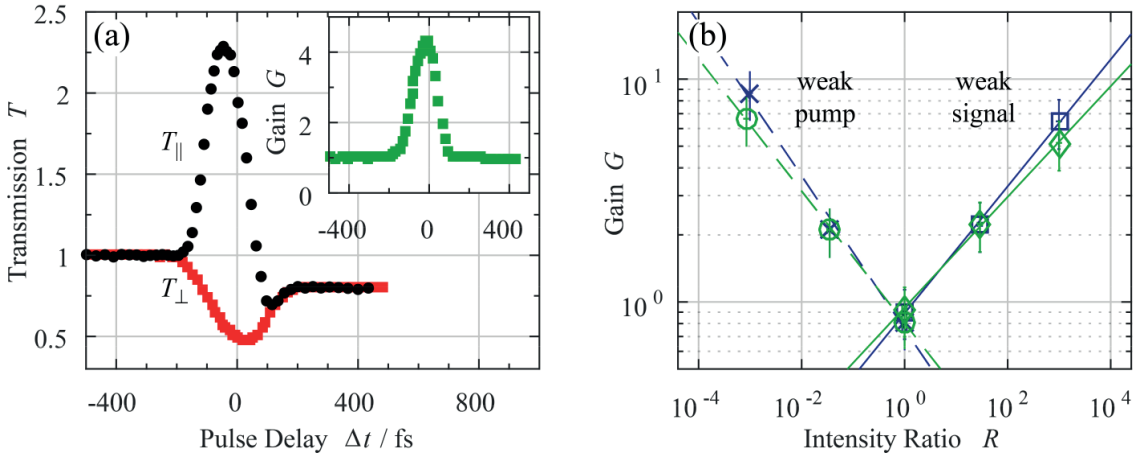

Figure 1: (a) Normalized transmission versus pulse delay Δt of the signal beam for two different polarization setups with extracted gain shown in the inset at a pulse duration $\tau = 80\,\mathrm{fs}$. (b) Maximum gain dependence from peak intensity ratio $R = I_\mathrm{P}/I_\mathrm{S}$.

Acknowledgements
The financial support of the Deutsche Forschungs Gemeinschaft (DFG) via projects IM37/5-2, INST 190/137-1 FUGG and INST 190/165-1 FUGG is gratefully acknowledged.

References

[1] S. Odoulov, A. Shumelyuk, H. Badorreck, S. Nolte, K. M. Voit, M. Imlau. *Interference and holography with femtosecond laser pulses of different colours.* Nat. Commun. **6**, 5866 (2015).

[2] M. Imlau, H. Badorrec, C. Merschjann. *Optical nonlinearities of small polarons in lithium niobate.* Appl. Phys. Rev. **2**, 040606 (2015).

[3] H. Badorreck, S. Nolte, F. Freytag, P. Bäune, V. Dieckmann, M. Imlau. *Scanning nonlinear absorption in lithium niobate over the time regime of small polaron formation.* Opt. Mat. Express **5**, 2729 (2015).

[4] N. Kukhtarev, V. Markov, S. Odoulov. *Transient energy transfer during hologram formation in $LiNbO_3$ in external electric field.* Opt. Commun. **23**, 338 (1977).

B.7 Picosecond near-to-mid-infrared absorption of pulse-injected small polarons in lithium niobate

Picosecond mid-infrared absorption of pulse-injected small polarons in lithium niobate

Felix Freytag[1,*], Phillip Booker[2], Gábor Corradi[3], Simon Messerschmidt[1], Andreas Krampf[1], and Mirco Imlau[1]

[1] *School of Physics, Osnabrueck University, Barbarastr. 7, 49076 Osnabrueck, Germany*
[2] *Laser Zentrum Hannover e.V.. Hollerithallee 8, 30419 Hannover, Germany*
[3] *Wigner Research Centre for Physics, Institute for Solid State Physics and Optics, Hungarian Academy of Sciences, Konkoly-Thege u. 29-33, 1121 Budapest, Hungary*
[*] *Corresponding author: felix.freytag@uos.de*

Abstract: Fs-pulse-induced (E_{pump}=2.5 eV) picosecond mid-infrared (MIR) absorption is studied in the spectral region between 0.30 eV and 1.05 eV in $LiNbO_3$. We find a non-instantaneous MIR absorption peak in the time domain up to 1 ps and a broad-band, long-lived absorption (maximum at 0.85 eV, width $\approx$ 0.5 eV), for $t > 1$ ps. Modelling suceeds by considering small Nb_{Nb}^{4+} electron polaron formation along the sequence: (i) two-photon injection of hot electron-hole pairs at Nb-O-octahedra, (ii) electron cooling by electron-phonon-scattering, and (iii) electron self-localization by strong electron-phonon-coupling.

Pulse-induced transient absorption (TA) is a widely accepted nonlinear optical phenomenon in lithium niobate, $LiNbO_3$ (LN), prominently observed as green- or blue-induced infrared absorption (GIIRA and BLIIRA) with a relaxation time of several seconds [1, 2]. The interaction of TA with propagating laser pulses fosters to a great extent the appearance of laser-induced bulk- and surface damages, and limits the conversion efficiency mainly by damping [3, 4]. It may also cause phase-detuning via localized crystal heating and the thermo-optical effect [5]. In LN, pulse-induced TA is closely connected with the optical generation of small polarons of the hole and electron type, trapped at O^{2-} and $Nb_{Nb/Li}^{5+}$ sites and absorbing in the blue and near-IR region, respectively [6, 7]. Consequently, the amplitude of the absorption maximum is expected to become proportional to the small polaron number density and the TA spectrum should be determined by the broad-bandwidth optical absorption features of small polarons [8]. The temporal evolution of TA is expected to reflect the complex path of carrier cooling and self-localization via phonon-scattering and -coupling [9], subsequent small polaron transport via thermally activated hopping [10] and its termination, e.g., via electron-hole recombination [11]. As a result, TA in LN ranges

over 15 decades of time from sub-picoseconds up to seconds [12] and is best studied by a combination of ultrafast pump-probe spectroscopy (fs - ns) and conventional spectrophotometric techniques (ns - D.C.).

The effects of GRIIRA/BLIIRA can almost completely be suppressed by co-doping LN with Mg, Zn, etc. over their respective threshold concentrations [1]. The doping has the effect to eliminate Nb_{Li}^{5+} antisite defects in LN and, thus, suppresses the formation of Nb_{Li}^{4+} electron and Nb_{Li}^{4+}:Nb_{Nb}^{4+} (bi-)polarons. Although the optical damage resistance is fairly increased in the visible range [13] a significant TA in the visible as well as in the infrared spectral region at timescales $< 10^{-5}$ s becomes more dominant in Mg-doped LN [14]. Despite the broad knowledge on the dependence of GRIIRA/BLIIRA on the crystal composition only little is known about the spectral and temporal properties of TA. In particular, nearly nothing is known about the TA in the MIR on the ultrafast time scale which is mandatory for the further improvement of high-power mid-infrared optical parametric oscillators (OPOs).

This contribution focuses on the spectral detection of picosecond MIR-TA in LN:Mg related with small Nb_{Nb}^{4+} free polaron (FP) formation in the range between 0.30 eV and 1.05 eV that is difficult to access from the experimental point of view. Our study uncovers that free polaron TA is overlaid by a non-instantaneous, broad-band MIR absorption peak on timescales up to ≈ 1 ps that cannot be attributed to multi-photon absorption processes. Under the assumption of pulse-injection of hot-electron-hole pairs, electron-phonon-scattering and -coupling, both TA contributions can well be separated on the temporal axis. An undisturbed, broad-band small polaron absorption spectrum emerges at a temporal delay of 2 ps after the pump pulse. It is shown that the obtained data set is best modeled by theoretical expectations for the absorption of small, free Nb_{Nb}^{5+} polarons. These data are also in good agreement with experimental absorption features of small Nb_{Nb}^{4+} polarons determined with conventional spectrophotometric techniques in thermally pre-treated LN crystals [15, 16] and are in line with previous NIR TA-measurements in Mg-doped LN [9, 17].

The ps-MIR TA studies were performed by a home-made VIS-pump-MIR-probe spectrometer (schematically sketched in the insert of Fig. 1, for a typical setup see [18]) with a temporal resolution $\Delta t \approx 200$ fs, beam diameters of $d_{\mathrm{pump}} = (500 \pm 50)\,\mu$m, $d_{\mathrm{probe}} = (400 \pm 50)\,\mu$m and an intersection angle of $\alpha = (8 \pm 1)^\circ$. The pump (2.5 eV; $\tau_{\mathrm{pump}} = (100 \pm 10)$ fs; I_{pump} up to 2.5 PW·m^{-2}; $f_{\mathrm{pump}} = 500$ Hz) and the probe (0.30 eV - 1.05 eV; $\tau_{\mathrm{probe}} \approx 170$ fs; $I_{\mathrm{probe}} < 0.03\,\mathrm{PW \cdot m^{-2}}$, $f_{\mathrm{pump}} = 1$ kHz) pulses are polarized along the c-axis and within the plane of the incident pulses. The infrared signal was detected with a spectral resolution of $\Delta\omega/\omega < 10^{-3}$ and a sensitivity $\Delta\alpha/\alpha \approx 2 \cdot 10^{-2}$ (exemplarily at 0.6 eV) using a combination of a Czerny-Turner spectrograph and a mercury-cadmium-telluride-detector pixel array (32-elements). The pulse energy of the signal generated via difference frequency generation during the interaction of pump and probe pulses (photon energy at about 2 eV) was measured by a standard Si-detector in transmission geometry. A single crystal (dimensions $6 \times 7\,\mathrm{mm^2}$; thickness $(200 \pm 10)\,\mu$m) of near-stoichiometric $LiNbO_3$:Mg (residual iron content below 5 ppm, solid solution MgO concentration of 1.0 molar %), grown at the *WIGNER Research Centre for Physics*, Budapest, Hungary is used with a fundamental absorption in the near- to mid-infrared spectral range not exceeding $\alpha_0 = 100\,\mathrm{m^{-1}}$ over the spectral range under investigation (0.30 eV−1.05 eV), apart from absorption due

to OH^--stretching vibrations in the spectral window $E = (0.424 - 0.443)\,\mathrm{eV}$ [13]. The two-photon absorption coefficient is determined to $\beta = (7.9 \pm 0.3)\,\mathrm{m^2/GW}$. Laser-induced damages of surface and bulk as well as cumulative effects of the TA between two sequential pump events were carefully checked, but not observed for $I_{\mathrm{pump}} = 1.4\,\mathrm{PW/m^2}$.

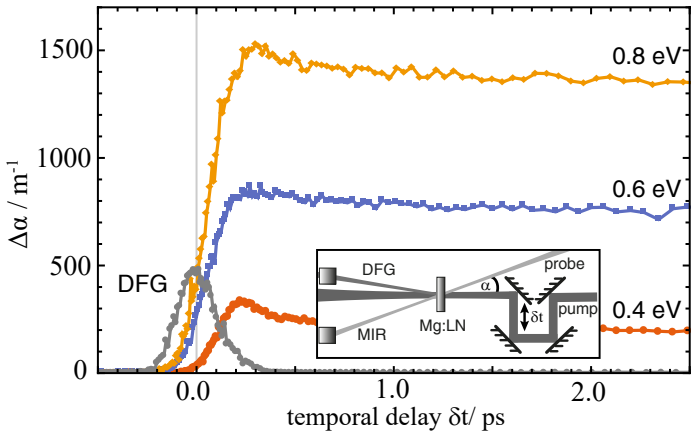

Figure 1: Transient absorption in the ps range for a 2.5 eV pump pulse ($I_{\mathrm{pump}} = (1.4 \pm 0.2)\,\mathrm{PW/m^2}$) and probe photon energies $E_{\mathrm{probe}} = 0.40\,\mathrm{eV}$ (3000 nm), 0.60 eV (2066 nm), 0.80 eV (1550 nm). The transient absorption is defined as $\Delta\alpha(E_{\mathrm{probe}}, \delta t) = \alpha(E_{\mathrm{probe}}, \delta t)_{\mathrm{pumped}} - \alpha(E_{\mathrm{probe}}, \delta t)_{\mathrm{unpumped}}$. The gray peak is a DFG correlation signal between pump and probe pulse (schematic setup shown in the insert).

Figure 1 shows the transient absorption $\Delta\alpha(\delta t)$ of LN:Mg for three probe photon energies ($E_{\mathrm{probe}} = 0.4\,\mathrm{eV}$, 0.6 eV, and 0.8 eV) as examples. The vertical gray line (cf. Fig. 1) marks the zero point $\delta t = 0$ defined as the maximum of DFG between pump and probe pulses (type-II eoe phasematching). The cross-correlation signal (dark gray dots in Fig. 1) has a FWHM of $(200 \pm 10)\,\mathrm{fs}$.

All transients of Fig. 1 show a qualitatively similar TA dynamics: A moderate non-instantaneous absorption peak dominates the time domain up to 1 ps after the pump pulse. Its maximum shows a marked dependence on the photon energy of the probe pulse and increases from $\delta\alpha^{\mathrm{max}} \approx 340\,\mathrm{m^{-1}}$ (0.4 eV) up to $\delta\alpha^{\mathrm{max}} \approx 1520\,\mathrm{m^{-1}}$ (0.8 eV). It is important to note that this absorption peak has a remarkable temporal shift of $\Delta t^{\mathrm{peak}} \approx (270 \pm 30)\,\mathrm{fs}$ (0.6 eV) compared to the pump pulse. In the time domain $t > 1\,\mathrm{ps}$, a plateau absorption materializes with an amplitude that also depends on the photon energy. The values, e.g., at $\delta t = 2.5\,\mathrm{ps}$, rise from $\delta\alpha(2.5\,\mathrm{ps}) = (200 \pm 10)\,\mathrm{m^{-1}}$ (0.4 eV) up to $\delta\alpha(2.5\,\mathrm{ps}) = (1350 \pm 20)\,\mathrm{m^{-1}}$ (0.8 eV) and remain constant all over the sub-ns time domain. Similar data sets were obtained for all probe photon energies in the investigated range between 0.30 eV and 1.05 eV. For photon energies below 0.4 eV as well as those above 0.8 eV, the MIR-TA shows a clear tendency to smaller values of $\delta\alpha^{\mathrm{max}}$ and $\delta\alpha(2.5\,\mathrm{ps})$.

These data cannot be explained straightforwardly with the state-of-the-art knowledge of picosecond TA in LN and provide further insights into the optical formation of small $\mathrm{Nb}^{4+}_{\mathrm{Nb}}$ electron polarons. In particular, to our knowledge, there are no reports on a temporal shift of the absorption peak of the TA with respect to the incident pump pulse in LN for any probe energy. This observation most likely remained inac-

cessible since the zero point $\delta t = 0$ has been assigned to the time of the maximum value of the absorption peak in recent studies. Consequently, the absorption peak itself was attributed to a *quasi-instantaneous* non-linearity, i.e., non-degenerate two- or multi-photon absorption in Refs. [17, 19, 20] using probe energies E_{probe}=1.55 eV in nominally undoped LN and LN:Mg. For the given fs-pump-probe technique some delay between the pump and a non-degenerate TPA peak might indeed be expected due to the different group velocities of the probe and pump pulse, as it has been discussed comprehensively by Beyer et al. [19]. Considering our experimental parameters, however, an estimate of the corresponding shift does not yield values exceeding $\delta t = (50 \pm 10)$ fs. Furthermore, the probe photon energies between 0.30 eV and 1.05 eV of our experiment are insufficient to enable non-degenerate two-photon absorption with a pump photon energy of 2.5 eV at a band gap energy of LN of $\approx$ 3.92 eV [21]. Three-photon interaction of two VIS and one MIR photons may be assumed, instead, but this does not comply with the considerable TA signal amplitudes of our study. However a similar shift of the peak-absorption, dependent on the photon energy, has been reported for diamond [22]. The authors attribute this phenomenon to the long-lasting presence of electrons within the conduction band.

In what follows, we attribute our findings to small $\text{Nb}^{4+}_{\text{Nb}}$ electron polaron formation according to the process schematically depicted in Fig. 2.

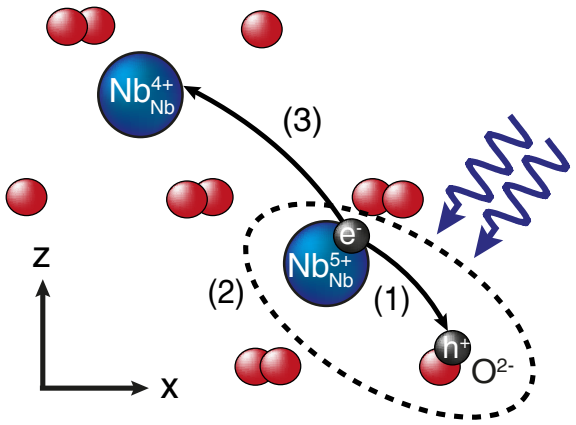

Figure 2: Model of small $\text{Nb}^{4+}_{\text{Nb}}$ electron polaron formation in LN (for details cf. text).

It is reasonable to expect the excitation of hot electron-hole pairs (hot excitons) to occur in a process localized within a Nb-O-octahedron of the LN structure. Such e^--h^+-pairs may recombine immediately (1) or may become self-trapped as self-trapped excitons (STE) [23] by strong coupling to the lattice (2). According to the phonon frequencies in LN up to the 10 THz range [24], the latter process will be delayed by a few hundreds of femtoseconds. It is noteworthy that the STE decay is closely connected with the emission of light in the blue-green spectrum in Mg-doped LN crystals [25] as used in our present study. Path (3) marks the possibility of phonon-assisted small polaron formation from an essentially unrelaxed e^--h^+-pair [26] by transfer of the electron to a next-neighboring $\text{Nb}^{5+}_{\text{Nb}}$ion (analogously, a transfer of a hole to a next neighboring O^{2-} also resulting in the dissociation of the e^--h^+-pair may also be considered). This electron will be cooled by means of electron-phonon scattering prior to self-localization via electron-phonon coupling. From the

perspective of our experiment, we will be able to detect the MIR absorption features of cooled electrons and Nb_{Nb}^{4+} electron polarons. In contrast, hot exciton states, that most probably show a UV/blue absorption feature, may not be accessible within the spectral region of our probe pulse. As a result, the transients in the MIR should reflect at least two main characteristic time constants: τ_c that takes into account the phonon-assisted cooling process of hot electrons and τ_p that is determined by the response time of the lattice.

A very similar understanding of TA related with small free Nb_{Nb}^{4+} polaron formation in MgO-doped LN was presented by Qiu et al. [9]. Although a non-instantaneous absorption peak of TPA was not observed, after a delay of the order of 1 ps a long-lived absorption plateau with rise time of about 200 fs at room temperature was clearly discovered and attributed to the formation of Nb_{Nb}^{4+} polarons. The delay was assigned to phonon-assisted cooling of optically excited hot carriers and the time required for carrier localization by electron-phonon coupling. In agreement with a theoretical estimate, a delay time of about 80 fs [9] was deduced for the cooling process. In a recent work of Badorreck et al. [27], we were able to verify this delay-time experimentally in nominally undoped, congruent LN with a value of $\tau_c \approx 80$ fs for a TPA excitation process at 2.5 eV, i.e., equivalent to this work.

The characteristics of the absorption plateau remain in full accordance with the state-of-the-art knowledge on TA in the near-infrared spectral range. Its interpretation via small, strong-coupling Nb_{Nb}^{4+} electron polarons is verified by a temperature dependent formation time of a few hundred femtoseconds [9, 17, 19, 20]. The respective decay process obeys a stretched exponential behavior with a decay time in the regime of a few hundred nanoseconds (over-threshold LN:Mg) [14,17,20]. This is short enough to avoid cumulative effects upon repetitive polaron formation at frequencies of 1 kHz. Based on these considerations, we will now turn to the numerical analysis of our data applying the following set of rate equations:

$$\frac{\partial N_h(L,t)}{\partial t} = \frac{\beta I^2(L,t)}{2\hbar\omega} - \frac{N_h(L,t)}{\tau_c} \quad (1)$$

$$\frac{\partial N_c(L,t)}{\partial t} = \frac{N_h(L,t)}{\tau_c} - \frac{N_c}{\tau_p} \quad (2)$$

$$\frac{\partial N_p(L,t)}{\partial t} = \frac{N_c}{\tau_p}, \quad (3)$$

where L is a coordinate along the light propagation direction in the crystal, β denotes the TPA-coefficient at the photon energy of the pump pulse ($\hbar\omega$), and $N_{h,c,p}$ the number densities of initially injected hot excitons, cold electrons and polarons, respectively. The derivative of the transient absorption signal then is given by the sum of three individual number densities multiplied by their respective absorption cross sections:

$$\frac{\partial \alpha(L,t)}{\partial L} = (-\sigma_p N_p(L,t) - \sigma_h \cdot N_h(L,t) - \sigma_c \cdot N_c(L,t))\frac{1}{d}. \quad (4)$$

This interplay of three types of carriers is the key for a successful modelling of the determined characteristics of the MIR-TA. According to the sequence of carriers in

our approach, the fitting procedure is performed with the following restrictions to the fitting parameters: (i) The number densities initially have to fulfill the relation $N_{\mathrm{h}}^{\mathrm{total}} \geq N_{\mathrm{c}}^{\mathrm{total}} \geq N_{\mathrm{p}}^{\mathrm{total}}$, (ii) the absorption cross section of hot excitons in the MIR is neglected: $\sigma_{\mathrm{hot}} \approx 0$, and (iii) for the sum of the decay times required for reaching the plateau absorption: $\tau_{\mathrm{c}} + \tau_{\mathrm{p}} \ll 1\,\mathrm{ps}$. For the comparison with experiment the final width of the probe pulse absorption has to be taken into account by convolving the modelled absorption with the temporal envelope of the probe pulse for fixed time delays. Again, we note that losses of the probe pulse by three-photon absorption including the pump pulse are not considered.

Fig. 3 compares the spatially integrated, convolved outcome of fitting equation (4) (green line) to the experimental data set (green dots), exemplarily for $E_{\mathrm{probe}} = 0.6\,\mathrm{eV}$. Successful fitting was performed for all spectra with the values $\tau_{\mathrm{c}} = 100\,\mathrm{fs}$, $\tau_{\mathrm{p}} = 150\,\mathrm{fs}$ the temporal evolution of the individual number densities $N_{\mathrm{h}}(t)$, $N_{\mathrm{c}}(t)$ and $N_{\mathrm{p}}(t)$ are depicted as determined from the solution of the rate equations (1)-(3). All fitting

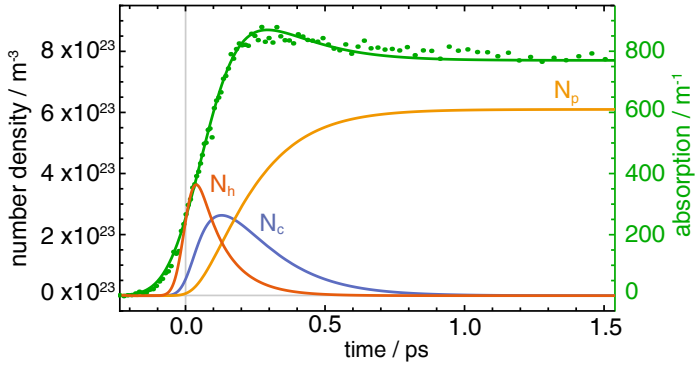

Figure 3: Numerical fit of the transient absorption (green line) and the data set (green dots) at 0.6 eV. Fitting parameters: $\tau_{\mathrm{c}} = 100\,\mathrm{fs}$ and $\tau_{\mathrm{p}} = 150\,\mathrm{fs}$. The calculated dynamics of the individual number-densities are plotted as orange (N_{h}), blue (N_{c}) and yellow (N_{p}) lines.

parameters agree very well with previously reported values of the polaron generation time (cf. $\tau_{\mathrm{FP}} \approx 100\,\mathrm{fs}$ in [17], $\tau_{\mathrm{GP}} < 400\,\mathrm{fs}$ in [12], [28]) and the free electron cooling time (cf. $\tau_{\mathrm{c}} \approx 80\,\mathrm{fs}$ in [9, 27]), confirming our assumptions. In the time range of $-0.2\,\mathrm{ps} < t < 1\,\mathrm{ps}$, we find that the number densities of all three carriers contribute to the overall TA signal. For $t > 1\,\mathrm{ps}$, on the other hand, TA is solely determined by the absorption of small, strong-coupling polarons.

Based on these findings, it is possible to deduce the absorption fingerprint of $\mathrm{Nb}_{\mathrm{Nb}}^{4+}$ electron polarons by plotting the spectral dependence of the TA signal at a fixed delay time of $t = 2\,\mathrm{ps}$ as displayed in Fig. 4. The data reveal a broad spectral distribution with a maximum at $E(\hbar\nu)_{\mathrm{peak}} \approx 0.80\,\mathrm{eV}$ that can be applied for an estimate of the small-polaron stabilization energy E_{p} due to the induced lattice distortion: $E_{\mathrm{p}} = (1/2)E(\hbar\nu)_{\mathrm{peak}} \approx 0.40\,\mathrm{eV}$. A more precise approach with respect to the asymmetric shape of the spectral distribution is given by EminÂ´s theory of small free polarons at elevated temperatures [8]:

$$\Delta\alpha(\hbar\omega) \propto \frac{1}{\hbar\omega} \exp[-(2E_{\mathrm{p}} - \hbar\omega)^2/(8E_{\mathrm{p}}k_{\mathrm{B}}T)], \tag{5}$$

describing the lineshape in excellent agreement with experimental data (cf. solid line

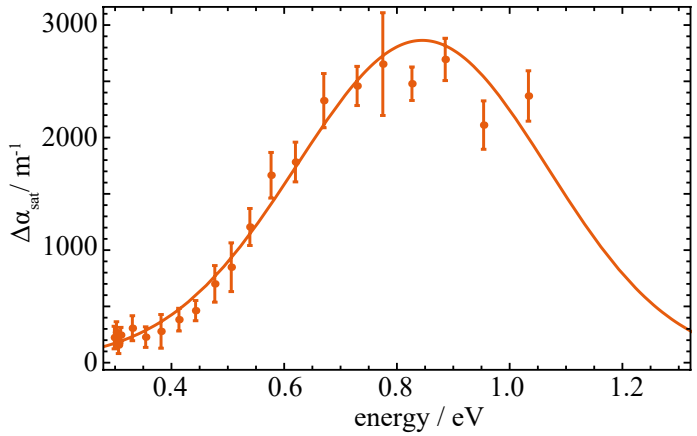

Figure 4: Absorption fingerprint of fs-pulse induced free polarons at a fixed time delay of $t = 2\,\mathrm{ps}$ ($I_{\mathrm{pump}} = 2.5\,\mathrm{PW/m^2}$). The continuous line fits Eq. 5 to the experimental data set.

in Fig. 4), with k_{B} being the Boltzmann constant. The fit yields the free polaron binding energy $E_{\mathrm{p}} = (0.445 \pm 0.020)\,\mathrm{eV}$, a peak maximum at $E(h\nu)_{\mathrm{peak}} = (0.835 \pm 0.040)\,\mathrm{eV}$ and a half width at half maximum of $W = (0.262 \pm 0.004)\,\mathrm{eV}$ at room temperature. A comparison of the values obtained in this study with previous investigations using thermally stabilized small polarons is given in Tab. 1. The peak position is in agreement with previous studies, whereas slight differences can be seen in the case of the spectral width.

The discovered differences can be attributed to (i) the use of an asymmetric fitting function and (ii) the impact of a non-equilibrium electronic state that has to be expected on the picosecond time scale after exposure to an intense fs-laser pulse. Driving evidence for the latter conclusion is the short lifetime of a few μs of the transient absorption with a complete recovery of the involved electronic state.

E_{p}(eV)	W(eV)	T(K)	Reference
0.445± 0.020	0.262 ± 0.004	295	this study
0.48	≈ 0.23	295	[15]
0.54	≈ 0.40	6	[15]
0.54	0.37	295	[7]
0.47	≈0.25	295	[16]

Table 1: Polaron stabilization energy E_{p} and half width at half maximum W of the MIR absorption feature in comparison.

In conclusion, our analysis reveals the picosecond transient absorption of femtosecond-pulse injected small free $\mathrm{Nb}_{\mathrm{Nb}}^{4+}$ electron polarons in the spectral range of 0.30 eV up to 1.05 eV. It extends the knowledge about the optical properties of small electron polarons to the ultrafast time regime that also comprises small polaron formation. The ps-MIR TA may be considered in forthcoming LN-based NLO devices dealing with MIR pulse generation and propagation. Furthermore, the fair agreement of peak position and spectrum of the absorption feature with expectations from small polaron theory supports the validity of the Holstein-Emin approach in solid state femtophysics. A specific result of our study is the discovery of a non-instantaneous

transient absorption peak that cannot be attributed solely to the action of multiphoton absorption. It rather supports the existing models for small polaron formation considering a multi-step flow of electronic energy upon two-photon absorption. It may also serve as a hint for the need of a further subdivision of the small polaron formation process and will push forward studies on the appearance and transport of hot excitons by probing the UV/VIS spectral range.

The authors gratefully acknowledge crystal preparation by K. Polgár and coworkers at the Wigner Research Centre for Physics, Budapest. Financial support of the Deutsche Forschungsgemeinschaft (DFG) via projects IM37/5-2, INST 190/137-1 FUUG and INST 190/165-1 is kindly acknowledged.

References

[1] Y. Furukawa, K. Kitamura, A. Alexandrovski, R. K. Route, M. M. Fejer, G. Foulon. *Green-induced infrared absorption in MgO doped $LiNbO_3$.* Appl. Phys. Lett. **78**, 1970–1972 (2001).

[2] J. Hirohashi, V. Pasiskevicius, S. Wang, F. Laurell. *Picosecond blue-light-induced infrared absorption in single-domain and periodically poled ferroelectrics.* J. Appl. Phys. **101**, 033105 (2007).

[3] S. Favre, T.C. Sidler, R.-P. Salathe. *High-power long-pulse second harmonic generation and optical damage with free-running Nd: YAG laser.* IEEE Journal of Quantum Electronics **39**, 733–740 (2003).

[4] R. M. Wood. *Laser-Induced Damage of Optical Materials (Series in Optics and Optoelectronics).* CRC Press (2003).

[5] G. Li, X. Xu. *Thermally induced dephasing of high power second harmonic generation in $MgO:LiNbO_3$ waveguides.* Chin. Opt. Lett. **9**, 121901–121904 (2011).

[6] O F Schirmer. *O-bound small polarons in oxide materials.* J. Phys. Conden. Matter **18**, R667–R704 (2006).

[7] O. F. Schirmer, M. Imlau, C. Merschjann, B. Schoke. *Electron small polarons and bipolarons in $LiNbO_3$.* J. Phys. Conden. Matter **21**, 123201 (2009).

[8] David Emin. *Optical properties of large and small polarons and bipolarons.* Phys. Rev. B **48**, 13691–13702 (1993).

[9] Yong Qiu, K. B. Ucer, R. T. Williams. *Formation Time of a Small Electron Polaron in LiNbO3: Measurements and Interpretation.* Phys. Status Solidi C **2**, 232–235 (2005).

[10] T. Holstein. *Studies of polaron motion.* Annals of Physics **8**, 343–389 (1959).

[11] D. Berben, K. Buse, S. Wevering, P. Herth, M. Imlau, T. Woike. *Lifetime of small polarons in iron-doped lithium–niobate crystals.* J. Appl. Phys. **87**, 1034–1041 (2000).

[12] O. Beyer, D. Maxein, Th. Woike, K. Buse. *Generation of small bound polarons in lithium niobate crystals on the subpicosecond time scale.* Appl. Phys. B **83**, 527–530 (2006).

[13] D. A. Bryan, Robert Gerson, H. E. Tomaschke. *Increased Optical Damage Resistance in Lithium Niobate.* Appl. Phys. Lett. **44**, 847 (1984).

[14] D Conradi, C Merschjann, B Schoke, M Imlau, G Corradi, K Polgár. *Influence of Mg doping on the behaviour of polaronic light-induced absorption in LiNbO3.* Phys. Status Solidi RRL **2**, 284–286 (2008).

[15] B. Faust, H. Müller, O. F. Schirmer. *Free small polarons in LiNbO3.* Ferroelectrics **153**, 297–302 (1994).

[16] G.K. Kitaeva, K.A. Kuznetsov, V.F. Morozova, I.I. Naumova, A.N. Penin, A.V. Shepelev, A.V. Viskovatich, D.M. Zhigunov. *Reduction-induced polarons and optical response of Mg-doped LiNbO3 crystals.* Appl. Phys. B **78**, 759–764 (2004).

[17] Satoru Sasamoto, Junji Hirohashi, Satoshi Ashihara. *Polaron Dynamics in Lithium Niobate upon Femtosecond Pulse Irradiation: Influence of Magnesium Doping and Stoichiometry Control.* J. Appl. Phys. **105**, 083102 (2009).

[18] G. M. Greetham et al. *Ultra: A Unique Instrument for Time-Resolved Spectroscopy.* Appl. Spectrosc. **64**, 1311–1319 (2010).

[19] O. Beyer, D. Maxein, K. Buse, B. Sturman, H. T. Hsieh, D. Psaltis. *Investigation of Nonlinear Absorption Processes with Femtosecond Light Pulses in Lithium Niobate Crystals.* Phys. Rev. E **71** (2005).

[20] Dominik Maxein, Stephan Kratz, Peter Reckenthaeler, Johanna Bückers, Daniel Haertle, Theo Woike, Karsten Buse. *Polarons in Magnesium-Doped Lithium Niobate Crystals Induced by Femtosecond Light Pulses.* Appl. Phys. B **92**, 543–547 (2008).

[21] X. Yang, G. Xu, H. Li, J. Zhu, X. Wang. *Optical Absorption Edge of Mg + Zn: $LiNbO_3$.* Cryst. Res. Technol. **31**, 521–527 (1996).

[22] T Roth, R Laenen. *Absorption of free carriers in diamond determined from the visible to the mid-infrared by femtosecond two-photon absorption spectroscopy.* Opt. Commun. **189**, 289–296 (2001).

[23] R.T. Williams, K.S. Song. *The self-trapped exciton.* J. Phys. Chem. Solids **51**, 679–716 (1990).

[24] Marc D. Fontana, Patrice Bourson. *Microstructure and defects probed by Raman spectroscopy in lithium niobate crystals and devices.* Applied Physics Reviews **2**, 040602 (2015).

[25] G. Blasse. *Fluorescence of Niobium-Activated Antimonates and an Empirical Criterion for the Occurrence of Luminescence.* J. Chem. Phys. **48**, 3108–3114 (1968).

[26] David Emin. *Dynamics of the optically induced properties of a small-polaronic glass.* J. Non-Cryst. Solids **35-36**, 969–973 (1980).

[27] Holger Badorreck, Stefan Nolte, Felix Freytag, Pia Bäune, Volker Dieckmann, Mirco Imlau. *Scanning Nonlinear Absorption in Lithium Niobate over the Time Regime of Small Polaron Formation.* Opt. Mater. Express **5**, 2729 (2015).

[28] Mirco Imlau, Holger Badorreck, Christoph Merschjann. *Optical Nonlinearities of Small Polarons in Lithium Niobate.* Appl. Phys. Rev. **2**, 040606 (2015).

C Beiträge zu Konferenzen

Während der Promotionzeit sind folgende Beiträge zu/in nationalen und internationalen Konferenzen/Instituten vorgestellt worden:

- Felix Freytag, Phillip Booker, Gábor Corradi und Mirco Imlau.
  Atomic insight to small, strong-coupling hole polarons in lithium niobate by local probing of OH^--bonds
  International Conference on Defects in Insulating Materials (ICDIM) 2016, Lyon, Frankreich (Vortrag)

- Felix Freytag.
  Optical Nonlinearities of Small Polarons in Lithium Niobate
  L'Institut national de la recherche scientifique (INRS) 2016, Montreal, Kanada (Kolloquiumsvortrag)

- Felix Freytag, Gábor Corradi und Mirco Imlau.
  Atomic insight to small, strong-coupling hole polarons in lithium niobate by local probing of OH^--bonds
  Photonics North 2016, Quebec, Kanada (Vortrag)

- Felix Freytag, Holger Badorreck, Stefan Nolte, Pia Bäune, Volker Dieckmann und Mirco Imlau.
  Scanning nonlinear absorption in lithium niobate over the time regime of small polaron formation
  International OSA Network of Students 2016, Quebec, Kanada (Vortrag)

- Felix Freytag, Holger Badorreck, Stefan Nolte, Pia Bäune und Mirco Imlau.
  Scanning nonlinear absorption in lithium niobate over the time regime of small polaron formation
  DPG-Frühjahrstagung 2016, Regensburg, Deutschland (Vortrag)

- Felix Freytag, Phillip Booker und Mirco Imlau.
  OH^- as local, vibrational probe for the inspection of small, strong-coupling polarons
  DPG-Frühjahrstagung 2016, Regensburg, Deutschland (Vortrag)

- Felix Freytag.
  Interaction of ultrashort laser pulses with small polarons in lithium niobate
  International Workshop LN, 2015, Tianjin, China (eingeladener Vortrag)

- Felix Freytag, Holger Badorreck, Stefan Nolte und Mirco Imlau.
  Lattice deformation of small polarons probed by OH^--defects in $LiNbO_3$ using transient fs-MIR spectroscopy
  Photorefractive Photonics (PR), 2015, Villars-Sur-Ollon, Schweiz (Poster)

- Felix Freytag, Phillip Booker und Mirco Imlau.
  Light induced changes in the OH^--stretching bond by frequency-resolved femtosecond infrared absorption spectroscopy in congruent $LiNbO_3$
  DPG-Frühjahrstagung 2015, Berlin, Deutschland (Vortrag)

Danksagung

An erster Stelle gilt mein besonderer Dank Herrn Prof. Dr. Mirco Imlau für die außerordentlich vielseitige Aufgabenstellung und zahlreiche motivierende Diskussionen. Vielen Dank für die über sechs Jahren in ihrer Arbeitsgruppe *Ultrakurzzeitphysik*.

Ein besonderer Dank geht außerdem an Prof. Dr. Dominik Schaniel für die Begutachtung dieser Arbeit.
Als nächstes möchte ich allen Mitgliedern der Arbeitsgruppe für die ständige Hilfs- und Diskussionsbereitschaft und das wunderbare Miteinander danken. Besonderen Dank spreche ich an meine beiden Bürokollegen Herrn Simon Messerschmidt und Herrn Björn Bourdon aus, welche durch (wenn auch manchmal schlechte) Witze für eine wunderbare Atmosphäre während der Arbeit gesorgt haben.
Für die außerordentlich produktive wissenschaftliche Zusammenarbeit auch auf internationaler Ebene möchte ich Herrn Prof. Dr. Simone Sanna, Herrn Prof. Dr. Ortwin Schirmer, Herrn Prof. Dr. Serguey Odulov, Herrn Dr. Marco Bazzan und Herrn Dr. Krisztián Lengyel danken. Hierbei bekunde ich außerordentlichen Dank an Herrn Dr. Gábor Corradi, welcher mir durch rege Diskussion und seine sprachliche Präzision eine große Hilfe war in der wissenschaftlichen Welt Fuß zu fassen.
Herrn Dr. Alexandr Shumelyuk und Herrn Björn Bourdon danke ich für die ausgezeichnete Zusammenarbeit und für die Kooperation bei der Erstellung der Messungen zur MIR-Holographie.
Ein besonderer Dank gilt dem ungarischen *WIGNER Research Centre for Physics* für die Bereitstellung, Bearbeitung und Beratung bezüglich der LN-Kristalle, insbesondere ist hierbei Frau Dr. Ivett Hajdara zu danken.
Bedanken möchte ich mich auch für eine außerordentlich kooperative Zusammenarbeit nicht nur während seiner Bachelor- und Masteranden Zeit bei Herrn Phillip Booker.
Ganz besonderer Dank gilt den Mitarbeitern der elektronischen und den feinmechanischen Werkstätten, insbesondere Herrn Rainer Svajda, Herrn Uwe Klink und Herrn Holger Heine.
Besonders danke ich Frau Dr. Magdalena Zawadzki, Herrn Stefan Nolte und Herrn Björn Bourdon für die Durchsicht dieser Arbeit.
Der Deutschen Forschungsgemeinschaft (DFG) danke ich für die finanzielle Unterstützung im Rahmen des Drittmittelprojektes INST 190/137-1 FUUG und INST 190/165-1.

Mein letzter Dank und wichtigster Dank gilt meiner Familie und meinen Freunden, ohne deren stetige Unterstützung mein Studium der Physik und meine Promotion nicht möglich gewesen wäre.

Eidesstattliche Erklärung

Hiermit versichere ich, die vorliegende Dissertation selbstständig, ohne fremde Hilfe und ohne Benutzung anderer als der von mir angegebenen Quellen angefertigt zu haben. Alle aus fremden Quellen direkt oder indirekt übernommenen Gedanken sind als solche gekennzeichnet. Die Arbeit wurde noch keiner Prüfungsbehörde in gleicher oder ähnlicher Form vorgelegt.

Osnabrück, den 30. November 2018.